

63-4-1

406 838

CATALOGED BY DDG

AS AD NO. 406 838

PROGRESS REPORT NO. 23

1 OCTOBER 1962 through 31 MARCH 1963

to

THE JOINT SERVICES TECHNICAL ADVISORY COMMITTEE

Representing: The Air Force Office of Scientific Research
The U.S. Army Research Office
The Office of Naval Research

A summary of current research at
The MICROWAVE RESEARCH INSTITUTE

DDC
RECEIVED
JUN 18 1963
TISIA B

Report
R-452.23-63

for
Grant AF-AFOSR-62-295
Task No. 4751

POLYTECHNIC INSTITUTE OF BROOKLYN
MICROWAVE RESEARCH INSTITUTE

Topics representative of most of the Microwave Research Institutes' research activities have been included in this report. The various sponsoring agencies and their contract numbers are individually acknowledged at the end of each item.

This comprehensive semi-annual report to the Joint Services Technical Advisory Committee is made possible through the support of the Air Force Office of Scientific Research of the Office of Aerospace Research; the Department of the Army, Army Research Office; and the Department of the Navy, Office of Naval Research; under Grant AF-AFOSR-62-295, Task No. 4751.

PROGRESS REPORT NO. 23

1 OCTOBER 1962 through 31 MARCH 1963

**to
THE JOINT SERVICES TECHNICAL ADVISORY COMMITTEE**

**Representing: The Air Force Office of Scientific Research
The U.S. Army Research Office
The Office of Naval Research**

**Submitted by: ERNST WEBER, President
Polytechnic Institute of Brooklyn**

Coordinated by: Walter K. Kahn, Associate Professor of Electrophysics

**Report
R-452.23-63**

**for
Grant AF-AFOSR-62-295
Task No. 4751**

TABLE OF CONTENTS

Research at the Microwave Research Institute of the Polytechnic Institute of Brooklyn	v
Participating Faculty and Research Staff	x

I. ELECTROMAGNETICS

Harmonic Amplitudes and Power Relations in Space-Time Periodic Media	1
Wave Propagation in a Sinusoidally Modulated Dielectric Medium	7
Diffraction in a Certain Stratified Medium	11

II. PLASMA ELECTROPHYSICS AND ELECTRONICS

Radiation from a Directive Antenna Embedded in an Anisotropic Plasma Half-Space	23
The Field of a Line Source above a Uniaxially Anisotropic Plasma Slab	27
Surface Waves on Plasma Slabs	31
A Study of the Cathode Fall Region in a Pulsed Glow Discharge	39
High-Power Microwave Plasma Interactions	49
One-Dimensional Isothermal Flow in an Infinitely Conducting Fluid	50

III. SOLID STATE AND MATERIALS RESEARCH

Acoustic Excitation of Magnetoelastic Waves in Ferrites	54
Harmonic Generation in Magnetic Materials through Galvanomagnetic Interactions	57
Active Structures Research	59
Low Temperature Studies	62
Biomedical Engineering Research	64

IV. MICROWAVE CIRCUITS

High-Power Facility	67
Interaction of High Microwave Fields with Metals	68
DC Triggered Microwave Spark Gap Switch	69
Electrical Breakdown at Microwave Frequencies of Gases at Relatively High Pressures	74
Absorbing Material Using Parallel Resistive Sheets	75

CONTENTS

C-Band Ferrite Switch	79
Symmetries of Uniform Waveguide Containing Anisotropic Materials	81

V. NETWORK THEORY

The Theory of Active Mode Generation Using Tunnel Diodes	90
Topology and Resistor Networks	92
Canonical Form of Two Tandem-Connected Four-Ports	93

VI. SYSTEMS AND CONTROL

Stability and Convergence Properties of Linear Time-Varying Systems	95
Studies in Optimal Control Theory	102
The Response of an Automatic Phase Control System to fm Signals and Noise	103
Synthesis of Optimal Control Systems with Control Input Constraints	106
Small Sample Sequential Detection	107
Reliability Research	109
Theory of Switching Circuits	110
Narrow-Band Television System	113
Publications and Reports	115
Colloquia and Seminars	122

RESEARCH AT THE MICROWAVE RESEARCH INSTITUTE
of the
POLYTECHNIC INSTITUTE OF BROOKLYN

Research efforts at the Polytechnic are motivated by a desire to fulfill an academic responsibility by providing a means for both faculty and graduate student body to participate in significant and fundamental research programs responsive to technological and national interests. The program at the Microwave Research Institute involves academic research activities of faculty primarily from the departments of electrophysics, electrical engineering, and physics and covers a broad spectrum ranging from basic theoretical programs in physics, mathematics, and engineering to experimental programs involving basic measurements and the development of devices and materials. Although the specific structure of this program is continually being refined, it appears desirable to provide an over-all summary of some of the present activity.

It is particularly desirable to provide such a summary in semi-annual reports to the Joint Services Technical Advisory Committee, as this permits a coherent presentation of the various phases of the program for the information of each of the various sponsoring agencies. These phases are sponsored not only by funds provided by Joint Service contract No. AF-AFOSR-62-295 but also, and in larger measure, by individual contracts with the various Services. In this connection, the funding provided by the Polytechnic Institute should not go unmentioned, as it frequently provides for the initiation of research programs and facilities which are subsequently sponsored by external agencies.

Contributions are compiled under six descriptive subject headings: electromagnetics, plasma electrophysics and electronics, solid state and materials research, microwave circuits, network theory, and systems and control. As may be anticipated from the summary of activities given below, these headings may be supplemented from time to time with reports of additional phases of research in which various groups of participating faculty are engaged.

ELECTROMAGNETICS

Under the heading of electromagnetics fall a large variety of problems dealing with the transmission of energy by electromagnetic waves and the diffraction of such waves.

"Non-conventional waveguides," by which is meant any waveguide structure other than conventional uniform waveguide having a homogeneous isotropic medium and perfectly conducting walls, are being investigated along a broad front. Non-conventional waveguides may be either transmission elements or antennas. They include "open" waveguides capable of propagating both a discrete and a continuous spectrum of guided waves; periodically open or closed waveguides admitting a band spectrum; and waveguides containing anisotropic media, electron beams or plasmas. Both theoretical and experimental investigations are directed toward the network description of propagation and discontinuity effects in such guides. Current activity is concerned with leaky-wave antennas, waveguides containing anisotropic and gaseous plasma, various types of periodic structures, surface-wave propagating structures, and media with time-varying properties.

Another research program, in quasi-optics, involves the calculation, via guided-wave techniques of the effects of large perturbing surfaces on the electromagnetic fields radiated by prescribed, but otherwise arbitrary, electric or magnetic current distributions. The as-

RESEARCH AT THE MICROWAVE RESEARCH INSTITUTE

sumed sources can be representative of incident plane waves (as in diffraction problems) or slots or dipoles on the surfaces (as in antenna problems). Asymptotic representations are used to highlight the quasi-optic nature of the field solutions in terms of geometric-optical, diffracted, "creeping" wave, etc., effects. Moreover, special attention is given to the transition phenomena appropriate to boundary regions between different, geometric-optical domains (for example, between illuminated and dark regions).

A multimode phase of research is motivated by the importance of millimeter-wave applications utilizing oversized waveguides. The current effort involves simplifying the frequently cumbersome formal multimode network theory which must be employed in engineering applications, and the deliberate exploitation of two or more propagating modes in the design of waveguide components.

PLASMA ELECTROPHYSICS AND ELECTRONICS

A project of considerable importance now under way is the design and construction of a facility to allow the interaction of high levels of microwave power with a supersonic plasma shock. This program is being carried out jointly by the Electrophysics and Aerospace Departments.

A plasma formed by a pulsed discharge is being studied by means of a microwave beam probe, in order to understand the fundamental process taking place in the plasma. Equipment is now being set up to study the interactions between the plasma and microwaves at high power levels.

Another experimental study is concerned with the ion oscillation phenomena in a plasma formed by an electron beam traversing a region of neutral gas molecules in a static magnetic field. Microwave plasma diagnostic experiments have been carried out on video pulsed discharges as well as on plasmas excited by high rf power levels.

The dynamical processes characteristic of a plasma are being studied theoretically and experimentally. Particular attention focusses on the coupling of electromagnetic and acoustic wave phenomena under both the linear and nonlinear regimes. The characteristics of a pure (electrodeless) high-current discharge are being studied with a view toward an adequate phenomenological description and direct application in high-power switching.

SOLID STATE AND MATERIALS RESEARCH

The activities in solid state research are primarily concerned with the interaction of microwave fields with ferrite materials and semiconductors. Research in ferrite materials and devices has been carried forward under two closely cooperating efforts. One of these directly concerns the basic physical properties of ferrites in both bulk and thin-film forms. These studies include spin wave interaction in thin films, fabrication and structure studies of spinel and garnet ferrites in thin-film forms, anisotropy studies, etc. Other work is continuing on the properties of metallic magnetic films.

The second phase of the ferrite activity is concerned with the application of these properties to devices and is currently devoted to ferrite components at millimeter waves, such as ferrite filters, isolators and circulators in non-conventional millimeter wave transmission lines.

The investigation of microwave-semiconductor interactions has been primarily concerned with microwave conductivity properties of germanium. A microwave modulator using a semiconductor switching element has been built and is being studied.

Paramagnetic resonance studies are being conducted utilizing the Institute's new mag-

RESEARCH AT THE MICROWAVE RESEARCH INSTITUTE

netic facility. The research program is jointly carried out by the electrophysics, physics and chemistry departments. The experiments are conducted to study the basic technology of magnetic resonance and spectroscopic techniques. As one application of paramagnetic resonance, this phenomenon is being used as a mechanism to achieve a highly stabilized oscillator. It is anticipated that the extension of this program to free radical observation may give rise to interesting studies in the fields of biology and biochemistry.

Another phase of the effort is concerned with the field theory calculation via guided wave techniques of the propagation and discontinuity (impurity) properties that characterize electron flow through solid-state structures. Band-structure properties are being studied on the basis of microscopic "electron-wave network theory" patterned along the lines of conventional network theory.

An interdepartmental program examining the properties of solid-state and gas optical masers has been started.

MICROWAVE CIRCUITS

Microwave components and equipment for requirements beyond those encountered in the present microwave art are being designed and constructed. Such requirements arise in connection with a super-high-power capability, millimeter operating wavelengths, extreme bandwidths, extremely short switching times, and other special response and performance characteristics. The approach is partially experimental, based on previous experience with microwave component development, and partially analytical, based on known solutions of field problems, known network theoretic considerations, application of new solid state effects and through interchange of information with other groups at MRI.

Current fields of interest in the high-power area include: the continued development of a high-power capability in excess of 30 megawatts, now utilizing a microwave flywheel; implementation of the interaction of this source and others with hypersonic plasmas, electrically excited plasmas, solid and liquid dielectrics and metals; development of high-power switches capable of switching in several nanoseconds time; and development of new techniques and components required for oversized waveguide operation.

In the millimeter area, present fields of interest include: continued development of H-guide transmission-line components, including all components for build-up of a radar front end; application of quasi-optic techniques to components using oversized guide; and methods of measurement in the multimode environment.

Our aim is to exploit new microwave circuit ideas and the properties of new materials measurement of the basic electrical properties of microwave components and systems. In the past this has led to the development of broadband precision power meters, microwave attenuators, impedance meters, etc., and has resulted in a better understanding of the errors implicit in the determination of such quantities as absolute power, impedance, and attenuation. For the future, under the stimulus of recent advances in the knowledge of solid state properties at microwave frequencies, added emphasis will be placed on the application of semiconductors and ferrites to microwave instrumentation and microwave devices. An additional activity in this area involves the writing of a new Handbook of Microwave Measurements which is a major revision and expansion of the original handbook published in 1954.

NETWORK THEORY

Lumped and distributed parameter networks and their application to the design of devices with optimum terminal performance, particularly in microwave wavelength regions, are under

RESEARCH AT THE MICROWAVE RESEARCH INSTITUTE

study. Of special interest are new and improved components employing special waveguide geometries, and the interaction of guided waves with solid-state materials to yield novel circuits. The use of these techniques for instrumentation and measurement methods also falls within the scope of the group.

The work done in network theory is aimed at obtaining unifying network principles, concepts, and synthesis techniques which encompass lumped-parameter as well as distributed-parameter circuits. The synthesis of lumped and transmission-line type networks, and the approximation of prescribed response characteristics for such circuits by physically realizable network functions is also being treated. This is associated with the general filter synthesis problem utilizing lumped-loaded lines. A class of network problems is being studied in which, for practical design reasons, special constraints are imposed on the final network form. Such constraints may include parasitic elements, special requirements on transformers (or lack of them), loss associated with the elements, permissible transmission-line configuration, synthesis of two-ports in Darlington cascade form, etc. Under this portion of the program, extensions of the theory of broadband matching and gain-bandwidth limitations in linear networks including negative resistances (tunnel diodes) are being investigated, including applications to the broadband high-frequency equalization of transistors and waveguide structures. The circuit theory of parametric and other active microwave systems is also being studied.

SYSTEMS AND CONTROL

Intensive research is in progress on the properties of and the design and analysis techniques for communication and control systems. The various phases of the work are closely correlated through the dependence upon the basic concepts of information theory, communication theory, network theory, and feedback theory in their broadest senses. Systems considered range from magnetoelectric circuits to point-to-point communication systems involving, as unifying aspects, the study of the fundamental informational characteristics of the system, and the formulation of synthesis procedures based upon the component parts defined as network elements.

Research in active networks covers investigations of nonlinear circuit analysis, design of nonlinear circuits, synthesis of active networks, and properties of feedback systems. Particular emphasis is placed on systems which utilize computers as control elements - of particular importance when process characteristics are exceedingly complex or when process characteristics vary with environmental conditions (as characterized, for example, by guidance systems, chemical process control, etc.). Subsidiary and related problems include investigations of experimental and theoretical techniques for the determination of the dynamic transfer characteristics of physical systems, both linear and nonlinear.

This work extends to the utilization of identification techniques in adaptive control systems, to the identification of the dynamical characteristics of human beings as elements of a human-mechanistic system, and to the investigation of the applied mathematical concepts which underlie the techniques for identification. The work on identification also includes the relation of measurement techniques to the configuration, particularly as the result influences the stability investigation for the system.

Modern statistical theory and its application to communication systems, signal detection and other fields is under study. Some specific projects which have been worked on include: general study of information theory; narrow-bandwidth transmission of television pictures; high-speed transmission of facsimile pictures; design of digital coding apparatus; problems involved in pulse transmission; reduction of multi-path echo distortion; application of recent statistical methods to basic communication theorems; study of abstract and practical proper-

RESEARCH AT THE MICROWAVE RESEARCH INSTITUTE

ties of digital codes; and the optimum detection of weak signals in noise and other random interferences. One of the features of modern communication theory is the ability to define quantitatively a quantity of information and a loss of information due to errors. Another feature is the consideration that a communication system must be designed to handle not one but an ensemble of signals and therefore a statistical approach is almost necessary.

Emphasis is also being placed on a study of learning processes: in particular, the programming of a computer to learn. Research in this area is again closely related with the work in communication systems on the development of design techniques for the improved transmission of signals in the presence of noise, and with the work in control on the development of design and evaluation techniques for adaptive and optimizing systems.

POLYTECHNIC INSTITUTE OF BROOKLYN

E. Weber, President
C. G. Overberger, Assistant Vice President for Research

MICROWAVE RESEARCH INSTITUTE
PARTICIPATING FACULTY AND RESEARCH STAFF

DEPARTMENT OF CHEMISTRY

Faculty

Fellows

F. Banks * R. F. Riley * N. H. Riederman P. Wagner

DEPARTMENT OF ELECTRICAL ENGINEERING

Faculty

M. Schwartz (Head)	K. Clarke	D. Hunt	L. Shaw
E. J. Angelo	S. Deutsch	W. A. Lynch	M. L. Shooman
C. Belove	P. Dorato	W. MacLean	E. J. Smith
L. Bergstein	R. F. Drenick	E. Mishkin	L. Strauss
W. B. Blesser	A. B. Giordano	M. Panzer	J. G. Truxal
J. J. Bongiorno	C. Hachemeister	A. Papoulis	G. Weiss
L. Braun, Jr.	R. Haddad	D. L. Schilling	F. Wohlers
J. Crump	D. Hess	A. Schillinger	
	S. Horing	H. Schlosser	

Research Associates and Instructors

F. T. Boesch	M. M. Drossman	F. M. Labianca	C. Shulman
R. R. Boorstyn	M. Gindoff	J. M. Mendel	J. Simes
R. Borrmann	R. Honigsbaum	E. Nelson	F. Stone
P. J. Crepeau	H. J. Hunt	R. L. Pickholtz	F. Weiser
C. Devieux	A. Kronfeld	R. Rifkin	

Research Assistants, Fellows and Graduate Assistants

J. Abbate	M. Karsky	E. Marom	J. Rubio
B. Albrecht	I. Kliger	R. Mauro	H. Schachter
G. Bernknopf	Z. Kohavi	S. Morse	G. Suzek
A. Bhojwani	E. Kushel	W. C.-W. Mow	J. Warshauer
S. Gurman	P. Lavalley	J. Palin	
Ch.-M. Hsieh	S. P. Lee	G. V. Raju	

* Faculty members engaged in other research besides that connected with MRI.

DEPARTMENT OF ELECTROPHYSICS

Faculty

H. J. Carlin (Head)	J. W. E. Griemsmann	N. Marcuvitz	L. I. Smilen
E. S. Cassedy, Jr.	A. Hessel	A. A. Oliner	M. Sucher
M. Ettenberg	W. K. Kahn	S. W. Rosenthal	T. Tamir
H. Farber	A. E. Laemmel	D. Schechter	D. C. Youla
L. B. Felsen	E. Levi	J. Shmoys	
	C. J. Marcinkowski	L. M. Silber	

Research Associates

H. M. Altschuler	Mary A. Eschwei	O. Lipszyc	K. Suetake
F. Bailey	D. Jacenko	R. Pepper	D. S. Wilson
L. Birenbaum	L. Levey	Beulah Rudner	M. Wohlers
Martha Crowell	K. T. Lian	M. Sandler	

Research Assistants

L. Almeleh	H. Goldie	R. F. Lohr, Jr.	M. L. Nussbaum
W. Bellmer	M. Klinger	Antoinette Lotito	D. Stoler

Fellows and Graduate Assistants

G. Bein	W. Kohler	S. Peng	H. Stadmore
H. Berger	E. Labuda	C. L. Ren	H. M. Stark
H. Bertoni	R. Larsen	S. Rosenbaum	K. Stuart
T. Bially	R. Li	M. Rothman	J. Van Nieuland
J. Freidberg	B. Mohr	J. M. Ruddy	H. C. Wang
H. Friedman	T. Morrone	B. Rulf	N. Worontzoff
P. Hirsch	V. Nanda	R. Sasiela	G. Zysman
H. S. Hou	H. C. Pande	J. Schlafer	

DEPARTMENT OF PHYSICS

Faculty

S. J. Freedman	W. Kiszenick	H. W. Schleuning	N. Wainfan
H. J. Juretschke*	M. Menes		

Instructor

M. Nahemow

Fellows and Graduate Assistants

A. Sobel	M. T. Stevens	M. Warshavsky	W. Yang
----------	---------------	---------------	---------

* Faculty members engaged in other research besides that connected with MRI.

ADMINISTRATIVE COMMITTEE

J. Fox (Chairman)

A. B. Giordano

W. K. Kahn

G. Zucker

The faculty and research staff is complemented by thirty full-time engineering assistants, laboratory technicians, computers, draftsmen, and machinists, and an office staff of twenty-six.

I - ELECTROMAGNETICS

Altschuler, H. M.	Hessel, A.	Marcinkowski, C. J.	Rulf, B.
Cassedy, E. S.	Kahn, W. K.	Marcuvits, N.	Shmoys, J.
Crepeau, P. J.	Labianca, F. M.	Oliner, A. A.	Tamir, T.
Felsen, L. B.	Levey, L.	Ren, C. L.	Wang, H. C.

A. HARMONIC AMPLITUDES AND POWER RELATIONS IN SPACE-TIME PERIODIC MEDIA

E. S. Cassedy, A. A. Oliner

Previous reports of this series have discussed the "sonic" region and temporal instabilities,¹ graphical (Brillouin diagram) techniques² and dispersion relations associated with electromagnetic waves propagating in a space-time periodically modulated medium.³ A comprehensive report covering all but the second of these topics has recently been completed.⁴ In addition, it discusses the behavior of harmonic amplitudes and power relations in this class of media. The discussion, summarized in this paper, indicates the connection between phenomena known from conventional (purely spatial) periodic structures and those associated with traveling-wave parametric frequency mixing.

The complete solution for space-time harmonic waves in the medium has been shown to be:

$$V(z, t) = \exp[j(\omega t - \kappa z)] \sum_{n=-\infty}^{\infty} V_n \exp[j(\omega_p t - k_p z) n] \quad (1)$$

where

ω = temporal frequency of the fundamental space-time harmonic wave;

κ = spatial (propagation) wavenumber of the fundamental wave;

ω_p = frequency of the pump modulation (assumed to be specified);

$k_p = 2\pi/a$ = wavenumber of the pump modulation (assumed to be specified);

V_n = amplitude of the n-th space-time harmonic.

The required dispersion relation ($\kappa(\omega)$ or $\omega(\kappa)$) for these waves³ has been discussed previously and is found using the same technique as that used for purely spatial periodic structures. Similarly, the method for determining the harmonic amplitudes may be carried over from periodic structures. That is, after solving the dispersion relation, the harmonic amplitudes may be computed for the following:

ELECTROMAGNETICS

$$\frac{V_n}{V_{n-1}} = \frac{1}{D_n - \frac{1}{D_{n+1} - \frac{1}{\ddots}}}, \text{ for } n \geq 0 \quad (2)$$

$$\frac{V_n}{V_{n+1}} = \frac{1}{D_n - \frac{1}{D_{n-1} - \frac{1}{\ddots}}}, \text{ for } n \leq 0$$

and

$$\frac{V_n}{V_0} = \frac{V_n}{V_{n-1}} \cdot \frac{V_{n-1}}{V_{n-2}} \cdots \frac{V_1}{V_0} \quad n \geq 0 \quad (3)$$

$$\frac{V_n}{V_0} = \frac{V_n}{V_{n+1}} \cdot \frac{V_{n+1}}{V_{n+2}} \cdots \frac{V_1}{V_0} \quad n \leq 0$$

The results of such computations are shown in Figs. I - 1 and I - 2, for the case of moving periodic modulation discussed previously.³ Figure I - 1 shows all the significant amplitudes in the propagating region of the principal stop band. Figure I - 2 does the same for the second stop band.

These results are reminiscent of those obtained for static periodic structures in that we find the dominant harmonic in the neighborhood of a given stop band to be exactly that predicted on the basis of phase synchronism arguments. For example, in Fig. I - 1 we see that the value of V_{-1}/V_0 approaches a magnitude near unity at the band edge. It is also at least an order of magnitude larger than any of the other harmonics at that point. Similar dominant harmonic behavior is evident near the band edge in Fig. I - 2 for the second interaction.

However, there is a noticeable difference between the static and moving modulation cases with regard to harmonic amplitudes. For static periodic structures, it is known that at stop-band frequencies (including the two band edges) there is a matching, in pairs, of all harmonics in amplitude and phase.

This matching in the static case, which occurs in the minor as well as in the dominant harmonics of the mode (see Fig. I - 3) acts to create standing waves at the band edges, and an exact zero of propagating power throughout the stop-band region.

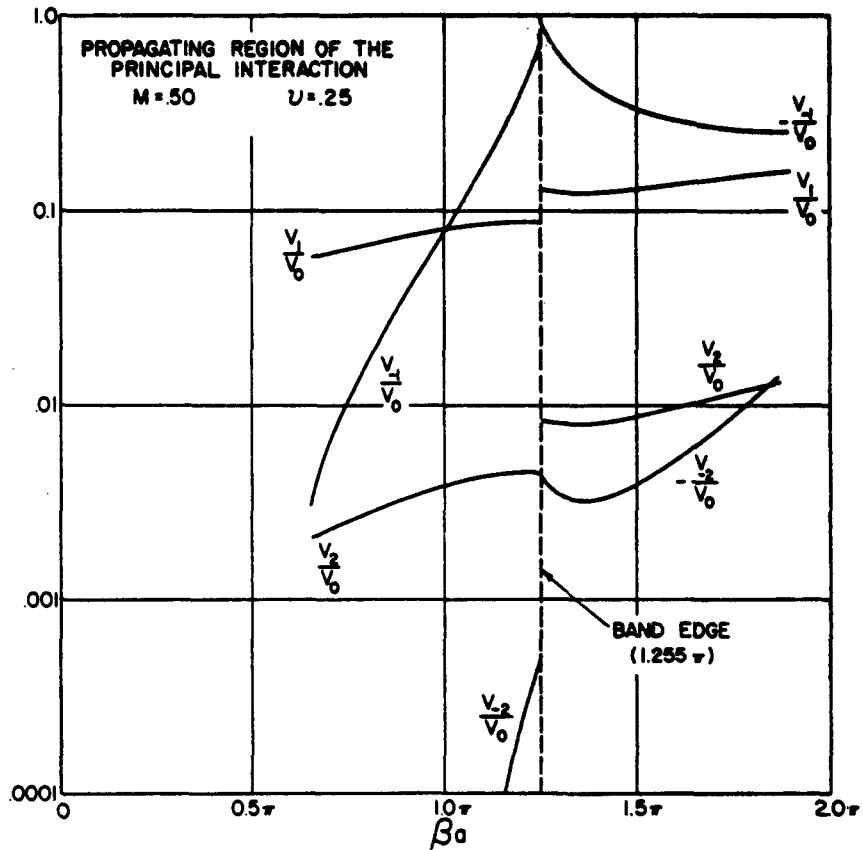


Fig. I-1 Relative amplitudes of space-time harmonics versus wavenumber

For example, in the case of the principal interaction of Fig. I-3, a symmetric matching of harmonic pairs exists on either side of the dominant pair of the form: $V_1 = V_{-2}$, $V_2 = V_{-3}$, etc. However, for moving modulation this simple matching is replaced by a more complicated system of frequency conversion effects.

The general energy laws obeyed in the stop bands for moving periodic modulation are the Manley-Rowe relations,⁵ generalized to cover the case of propagating waves, as discussed previously.³ In this paper we wish to report results obtained by using the Manley-Rowe relations together with the harmonic amplitudes accurately computed for the prediction of frequency conversion power ratios. The pertinent relation⁵ in the present case is:

ELECTROMAGNETICS

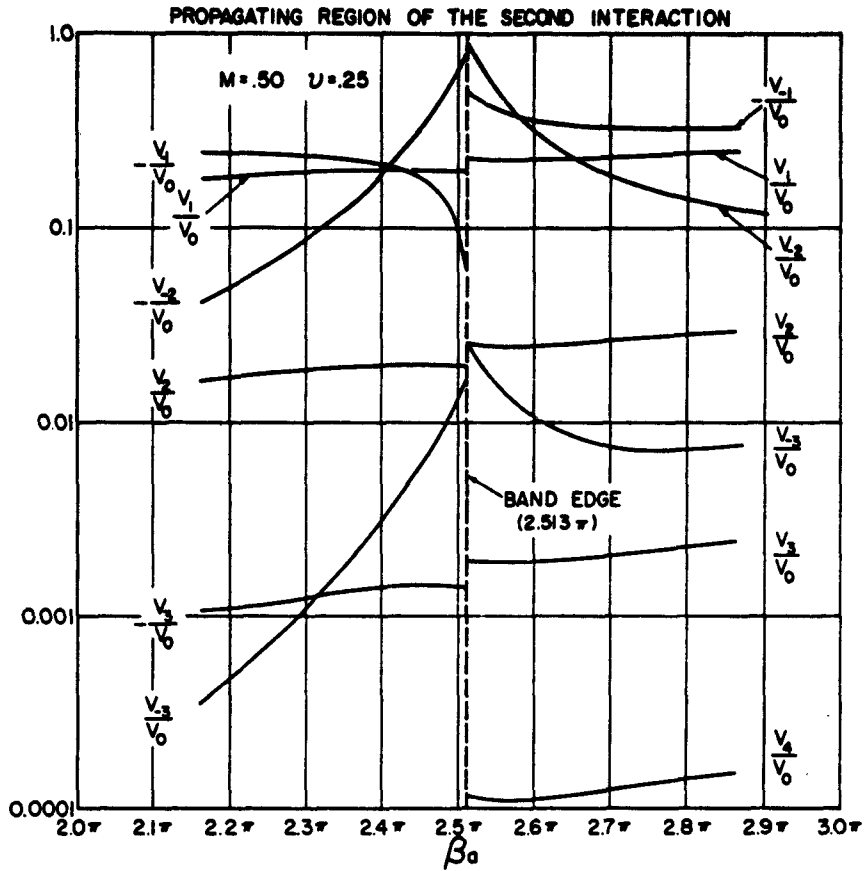


Fig. 1-2 Relative amplitudes of space-time harmonics versus wavenumber

$$\sum_{n=-\infty}^{\infty} \frac{P_n}{\omega + n\omega_p} = 0, \quad (4)$$

where

$$P_n = \text{power in } n\text{-th harmonic,}$$

$$= \text{Re} \left[\frac{\kappa^* + n\beta_p}{L_0(\omega + n\omega_p)} |V_n|^2 \right],$$

with

L_0 = distributed inductance per unit length of transmission-line model.

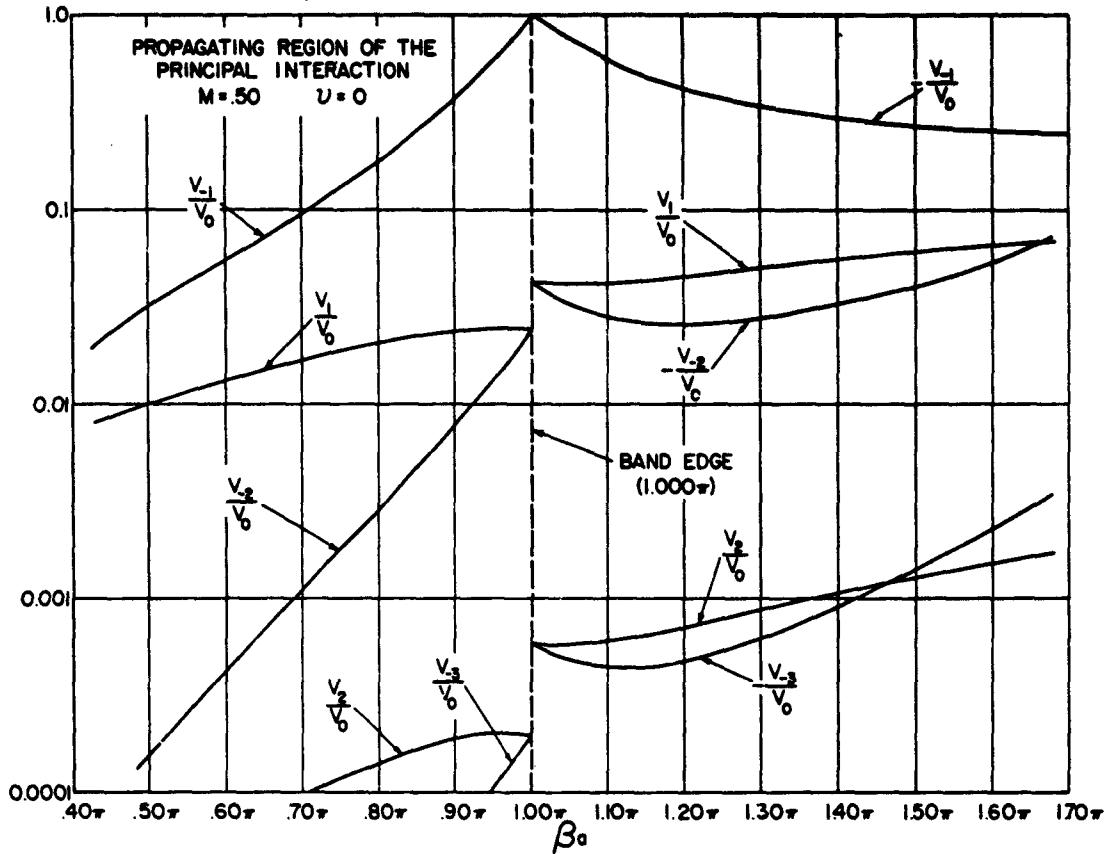


Fig. 1-3 Relative amplitudes of spatial harmonics versus wavenumber

Previous theories of traveling-wave parametric problems using the coupled mode approach have also yielded results which were stated to satisfy the Manley-Rowe relations, but only for an arbitrarily limited number of harmonics. Comparison with the present theory (which includes all the harmonics) indicates that these previous (coupled-mode) results satisfied the Manley-Rowe relations only in a way self-consistent with the assumption of a limited number of harmonics ("idler" frequencies).

Since the present theory is exact for the linear model, the error due to the assumption of a limited number of harmonics may be tested in any case of interest. The single harmonic assumption leads to the simple power relation,

$$\frac{P_n}{P_0} \approx \frac{\omega + n\omega}{\omega} P, \quad (5)$$

ELECTROMAGNETICS

for the prediction of the power converted from the fundamental to the (dominant) n -th harmonic. On the other hand, the results of the present analysis would indicate

$$\frac{P_n}{P_o} = \text{Re} \left[\frac{Y_n^* |V_n|^2}{Y_o^* |V_o|^2} \right] \quad (6)$$

to be the accurate ratio.

Several numerical comparisons may be made in the following table:

Number of Interaction	n	Lower Band-Edge Frequency		Mid-Band Frequency		Upper Band-Edge Frequency	
		$\frac{\omega + n\omega_p}{\omega}$	$\text{Re} \left[\frac{Y_n^* V_n ^2}{Y_o^* V_o ^2} \right]$	$\frac{\omega + n\omega_p}{\omega}$	$\text{Re} \left[\frac{Y_n^* V_n ^2}{Y_o^* V_o ^2} \right]$	$\frac{\omega + n\omega_p}{\omega}$	$\text{Re} \left[\frac{Y_n^* V_n ^2}{Y_o^* V_o ^2} \right]$
Principal	+1	1.780	1.761	1.645	1.619	1.569	1.540
Second	+2	1.678	1.603	1.653	1.510	1.627	1.437
Third	+3	1.664	1.422	1.653	1.373	1.645	1.322
Fourth	+4	1.657	1.210	1.657	1.173	1.653	1.153

This table has been computed for four cases of frequency up-conversion ($n > 0$), whereas the previous results for the dispersion effects and the amplitudes have been for cases of frequency down-conversion ($n < 0$). The up-conversion results may be obtained directly from the down-conversion results, however, due to the cell-pattern property of the dispersion diagram mentioned previously.² The calculation, as a matter of fact, amounts only to a relabeling of harmonic numbers. A detailed discussion of this point is made in the above-mentioned report.⁴

Power ratios of the type shown are understood to represent maximum attainable power exchange under conditions of no dissipation. We find that agreement between the single idler result and the exact treatment is good only for the principal interaction. The discrepancy between the exact and the single idler treatments is due to power residing in the minor harmonics, which are neglected in the approximate analysis.

The present results show that the accurate frequency power conversion ratios tend toward unity as the number of the interaction increases. The reason for decreasing conversion of power is evident when we consider the increasingly significant role

played by the minor harmonics in the higher interactions, particularly those harmonics residing between the two dominant harmonics for the higher interactions (e.g., see Fig. I - 2, the $n = -1$ harmonic).

Air Force Cambridge Research Laboratory
Office of Aerospace Research
AF-19(604)-7499

E.S. Cassedy

References

1. E.S. Cassedy, "Temporal Instabilities in Traveling-Wave Amplifiers," Progress Report No. 20 to the Joint Services Technical Advisory Committee, R-452.20-61, Microwave Research Institute, P.I.B., pp. 5-9.
2. E.S. Cassedy, "A Graphical Interpretation of 'Sonic Regions' in Traveling-Wave Parametric Amplifiers," Progress Report No. 21 to the Joint Services Technical Advisory Committee, R-452.21-62, Microwave Research Institute, P.I.B., pp. 1-7.
3. E.S. Cassedy, "Dispersion Relations in Space-Time Periodic Media," Progress Report No. 22 to the Joint Services Technical Advisory Committee, R-452.22-62, Microwave Research Institute, P.I.B., pp. 1-4.
4. E.S. Cassedy and A.A. Oliner, "Dispersion Relations in Time-Space Periodic Media: Part I -- Stable Interactions," Report PIBMRI 1122, Microwave Research Institute, P.I.B. (February 1963).
5. J.M. Manley and H.E. Rowe, "Some General Properties of Non-linear Elements-- Part I," Proc. IRE, Vol. 44, pp. 906-913 (1956).

B. WAVE PROPAGATION IN A SINUSOIDALLY MODULATED DIELECTRIC MEDIUM

A.A. Oliner, T. Tamir, H.C. Wang

The first part of a study of wave propagation in a sinusoidally modulated dielectric medium has been completed and a comprehensive discussion of the results will be presented in a forthcoming report. This portion of the study was concerned with an infinite medium which possesses a dielectric constant that varies in a sinusoidal manner along the z coordinate, as shown in Fig. I - 4.

There are several motivations for this investigation. One is concerned with electromagnetic wave propagation through a compressible medium which is influenced by acoustic or other mechanical waves. The results are applicable, for example, to acoustically modulated plasma media in the range $\epsilon > 0$.

In a second area of application, the above-mentioned study is regarded as a first step in the analysis of a sinusoidally modulated dielectric slab antenna, which employs a layer of this modulated medium. The next step in this study, on which work has begun, is the evaluation of the interface discontinuity between air and the modulated medium.

ELECTROMAGNETICS

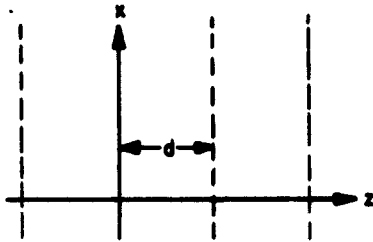


Figure 1-4

In a third area of application, a layer of this modulated medium, with air above and water below, is viewed as an approximation to water waves set up by a specific disturbance. Again, the interface problem must be solved before a complete equivalence may be obtained.

The relative dielectric constant of the modulated medium may be expressed as

$$\epsilon(z) = \epsilon_r [1 - M \cos 2\pi (z/d)] \quad (1)$$

where M is the modulation coefficient and d is the length of one "cell" in the medium. The fields are assumed to be uniform in the y direction, so that the problem is two-dimensional. The modes of propagation are of the E or H type. For the latter, the wave equation is

$$\left[\nabla^2 + k_0^2 \epsilon(z) \right] E(x, z) = 0 \quad (2)$$

where $E(x, z)$ is the electric field in the y direction. The wave equation for E modes is more complicated than that for H modes since it also involves the derivative of $\epsilon(z)$. Only H modes were considered in the present study.

For H modes, if the relation for $\epsilon(z)$ is substituted in the wave equation (2) above, and solutions in the form

$$E(x, z) = A(k_t; z) e^{ik_t x} \quad (3)$$

are assumed, one obtains:

$$\left[(d/dz)^2 - k_t^2 + k_0^2 \epsilon_r (1 - M \cos 2\pi (z/d)) \right] Z(k_t; z) = 0 \quad (4)$$

Equation (4) is in the form of a Mathieu differential equation. It may be noted that a Hill's differential equation is obtained if E modes are considered; the Mathieu equation pertaining to H modes is a particular case of this more general Hill's equation.

The solution for Eq. (4) may be written in the Floquet form:

$$Z(k_t; z) = e^{ik_t z} \sum_{n=-\infty}^{\infty} a_n e^{in(2\pi/d)z} \quad (5)$$

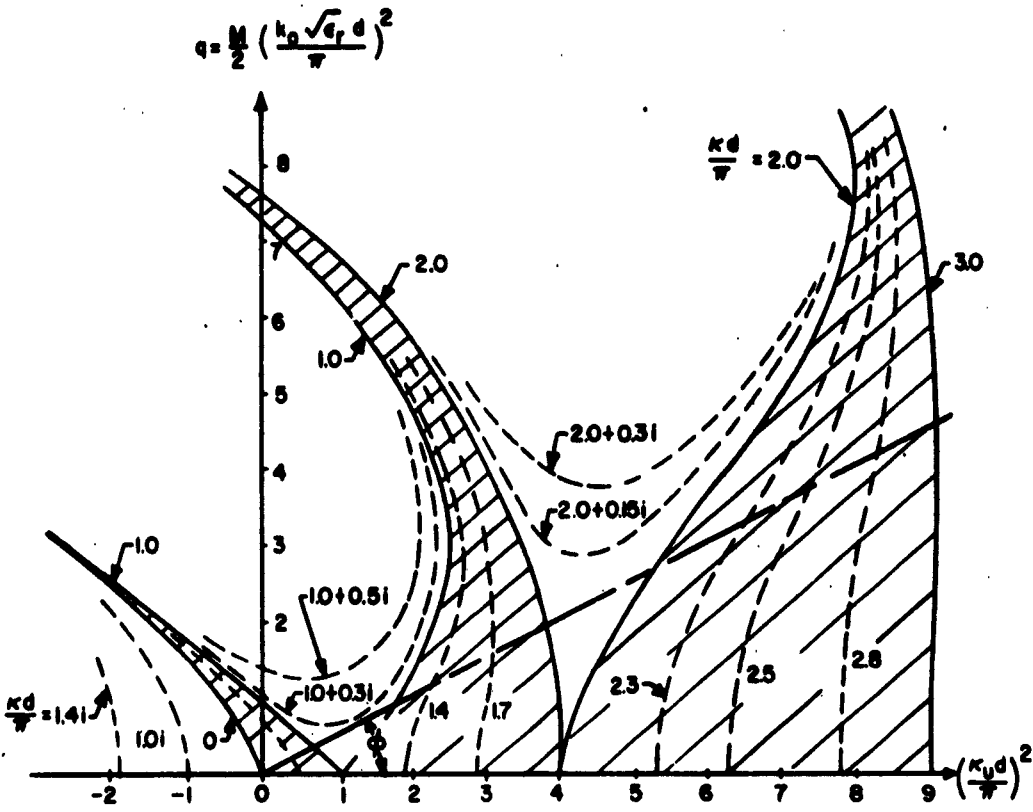


Figure 1-5

where K is the so-called characteristic exponent.

Equation (5) represents a mode characterized by the wavenumber k_t . It may be noted that both K and the constants a_n are dependent on k_t . The exponent K is regarded as a wavenumber in the z direction and each term a_n , together with its appropriate exponent, then represents a space harmonic.

The wave properties of the mode functions may be examined by means of the Mathieu stability diagram shown in Fig. 1 - 5. This diagram is essentially a plot of the dispersion relation

$$K = f(k, k_t) \tag{6}$$

in terms of the parameters ϵ_r and d , which characterize the medium. The abscissa in Fig. 1 - 5 is given by

$$(\kappa_u d/\pi)^2 = (kd/\pi)^2 - (k_t d/\pi)^2. \tag{7}$$

ELECTROMAGNETICS

One notes that k_u then represents the wavenumber in the z direction for the unmodulated medium. The ordinate in Fig. I - 5 is:

$$q = \frac{M}{2} (k_0 \sqrt{\epsilon_r} d/\pi)^2, \quad (8)$$

which is proportional to the modulation index M .

When the constants k_x , M , ϵ_r , d , and frequency are given, a point is specified in the stability chart and therefore the appropriate K is determined. For real values of k_x , one then has two possible mode types:

a) If K falls within one of the shaded regions of Fig. I - 5 (the so-called "stable" regions), its value is pure real. The mode then consists of harmonics, each of which is in the form of a plane wave propagating at a certain angle with respect to the striations formed by the modulation in the medium.

b) When K falls within one of the unshaded regions of Fig. I - 5 ("unstable" regions), its value is complex. This represents a mode which varies exponentially in z and propagates only in the x direction, i. e., along the striations. The mode is then actually "ducted" along the striations.

A rectangular waveguide containing a dielectric modulated as above was also considered, with the modulation present in the z (longitudinal) direction. The modes in this case are simply related to those in the infinite medium. It is shown that the first mode type mentioned above corresponds to the pass bands, while the ducted modes pertain to the stop bands of the waveguide. As before, the structure and width of these bands may be obtained directly from the Mathieu stability diagram.

The shape of the field within one cell of the periodically modulated structure was also examined for both the pass and the stop bands, as well as at the band edges. It is shown that the electric field component does not bear any direct relation to the variation of the dielectric constant within a cell.

Additional attention has been paid to the case of small values for the modulation index. For certain frequency ranges it is shown that the dispersion curves, band characteristics, and other features can be expressed in an analytic fashion by relations which involve the fundamental ($n = 0$) wave and the two nearest ($n = \pm 1$) space harmonics. These relations also permit a representation of the modulated medium, with regard to the propagation characteristics, in terms of a smooth transmission line periodically loaded with lumped elements.

The case of a plane wave incident on a semi-infinite modulated dielectric, shown

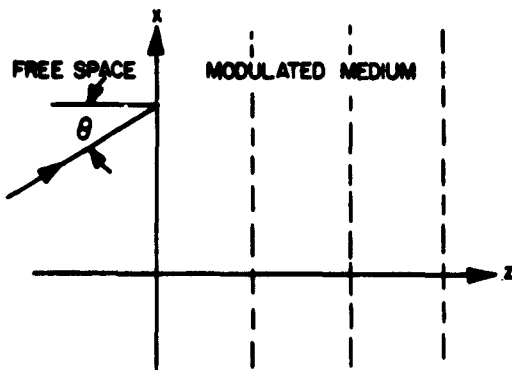


Figure 1-6

in Fig. 1 - 6, was also examined. It may be shown that the mode excited in the dielectric medium must have a value of κ which lies on the dashed straight line shown in Fig. 1 - 5. This line has a slope ϕ given by

$$\tan \phi = M/2 \cos^2 \theta . \quad (9)$$

The particular point of operation on this line can be determined by means of the ordinate q for the particular frequency. As frequency increases, this point moves up on the dashed line. Thus, as frequency

varies, one alternately obtains pass bands and stop bands.

In the stop bands, the refracted part of the wave is closely bound to the interface. In the pass bands, however, the refracted wave propagates in the modulated medium but each space harmonic travels in a different direction with respect to the striations.

Other propagation and field features were examined, particularly the relations obtained for small values of the modulation index M . In the range of small M , an explicit expression was also derived for the reflection coefficient which occurs for the incident plane wave of Fig. 1 - 6. All of these aspects have been incorporated in the comprehensive report describing this investigation.

Air Force Cambridge Research Laboratory
Office of Aerospace Research
AF-19(604)-7499

T. Tamir

C. DIFFRACTION IN A CERTAIN STRATIFIED MEDIUM

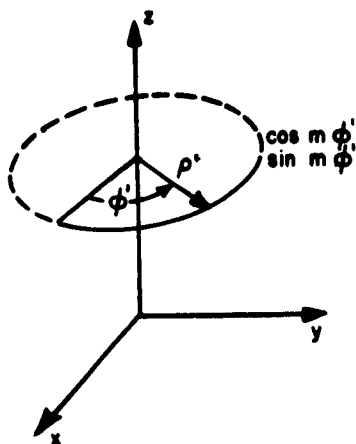
L.B. Felsen, L. Levey

Introduction

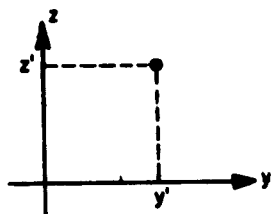
L.B. Felsen has shown how a class of scalar three-dimensional diffraction problems concerning ring sources in a homogeneous medium may be related to two-dimensional diffraction problems involving a uniform line source in a certain stratified medium.¹ In particular, reference 1 contains a transformation by means of which the field of a line source in a medium with wavenumber

$$k(y) = k \left\{ 1 - \frac{m^2 - (1/4)}{k^2 y^2} \right\}^{1/2} \quad (1)$$

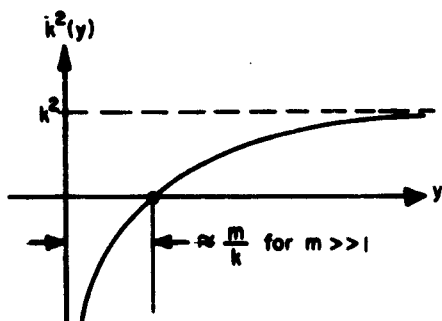
ELECTROMAGNETICS



(a)



(b)



(c)

Fig. 1-7 (a) Ring source in homogeneous medium; (b) Line source in stratified medium; (c) Variation of wavenumber of stratified medium.

may be obtained from the solution for a ring source with azimuthal variation $\cos m \phi'$ or $\sin m \phi'$ situated in a homogeneous medium with wavenumber k , as shown in Fig. 1 - 7.

In this paper, a simple geometrical correspondence is developed between the rays of the geometrical optics fields of these two related diffraction problems.

The field of the ring source may be expressed in the form

$$G^0(\underline{r}; \rho', z') = G(\rho, z; \rho', z') \begin{cases} \cos m \phi \\ \sin m \phi \end{cases} \quad (2a)$$

In brief, the transformation prescribed in reference 1 to obtain the field \bar{G} of the line source in the stratified medium described by Eq. (1) is given by

$$\bar{G}(y, z; y', z') = \sqrt{y/y'} G(y, z; y', z') \quad (2b)$$

In this paper, a graphical interpretation of this transformation is considered, by means of which the rays and caustic of the two-dimensional problem can be mapped from those of the three-dimensional configuration.

As explained in reference 1, the variation of wavenumber described by Eq. (1) for $m \geq 1$ is appropriate to an isotropic plasma medium in which collisions can be neglected. This reference also has shown how the transformation may be employed to yield rigorous solutions for the line source problem when certain obstacles are present. Significantly, some of these

obstacles have boundaries which are not coincident with the direction of stratification of the medium. This is a situation not encountered in the usual treatments dealing with diffraction in variable media.

The existence of exact solutions makes a check possible on proposed approximate procedures for problems in this category. The graphical interpretation of the transformation discussed here may also be extended to include the class of obstacles considered in reference 1. On a purely geometrical basis, it can thus provide an insight into the behavior of rays reflected from a curved or plane surface along which the properties of the medium are permitted to vary.

Rays in a homogeneous medium are of course straight lines. It is to be expected that, in the short wavelength limit, the ray pattern of the ring source will resemble that of an infinite line with a progressive phase variation. The rays of the latter² emanate conically from each element of the line, as shown in Fig. I - 8.

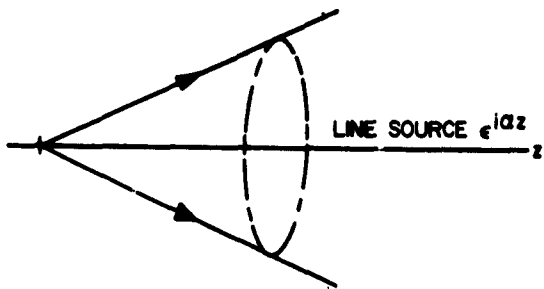


Figure I-8

The following section of this paper will show that a quantitative correspondence between the two configurations does in fact exist, with the rays shed by an element of the ring forming a cone. This is indicated in Fig. I - 11. There are field points, as distinguished from the line source with progressive phase variation, which are not included on any "ray cone" of the ring source. Thus the geometrical optics field contains shadow regions.

The curved rays in the stratified medium are refracted toward the region of higher real refractive index. Rays initially shed from the line source toward the portion of the medium which is non-propagating turn in direction. It will be shown that the rays form a family of hyperbolas (see Fig. I - 15), which have a caustic surface delimiting a shadow region.

Ray System of Ring Source in Homogeneous Medium

For convenience, let the ring source of radius ρ' be situated in the x-y plane, centered at the origin, as shown in Fig. I - 9. An azimuthal variation of $\exp[i m \phi]$, $m = 0, 1, 2, \dots$, is assumed, with time-dependent $\exp[-i \omega t]$ omitted (references 1 and 2 consider variations of $\cos m \phi$ and $\sin m \phi$, but no essential difference is involved).

The Green's function problem for the ring in a medium with wavenumber k is

ELECTROMAGNETICS

given by

$$G^0 = \rho' \int_0^{2\pi} \exp [i m \phi'] \frac{\exp [ik |\underline{r} - \underline{r}'|]}{|\underline{r} - \underline{r}'|} d\phi' \quad (3a)$$

$$= \rho' \int_0^{2\pi} \frac{\exp [i k f(\underline{r}, \phi')]}{|\underline{r} - \underline{r}'|} d\phi' ,$$

where

$$f(\underline{r}, \phi') = \sqrt{r^2 + \rho'^2 - 2 r \rho' \sin \theta \cos(\phi - \phi')} + (m/k) \phi' \quad (3b)$$

when the source is in the x-y plane.

The small wavelength ($k \rightarrow \infty$) asymptotic approximation for G^0 (i.e., the geometrical optics field) may be obtained by a stationary phase evaluation of the integral. The stationary phase points ϕ_s , satisfying $\partial f / \partial \phi' = 0$, are given implicitly by:

$$\frac{r \sin \theta \sin(\phi - \phi_s)}{\sqrt{r^2 + \rho'^2 - 2 r \rho' \sin \theta \cos(\phi - \phi_s)}} - \cos \psi = 0 \quad (4a)$$

where

$$\cos \psi = m/k\rho' . \quad (4b)$$

In terms of the cylindrical coordinates $\rho = r \sin \theta$ and $z = r \cos \theta$, Eq. (4) yields:

$$\cos(\phi - \phi_s) = \cos \psi / \rho \left[\rho' / \cos \psi \pm \sin \psi \sqrt{\frac{\rho^2}{\cos^2 \psi} - \frac{z^2}{\sin^2 \psi} - \rho'^2} \right] \quad 0 < \phi - \phi_s < \pi . \quad (5)$$

From Eq. (5) it is seen that there is only one stationary point when \underline{r} is on the hyperboloid of revolution defined by:

$$(\rho^2 / \cos^2 \psi) - (z^2 / \sin^2 \psi) = \rho'^2 . \quad (6)$$

This surface (see Fig. I - 10) divides the surrounding space into a shadow region, $(\rho^2 / \cos^2 \psi) - (z^2 / \sin^2 \psi) < \rho'^2$, for which there are no real stationary points, and an

illuminated region, $(\rho^2 / \cos^2 \psi) - (z^2 / \sin^2 \psi) > \rho'^2$, in which two real and distinct values of ϕ_s exist. The surface constitutes the caustic of the family of rays emanating from the ring source.

Equation (4) may also be viewed as defining a surface, all field points of which have the same stationary phase value ϕ_s . This surface is a right circular cone of central angle 2ψ with apex at $\phi' = \phi_s$ and axis tangent to the ring, as depicted in Fig. I - 11.

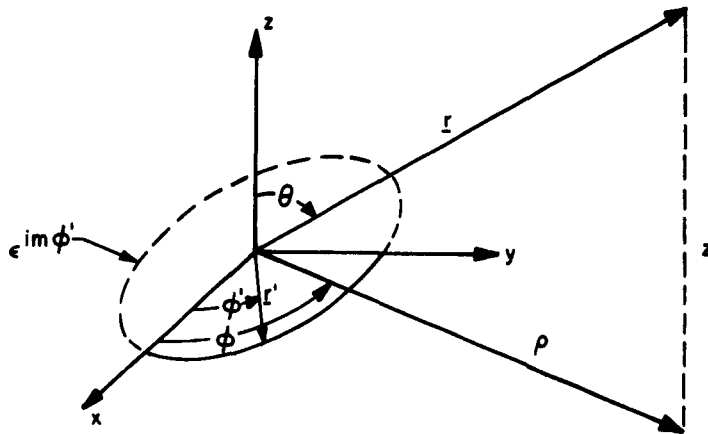


Figure I-9

The caustic surface of Fig. I - 10 is generated by revolving the cone of Fig. I - 11 about the z axis. The cone also defines the system of rays shed by the segment of the ring source at ϕ_s . Intuitively this is to be expected, since field points illuminated by rays emanating from the element at ϕ_s should have the common stationary phase value of ϕ_s . This consideration is pursued further in this paper.

As previously mentioned, each field point in the illuminated region has associated with it two real, stationary phase points $\phi_{s1, 2}$ defined by Eq. (5). In the stationary phase evaluation of G^0 these yield the phase functions:

$$k_{1, 2} = \sqrt{r^2 + \rho'^2 - 2r\rho' \sin \theta \cos (\phi - \phi_{s1, 2})} + (m/k) \phi_{s1, 2} \quad (7)$$

The rays of the ring source are the orthogonal trajectories of the surfaces $k_{1, 2} = \text{constant}$. Thus, there are two rays through each point in the illuminated region,

ELECTROMAGNETICS

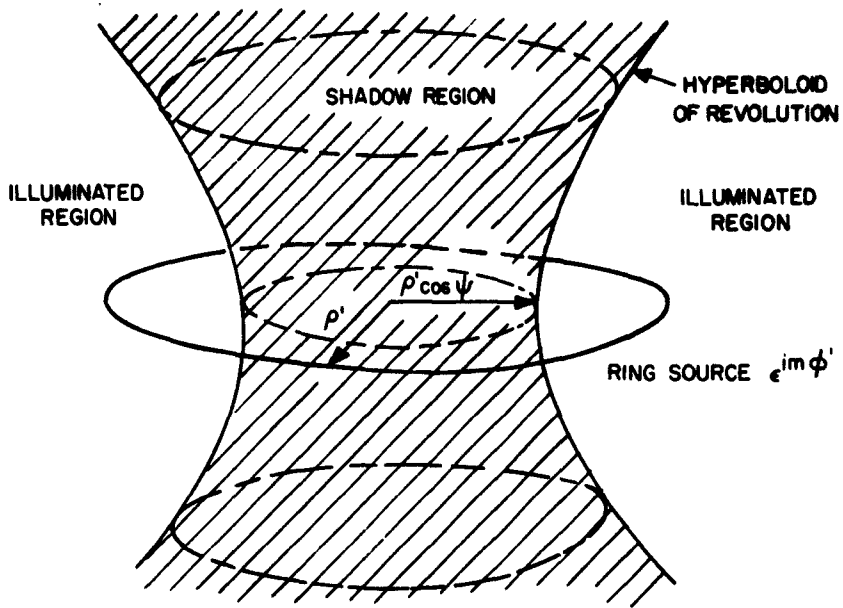


Figure 1-10

determined by the directions of $\nabla \kappa$ and $\nabla \kappa_2$.

For each ϕ_s , from Eq. (7),

$$\nabla \kappa = \frac{\underline{r} - \rho' \sin \theta \cos (\phi - \phi_s) \underline{r}_0 - \rho' \cos \theta \cos (\phi - \phi_s) \underline{\theta}_0 + \rho' \sin (\phi - \phi_s) \underline{\phi}_0}{\sqrt{r^2 + \rho'^2 - 2 r \rho' \sin \theta \cos (\phi - \phi_s)}} \quad (8)$$

By expressing \underline{r}_0 , $\underline{\theta}_0$, $\underline{\phi}_0$ in terms of the rectangular unit vectors \underline{x}_0 , \underline{y}_0 , \underline{z}_0 , Eq. (8) may be recast as:

$$\nabla \kappa = \frac{\underline{r} - \underline{\rho}'}{|\underline{r} - \underline{\rho}'|} \quad , \quad (9)$$

where

$$\underline{\rho}' = \rho' (\cos \phi_s \underline{x}_0 + \sin \phi_s \underline{y}_0) .$$

A construction for the vector $\underline{l} = \underline{r} - \underline{\rho}'$, which determines the ray direction at

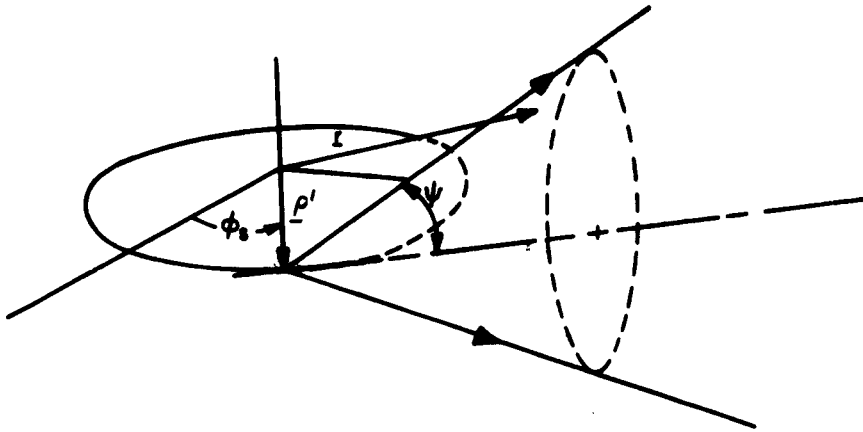


Figure I-11

the point \underline{r} , is shown in Fig. I - 12. As evidenced by the figure, the ray associated with the stationary phase value ϕ_s emanates from the ring source at $\phi' = \phi_s$.

The angle between the ray and the tangent \underline{t}_0 to the ring source is simply computed to be ψ , defined in Eq. (4b). Since ψ is determined only by the source parameters, the totality of rays shed by the source element at $\phi' = \phi_s$ must form the cone described by Eq. (4), which subsequently is referred to as the "ray cone." In this respect, each element of the ring behaves similarly to that of an infinite line source with a progressive phase variation of m/k (see reference 2).

Mapping of Rays in Line Source Problem

The geometrical optics field of the related two-dimensional problem (see Fig. I - 7(b)) may be obtained from the stationary phase evaluation of Eq. (3) by means of the transformation detailed in reference 1 and briefly outlined in the introduction of this paper. In particular, the phase functions appropriate to the line source in the stratified medium are derived from Eqs. (5) and (7) by suppressing the ϕ variable, substituting the rectilinear coordinate y for the cylindrical coordinate ρ and keeping the z dependence invariant. The rays in the two-dimensional problem are obtained from the directions of the gradients of the resulting phase functions.

For convenience in furnishing a geometrical interpretation, the transformation may be rephrased as follows: A ray element at (ρ, ϕ, z) in the ring source problem maps into one at $(y = \rho, z)$ in the allied line source problem. The two-dimensional ray element has y and z components which are equal to the ρ and z components,

ELECTROMAGNETICS

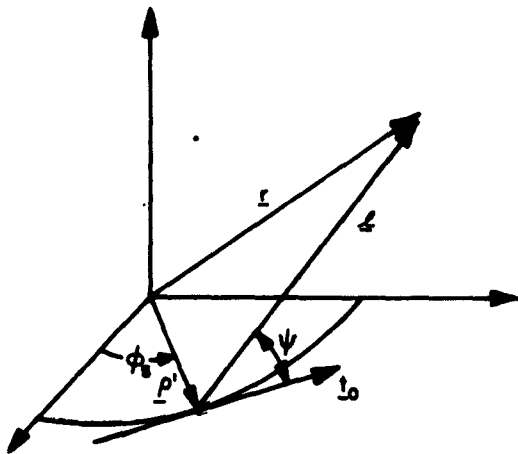


Figure 1-12

into the $\phi = \hat{\phi}$ plane. In the plane itself, ρ is interpreted as the rectilinear coordinate y of the line source problem. Two such projected points are shown in Fig. I - 13.

respectively, of the corresponding three-dimensional ray element.

The transformation procedure is illustrated geometrically in Fig. I - 13. Consider an arbitrary plane $\phi = \hat{\phi}$. The intersection of this plane with the ring source establishes the site of the line source in the two-dimensional problem. The family of two-dimensional rays is obtained by a projection onto the $\phi = \hat{\phi}$ plane of the three-dimensional rays emanating from the ring source at $\hat{\phi}$. The projection, in accordance with the relationship between ray components mentioned in the previous paragraph, is accomplished by rotating points on the three-dimensional rays about the z -axis

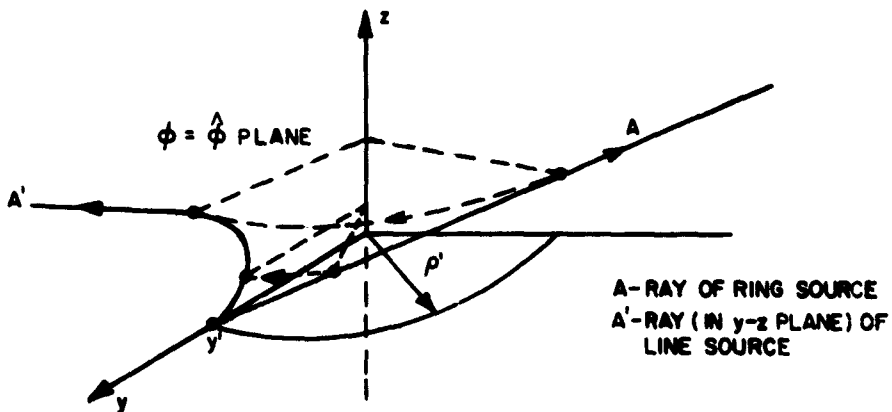


Figure 1-13

This mapping procedure highlights a number of properties of the ray system for the two-dimensional problem:

ELECTROMAGNETICS

1) The rays in the stratified medium are refracted toward the region of higher refractive index (positive y direction). The turning points of the rays correspond to the points of nearest approach to the z -axis of the associated three-dimensional rays.

2) A direct and a refracted ray pass through each point (\hat{y}, \hat{z}) in the illuminated region. These correspond in the ring problem to the two rays through the intersections ρ_1, ρ_2 , in Fig. I - 14, of the cylinder $\rho = \hat{y}$ and the hyperbolic trace of the ray cone on the plane $z = \hat{z}$. The direct and refracted rays through (\hat{y}, \hat{z}) are determined by the projections of the three-dimensional ray through ρ_1 and ρ_2 , respectively.

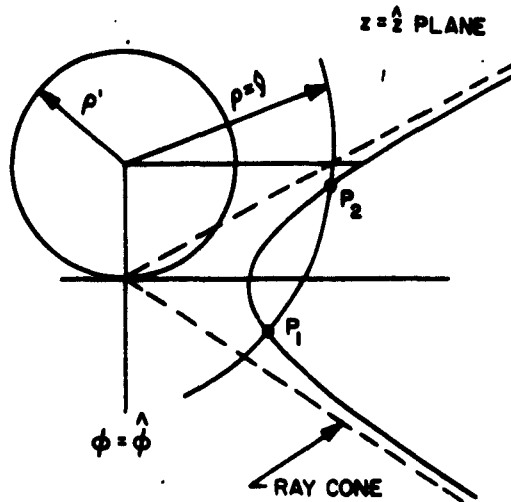


Figure I-14

3) The line source problem has regions of geometrical shadow and illumination. A point (\hat{y}, \hat{z}) will be in the geometrical shadow if the cylinder $\rho = \hat{y}$ in Fig. I - 14 does not intersect the trace of the ray cone on the plane $z = \hat{z}$. The boundary (caustic) curve between the illuminated and shadow regions is readily derived from consideration of Fig. I - 14, since it is determined by points for which the cylinder $\rho = \hat{y}$ has only one intersection with the cone trace. The ray cone in cylindrical coordinates is given by:

$$\frac{\rho \sin(\phi - \hat{\phi})}{\sqrt{\rho^2 + z^2 - 2\rho\rho' \cos(\phi - \hat{\phi})}} = \cos \psi \quad (10)$$

It is easily shown that there is only one value of ϕ satisfying this relationship

ELECTROMAGNETICS

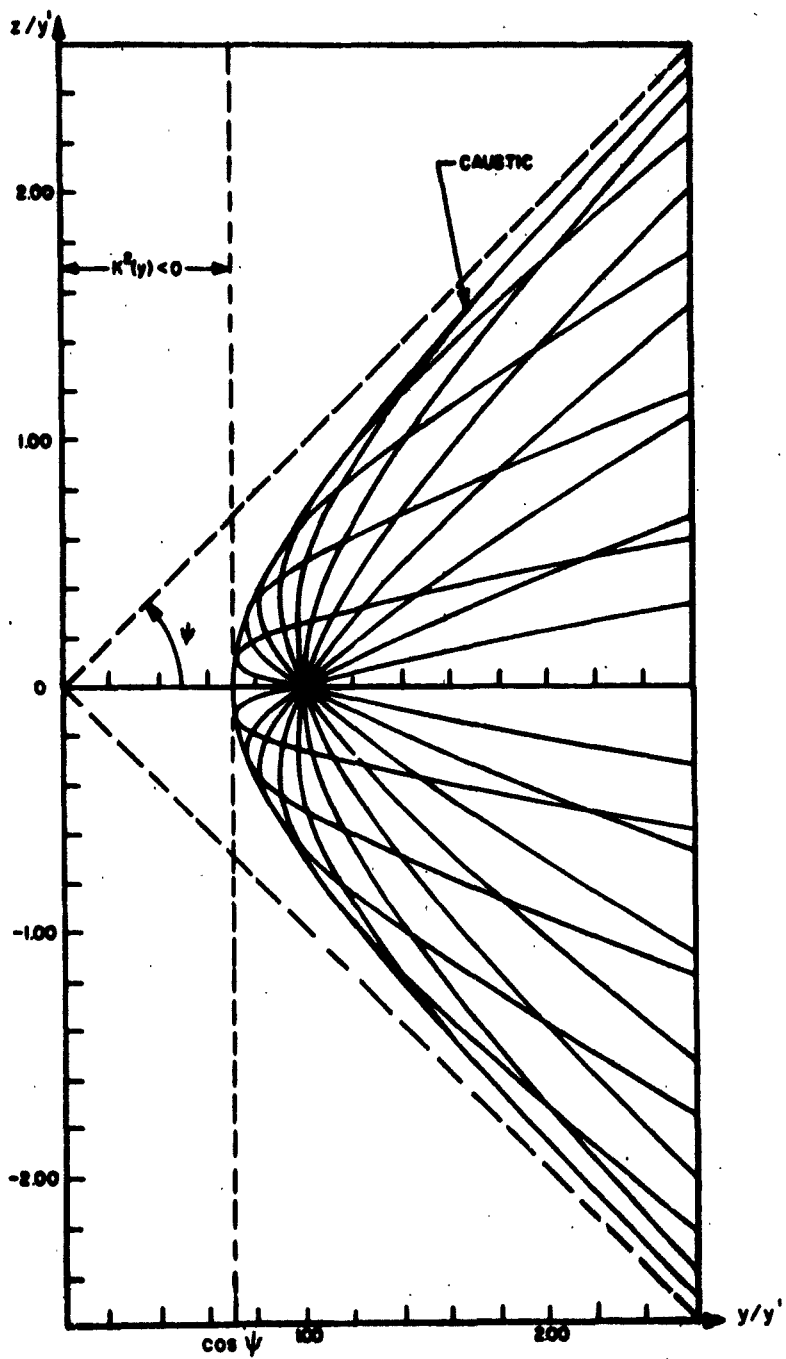


Figure 1-15

for $\rho = \hat{y}$, $z = \hat{z}$ when

$$\frac{\hat{y}^2}{\rho'^2 \cos^2 \psi} - \frac{\hat{z}^2}{\rho'^2 \sin^2 \psi} = 1 \quad (11)$$

This hyperbola constitutes the caustic in the two-dimensional problem with the line source at $(y' = \rho', 0)$. From this equation, ψ is seen to be the angle subtended by the asymptotes of the hyperbola and the positive y -axis. The two-dimensional caustic may also be derived by applying the transformation of variables to the equation for the three-dimensional caustic given by (6).

Analytical expressions for the rays of the line source problem may be obtained directly from those describing the family of three-dimensional rays. A ray emanating from the ring at $\phi' = \hat{\phi}$, whose projection in the $\phi = \hat{\phi}$ plane makes an angle of α with the positive x -axis, is described by the intersection of the plane

$$\rho \cos(\phi - \hat{\phi}) - z \cot \alpha = \rho' \quad (12)$$

and the ray cone (see Eq. (10)).

When $(\phi - \hat{\phi})$ is eliminated between these two equations and y is substituted for ρ , the result is

$$(y'^2 - y^2) \sin^2 \psi + z^2 (\cos^2 \psi + \cot^2 \alpha) + 2 y' z \sin^2 \psi \cot \alpha = 0. \quad (13)$$

This is the equation of a hyperbola, describing the two rays that emerge from the line source at angles of α and $\pi + \alpha$ with the y -axis.

The ray hyperbolas may be shown to have a common directrix at $y = m/k$. As y increases through this value, the wavenumber of the stratified medium (for $m \gg 1$) passes through zero, changing from pure imaginary to real. A plot of the ray system for the line source is given in Fig. I - 15 for the special case of $\psi = \pi/4$.

The envelope of the ray hyperbolas may be obtained by eliminating the parameter $\cot \alpha$ between Eq. (13) and its derivative with respect to $\cot \alpha$. When this is done, Eq. (11) results for the caustic.

ELECTROMAGNETICS

References

1. L. B. Felsen. "Diffraction by Objects in a Certain Variable Plasma Medium," Progress Report No. 16 to the Joint Services Technical Advisory Committee, R-452.16-59, Microwave Research Institute, P. I. B., pp. 27-32.
2. L. B. Felsen and N. Marcuvitz, "Modal Analysis and Synthesis of Electromagnetic Fields," Report PIBMRI-841-60, Microwave Research Institute, P. I. B. pp. 38-40 (July 1961).

II - PLASMA ELECTROPHYSICS AND ELECTRONICS

Bailey, F.	Hessel, A.	Lippsyc, O.	Pande, H.	Shmoys, J.
Bergstein, L.	Hirsch, P.	Marcinkowski, C.J.	Pepper, R.	Smith, E.J.
Bertoni, H.	Hou, H.	Marcuvitz, N.	Rosenthal, S.W.	Sucher, M.
Crepeau, P.J.	Labianca, F.M.	Mohr, B.	Rulf, B.	Tamir, T.
Ettenberg, M.	Labuda, E.	Morrone, T.	Sandler, M.	Veron, H.
Farber, H.	Larsen, R.	Nahemow, M.	Sasiela, R.	Wainfan, N.
Felsen, L.B.	Levi, E.	Oliner, A.A.	Schlafer, J.	Wilson, D.S.
Goldstone, L.O.	Lian, K.T.			

A. RADIATION FROM A DIRECTIVE ANTENNA EMBEDDED IN AN ANISOTROPIC PLASMA HALF-SPACE

L. B. Felsen, B. Rulf

To provide a first insight into the quantitative aspects and the physical mechanism of radiation from sources in bounded anisotropic media, a previous study^{1, 2} was concerned with the fields generated by electromagnetic line and point sources in a uniaxially anisotropic plasma half-space. An asymptotic evaluation of the rigorous solution has led to far field contributions which have been identified as incident, reflected and refracted waves, and also as lateral waves.

The manner in which reflected, refracted, and lateral wave fields can be constructed from a knowledge of the radiation field in an infinite medium has been shown, thereby providing quantitative support for certain ray-tracing procedures when the source is located inside, rather than exterior to, the anisotropic region. In this quasi-optical interpretation, the refractive index surfaces descriptive of plane wave propagation in the medium play a crucial role since they provide information on the directions of the following:

- a) the ray (energy flow) and wave normal (phase propagation) vectors, thereby facilitating the implementation of the radiation condition;
- b) the incident, reflected, and refracted rays;
- c) the critically refracted rays required to launch the lateral waves.

A physical basis has thereby been provided for the quantitative understanding of radiation phenomena which, though derived for uniaxially anisotropic media, may be expected to occur also in other types of anisotropy.

In the above analysis, the lateral wave fields were shown to have potential significance if the plasma possesses opaque regions in which the direct and reflected waves are exponentially small. Under these circumstances, the lateral waves, which decay with distance algebraically rather than exponentially, constitute the dominant field contribution. Since these waves are excited by a ray which strikes the interface at the critical angle (angle of total reflection) θ_c , it is to be expected that their relative

PLASMA ELECTROPHYSICS AND ELECTRONICS

amplitude would be enhanced by a directive source which has a sharp major radiation lobe along $\hat{\theta}$. Consequently, if the major lobe of a directive antenna is being scanned through the complete range of angles of propagation θ , an observer in the shadow region should see a sharply increased field response when $\theta = \hat{\theta}$. It should also be borne in mind that two critical angles $\hat{\theta}_{1,2}$ exist, each of which is associated with its own lateral wave. By pointing the major lobe of this antenna along one or the other of these directions, it should be possible to verify the validity of the rather unconventional lateral wave trajectories which were found in the previous study (see Fig. II - 1).² The analysis has confirmed these anticipations.

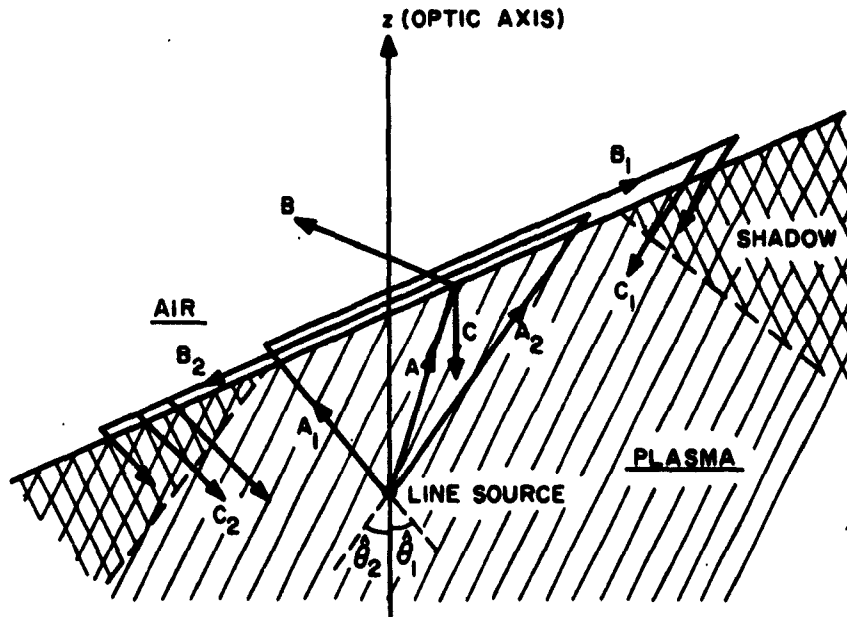


Fig. II-1 Ray paths when $\omega < \omega_p$; A = incident ray; B = refracted ray; C = reflected ray; (A₁, B₁, C₁) and (A₂, B₂, C₂) pertain to lateral ray paths.

These lateral wave aspects have provided the primary motivation for the present investigation involving a directive source distribution inside a uniaxially anisotropic plasma half-space. However, it was also desired to check how the properties of the direct, reflected, and refracted beams can be predicted from the previous point source results

PLASMA ELECTROPHYSICS AND ELECTRONICS

As in isotropic media, the radiation pattern of a finite antenna in an anisotropic medium is equal to the pattern of a point source multiplied by the array factor. If the antenna is linear, several wavelengths long, and of the traveling-wave type with a progressive phase variation $\exp(ib\xi)$ where ξ is the direction along the antenna and b is a real constant (see Fig. II - 2), one expects to find a strong maximum in the radiation pattern along or near the direction of propagation of a plane wave having the same phase dependence. In an anisotropic region, where the ray and wave normal are generally not

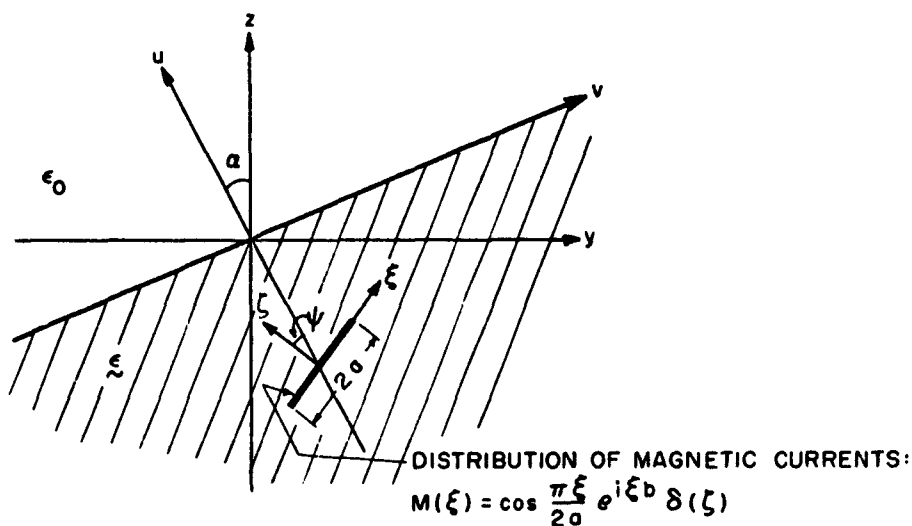


Fig. II-2 Physical configuration

parallel, the pattern maximum should occur essentially along the ray direction which defines the direction of energy flow. This expectation is confirmed by the analysis, and the ray direction corresponding to a given phase variation along ξ can be determined either analytically, or from the refractive index diagram for the medium (Fig. II - 3).

Similarly, the directions of the reflected and refracted (transmitted) beams arising in the presence of a semi-infinite plasma are found to coincide essentially with those of the reflected and transmitted rays as specified by the refractive index plot. Thus, the major features of the radiation pattern are found to be predictable from a study of the refractive index curves. The quantitative field description can be

PLASMA ELECTROPHYSICS AND ELECTRONICS

obtained by combining these plane wave considerations with the known radiation formulas for a point source.

Although the validity of these results is demonstrated below for the uniaxially anisotropic medium only, the same procedure will also yield the pattern characteristics for directive antennas in gyrotropic plasmas provided that the expressions for the point source radiation fields there are combined with the correspondingly more complicated refractive index plots for the ordinary and extraordinary waves. For this more general case it must also be kept in mind that an interface may couple these wave types. For this reason a single incident beam may produce two reflected or refracted beams.

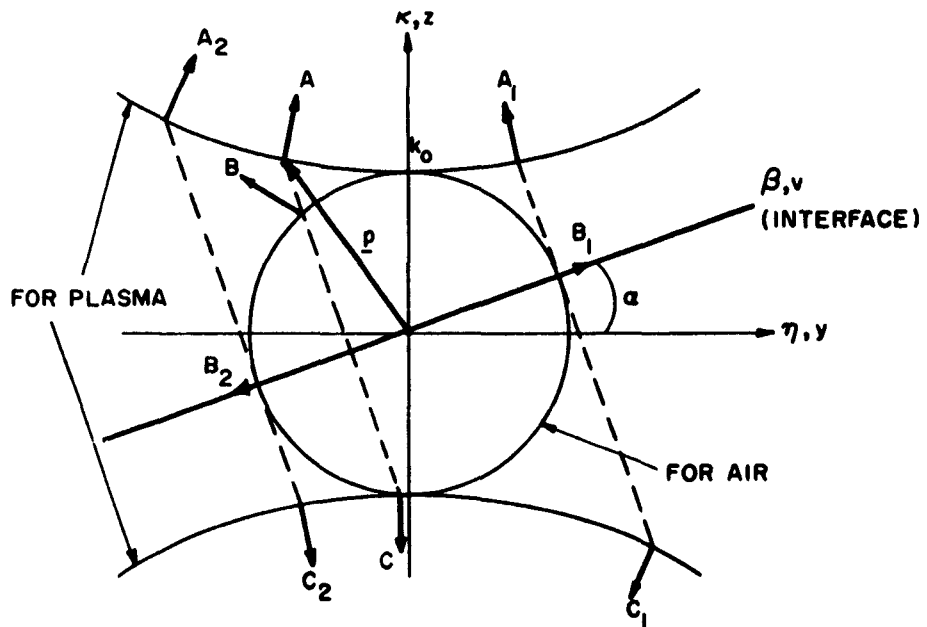


Fig. 11-3 Refractive index plots and ray directions when $\omega < \omega_p$; A = incident ray; B = refracted ray; C = reflected ray; p = wave normal for incident ray; (A_1, B_1, C_1) and (A_2, B_2, C_2) pertain to lateral rays.

In addition to the analytical verification of the above statements, a representative set of numerical data is being calculated in order to provide a feeling for the orders of magnitude of the various field contributions. If the lateral wave is included, it is not possible to consider merely the angularly dependent radiation pattern since the

PLASMA ELECTROPHYSICS AND ELECTRONICS

distance dependence of the lateral waves differs from that of the direct, reflected and refracted waves. Consequently, the field magnitudes have been calculated for various radial distances from the source region.

Preliminary results show, as expected, that the influence of the lateral waves diminishes with distance from the source except in the vicinity of the angle of total reflection. In the illuminated region, the lateral wave amplitude is very small compared with that of the direct or reflected fields; the amplitude is also small in the shadow region but there it greatly dominates the other exponentially decaying field constituents. Its experimental detection is probably accomplished most easily by placing a detector into the shadow region, employing a scanned directive source and noting the maximum response, as mentioned previously. This method may perhaps be useful for diagnostic purposes below the plasma frequency if the plasma can be rendered partially transparent by the application of a strong magnetic field.

In connection with the problem of radiation from a plasma half-space, the energy diverted into the lateral waves constitutes a small effect (at least for the uniaxial medium) which can be minimized further by avoiding large primary field amplitudes in the vicinity of the angle of total reflection. Formulas and typical radiation patterns will be presented in the next Progress Report.

Air Force Cambridge Research Laboratory
Office of Aerospace Research
AF-19(628)-2357

L. B. Felsen

References

1. L. B. Felsen, "Lateral Waves on an Anisotropic Plasma Interface," IRE Trans. on Antennas and Propagation, Vol. AP-10, p. 347 (May 1962).
2. L. B. Felsen, "Radiation from a Uniaxially Anisotropic Plasma Half-Space," Report PIBMRI-1058-62, Microwave Research Institute, P. I. B. (August 1962); to be published in IEEE Trans on Antennas and Propagation, July 1963.

B. THE FIELD OF A LINE SOURCE ABOVE A UNIAXIALLY ANISOTROPIC PLASMA SLAB

P. J. Crepeau, L. O. Goldstone, F. M. Labianca

The properties of electromagnetic waves guided by a homogeneous, isotropic, plasma slab have been thoroughly investigated in recent literature.^{1,2} In the problem described in this article, the geometry is the same, but the plasma slab is uniaxially anisotropic with the infinite magnetic field applied perpendicular to the magnetic line source. This situation is illustrated in Fig. II - 4.

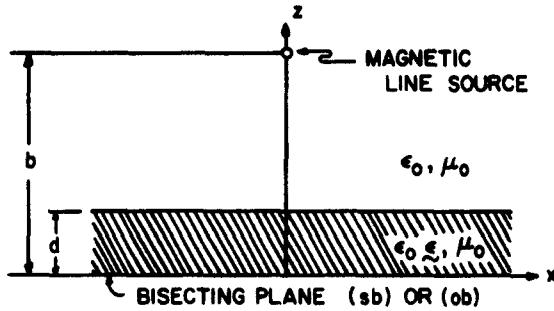


Fig. II-4 Source-excited plasma layer

As indicated in Fig. II - 4, the symmetry of the problem has been exploited, so that the total solution is obtained as the superposition of the solutions to the short circuit (sb) and open circuit (ob) bisections of the original geometry. The relative dyadic permittivity of the slab in Fig. II - 4 has the form:

$$\xi = \epsilon_p \frac{x_0 x_0}{z_0 z_0} + \frac{y_0 y_0}{z_0 z_0} + \frac{z_0 z_0}{z_0 z_0}$$

$$\epsilon_p = 1 - (\omega_p / \omega)^2 \quad (1)$$

where ω_p is the plasma frequency.

With the magnetic line source outside the slab as indicated, the magnetic field can be represented as follows:

a) For $0 \leq z \leq d$,

$$H_y = - \frac{1}{2\pi} \int_{-\infty}^{\infty} \frac{\exp[-j k_z (b-d)]}{Z(d)} \frac{\cos \kappa_z z}{\cos \kappa_z d} \exp[-j \xi x] d\xi, \quad (sb), \quad (2a)$$

$$H_y = - \frac{1}{2\pi} \int_{-\infty}^{\infty} \frac{\exp[-j k_z (b-d)]}{Z(d)} \frac{\sin \kappa_z z}{\sin \kappa_z d} \exp[-j \xi x] d\xi, \quad (ob), \quad (2b)$$

b) For $z > d$,

$$H_y = - \frac{\omega \epsilon_0}{4\pi} \int_{-\infty}^{\infty} \left[\exp[-j k_z |z-b|] - \tilde{\Gamma}(d) \exp[-j k_z (z+b-2d)] \right] \frac{\exp[-j \xi x]}{k_z} d\xi \quad (3)$$

In Eqs. (2) and (3) κ_z and k_z are the wavenumbers in the z direction inside and outside the plasma slab respectively, and ξ is the wavenumber in the x direction. The dispersion relations are:

$$\xi^2 \epsilon_p + \kappa_z^2 = k_0^2 \epsilon_p$$

$$\xi^2 + k_z^2 = k_0^2 \quad (4)$$

where

$$k_0^2 = \omega^2 \mu_0 \epsilon_0$$

The other quantities of interest are

$$\vec{Z}(d) = \begin{cases} j(\kappa_z / \omega \epsilon_0 \epsilon_p) \tan \kappa_z d + (k_z / \omega \epsilon_0) & \text{(sb)} \\ -j(\kappa_z / \omega \epsilon_0 \epsilon_p) \cot \kappa_z d + (k_z / \omega \epsilon_0) & \text{(ob)} \end{cases} \quad (5)$$

and

$$\vec{\Gamma}(d) = \begin{cases} \frac{j(1/\epsilon_p) \kappa_z \tan \kappa_z d - k_z}{j(1/\epsilon_p) \kappa_z \tan \kappa_z d + k_z} & \text{(sb)} \\ \frac{j(1/\epsilon_p) \kappa_z \cot \kappa_z d + k_z}{j(1/\epsilon_p) \kappa_z \cot \kappa_z d - k_z} & \text{(ob)} \end{cases} \quad (6)$$

The evaluation of the integrals in (2) and (3) and consequently the properties

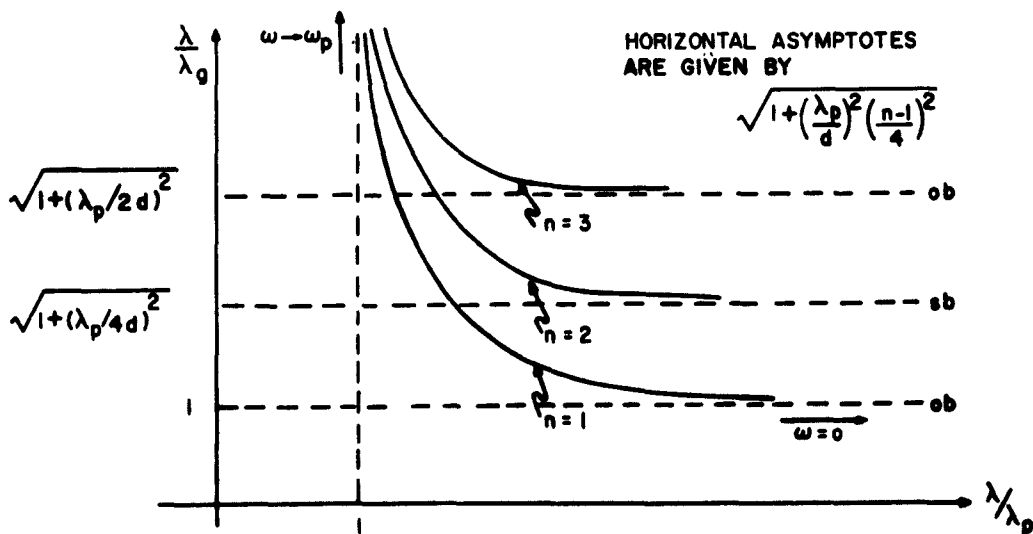


Fig. 11-5 Dispersion curves for surface waves

PLASMA ELECTROPHYSICS AND ELECTRONICS

of the fields depend on the roots of the following equations:

$$q = \begin{cases} j (1/\epsilon_p) p \tan p & (7a) \\ -j (1/\epsilon_p) p \cot p & (7b) \end{cases}$$

and

$$p^2 - \epsilon_p q^2 = 0 \quad (8)$$

where

$$p = \kappa_z d = p_r + j p_i$$

$$q = k_z d = q_r + j q_i$$

A thorough study of Eqs. (7) and (8) reveals the existence of a discrete infinity of surface wave poles in the range of frequencies $0 < \omega < \omega_p$. It is also found that all

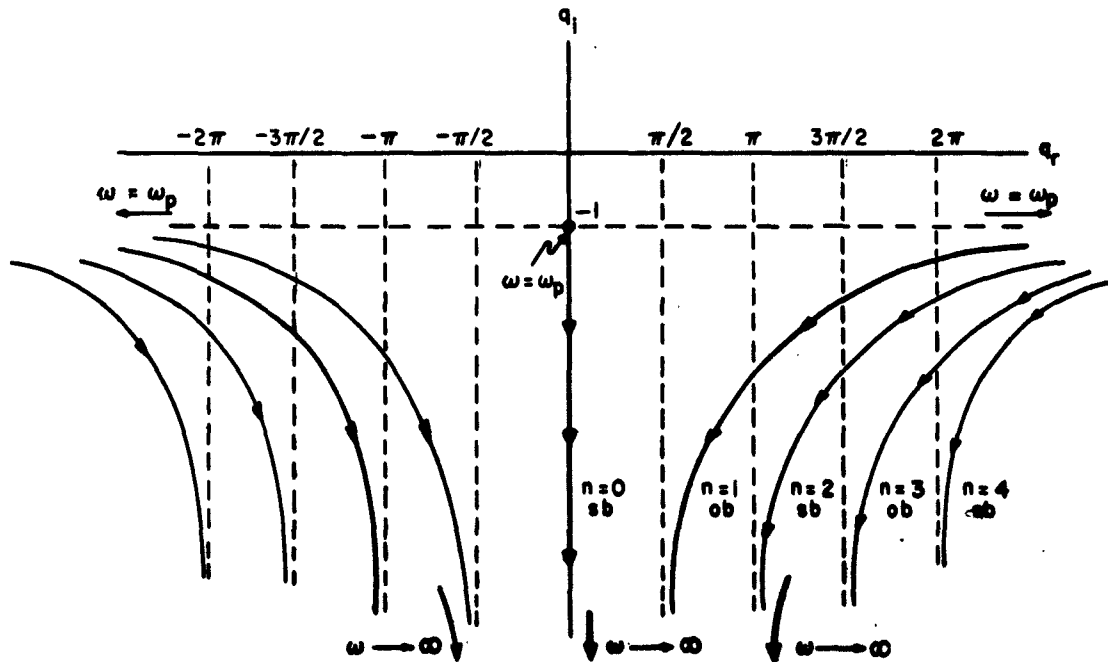


Fig. 11-6 Loci of leaky wave poles in q-plane

PLASMA ELECTROPHYSICS AND ELECTRONICS

of these poles contribute residus terms to the fields when the method of steepest descent is used to evaluate the integrals in (2) and (3). The resultant surface wave field is expressed as a convergent series. The spatial variation of the surface waves is sinusoidal within the slab and exponentially decaying outside the slab.

Insofar as propagation in the x direction is concerned, the surface wave contributions are all forward waves. This fact is evident from a study of the dispersion curves shown in Fig. II - 5. In Fig II - 5, λ_g is the wavelength in the x direction and λ_p is the plasma wavelength.

In the range of frequencies $\omega > \omega_p$, Eqs. (7) and (8) indicate the existence of an infinite number of leaky wave poles, only a finite number of which contribute to the field. The loci of these leaky wave poles in the q -plane, with frequency as a parameter, are illustrated in Fig. II - 6. The loci of the leaky wave poles are given by the equation

$$q_i = - (2 q_r / n\pi) \coth^{-1} (2 q_r / n\pi) \quad n = 1, 2, 3, \dots \quad (9)$$

Joint Services Technical Advisory Committee
AF-AFOSR-62-295

F.M. Labianca

References

1. S. Barone, "Leaky Wave Contributions to the Field of a Line Source above a Dielectric Slab," Report PIBMRI R-532-56, Microwave Research Institute P.I.B. (November 1956).
2. T. Tamir, "The Electromagnetic Field of a Source-Excited Plasma Slab," Report PIBMRI-932-61, Microwave Research Institute, P.I.B. (September 1961).

C. SURFACE WAVES ON PLASMA SLABS

P. Hirsch, J. Shmoys

To gain insight into the problem of the propagation of surface waves along a gradual transition between two uniform plasma regions, a simplified model has been constructed and analyzed.

In the linear approximation (it is assumed that all signals are small and that only the electrons are mobile), the plasma acts like an isotropic medium whose dielectric constant depends only on the electronic number density as in the formula:

$$\epsilon = \epsilon_0 \left[1 - (n/n_c) \right]$$

where the critical density is given by:

PLASMA ELECTROPHYSICS AND ELECTRONICS

$$n_c = \omega^2 \epsilon_0 m / e^2 = n \omega^2 / \omega_p^2 \quad (2)$$

and where

$$\omega_p^2 = e^2 n / \epsilon_0 m, \text{ the plasma frequency;}$$

ω = the radian frequency of the electromagnetic wave;

m = the electronic mass;

e = the electronic charge.

The gradual increase in electron density from the one uniform region to the other is to be approximated by a series of steps. The propagation of surface waves

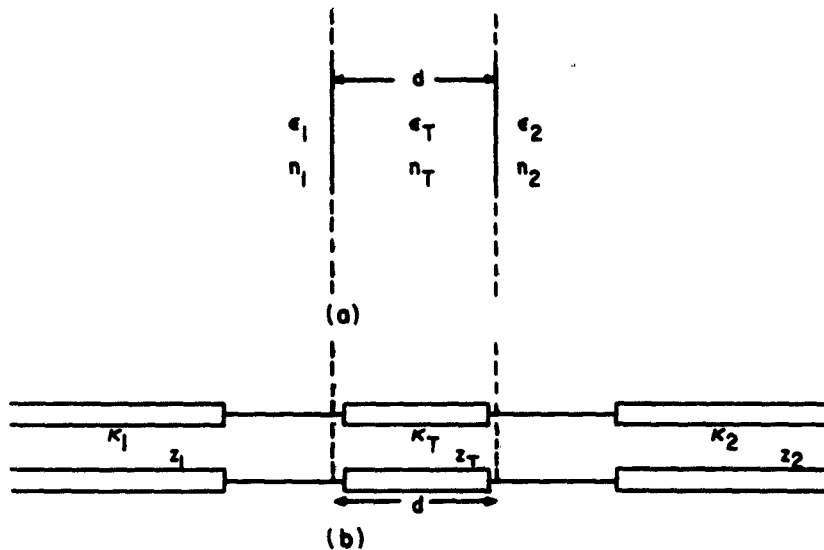


Fig. II-7 (a) Physical configuration; (b) network equivalent.

along an abrupt, single-step transition between two semi-infinite dielectric media has been described by Epstein.¹ The purpose of this paper is to examine the conditions which must be satisfied for surface waves to propagate along a two-step transition, as in Fig. II - 7(a). Here $\epsilon_1, \epsilon_T, \epsilon_2$ are the relative dielectric constants of the three regions, with

$$\epsilon_1 < 0 < \epsilon_2, \quad (3)$$

and

$$\epsilon_1 < \epsilon_T < \epsilon_2 \quad (4)$$

Since the regions are uniform in every plane which is parallel to the discontinuity planes, propagation can be described in terms of uniform transmission lines whose propagation constants are the wavenumbers in the direction normal to the discontinuity planes, and whose characteristic impedances are the corresponding wave impedances. The equivalent circuit is shown in Fig. II - 7(b).

From a transverse resonance analysis, it was found that the magnetic field vector of all surface waves must be parallel to the discontinuity planes, and that their wavenumbers must satisfy the equation

$$\frac{\tanh (ukd \sqrt{\epsilon_2})}{u} = \frac{\eta_T \left[\sqrt{\eta_T - \eta_1 + u^2} + \eta_1 \sqrt{\eta_T - 1 + u^2} \right]}{-\eta_1 u^2 - \eta_T^2 \sqrt{(\eta_T - \eta_1 + u^2)(\eta_T - 1 + u^2)}} \quad (5)$$

where

d = the thickness of the transition layer;

k = the free space wavenumber;

$$\eta_T = \epsilon_T / \epsilon_2;$$

$$\eta_1 = \epsilon_1 / \epsilon_2 ;$$

$$-ju = \kappa_T / k\sqrt{\epsilon_2} \quad , \quad \text{the normalized wavenumber in the transition region;}$$

and u is real.

As (5) now stands, the thickness of the transition layer is normalized to the wavelength in region 2: $k\sqrt{\epsilon_2} = 2\pi/\lambda_2$. In order to plot a dispersion curve, it will be better to normalize with respect to c/ω_{p1} , the plasma wavelength in region 1.

For this purpose it is now assumed that region 2 is vacuum, i. e., that $\epsilon_2 = 1$. A new normalized thickness, $D \equiv kd\sqrt{1 - \eta_1} = (c/\omega_{p1})d$, is defined. Then the left-hand side of (5) becomes

$$L = \frac{\tanh (uD/\sqrt{1 - \eta_1})}{u} = \frac{\tanh ukd}{u} \quad (6)$$

For brevity in the following discussion, the right-hand side of (5) will be

PLASMA ELECTROPHYSICS AND ELECTRONICS

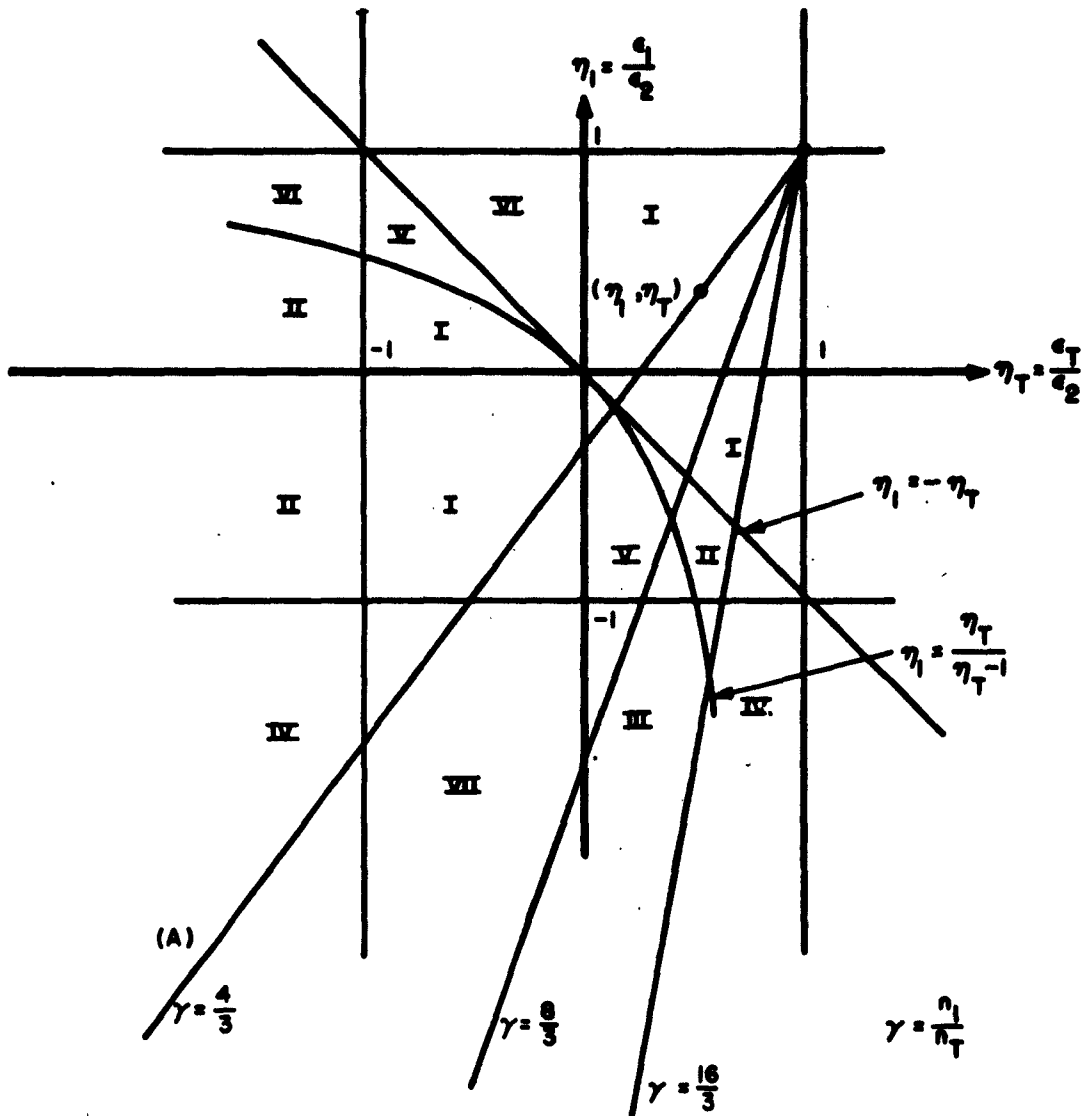


Fig. 11-8 Regions of different behavior of the surface waves

denoted by:

$$R \equiv \frac{\eta_T \left[\sqrt{\eta_T - \eta_1 + u^2} + \eta_1 \sqrt{\eta_T - 1 + u^2} \right]}{-\eta_1 u^2 - \eta_T^2 \sqrt{(\eta_T - \eta_1 + u^2)(\eta_T - 1 + u^2)}} \quad (7)$$

Obviously, (5) has a solution wherever $L = R$. Both quantities represent families of

curves when plotted as functions of u , and the possible solutions of (5) have been investigated in terms of these families.

Fig. II - 8 shows the η_1, η_T plane divided into a set of zones. The surface wave behavior depends on the possibility of intersection of L and R in these zones:

- Zone I: No surface waves can propagate.
- Zone II: Surface waves propagate for all D except $D = 0$.
- Zone III: There is a critical value of D , which depends on the particular coordinate in the η_1, η_T plane. Surface waves propagate only for values of D which is smaller than the critical, and also at the limit $D = \infty$. The behavior of u , the normalized wavenumber in the transition region, as D is increased is shown in Fig. II - 9.
- Zone IV: Surface waves propagate for all D .
- Zone V: There is a critical upper value of D , and surface waves can propagate for all D smaller than this, except at the limit $D = 0$.
- Zone VI: There is a critical lower value of D , and surface waves can propagate for all D greater than this. Note that this behavior is actually not possible in the case which approximates a monotonic transition, where it is required that $\eta_T > \eta_1$.
- Zone VII: Surface waves can propagate for every D (including $D = 0$) which is smaller than some critical value. This is the only zone in which R and L can intersect more than once for each set of parameters. This suggests the existence of backward waves, because the dispersion curve for this mode will be multiple-valued.

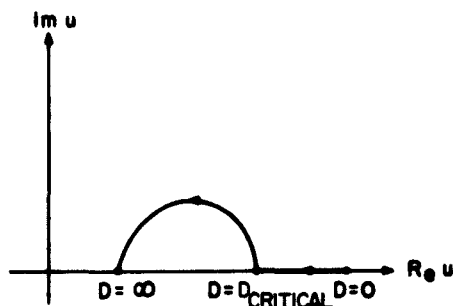


Fig. II-9 Behavior in the complex U plane

To study the dispersion curve, a frequency independent parameter γ is defined as the ratio of electron number densities:

$$\gamma \equiv n_1 / n_T \quad (8)$$

To satisfy the condition $\epsilon_1 < \epsilon_T < \epsilon_2$, it is necessary that $\gamma > 1$. Since

$$\eta_i \equiv \epsilon_i / \epsilon_2; \quad i = 1, 2, T, \quad (9)$$

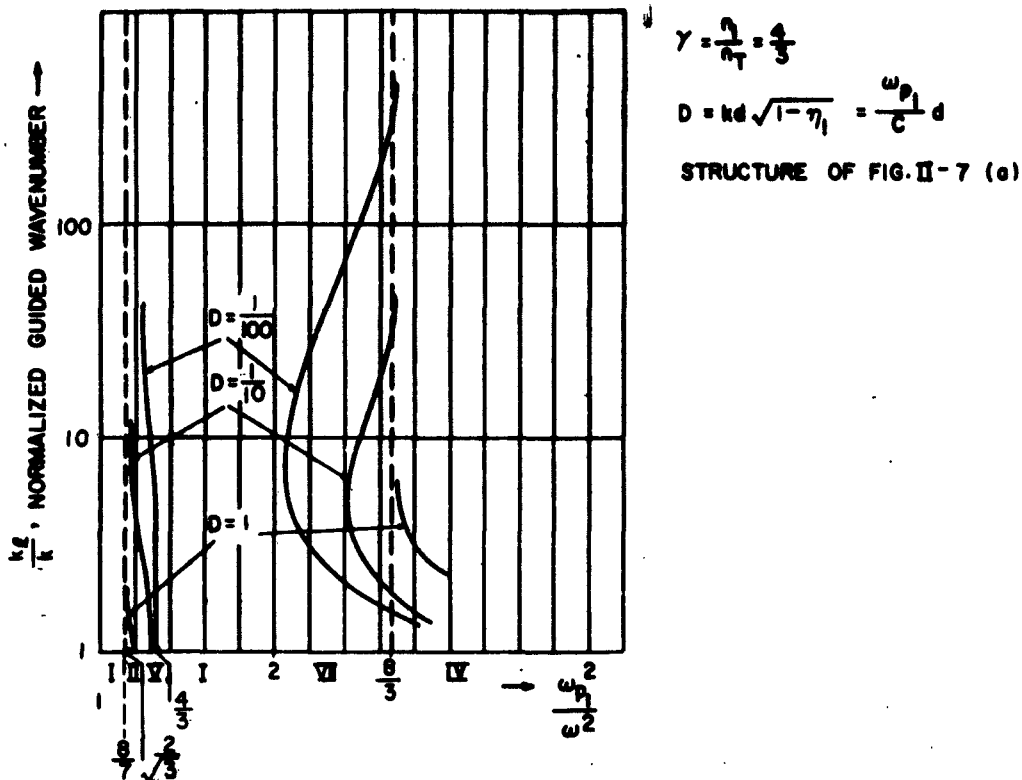


Fig. II-10 Dispersion curve

and

$$\epsilon_1 = \epsilon_0 \left[1 - (n_i/n_c) \right] , \tag{10}$$

then

$$\eta_1 = 1 - \gamma (1 - \eta_T) . \tag{11}$$

The solutions of Eq. (5) can now be plotted in terms of the normalized longitudinal wavenumber:

$$k_z / k\sqrt{\epsilon_2} = \sqrt{u^2 + \eta_T} , \tag{12}$$

and normalized frequency:

$$\omega_{p1}^2 / \omega^2 = 1 - \eta_1 , \tag{13}$$

with γ and D as parameters.

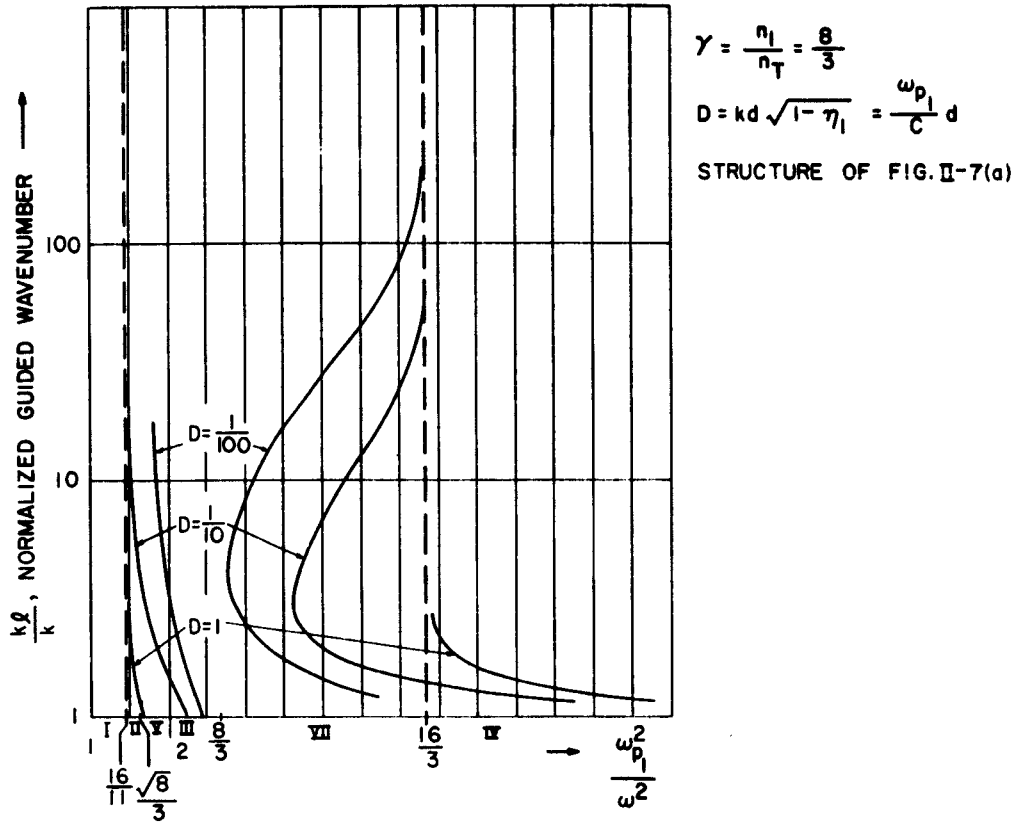


Fig. II-11 Dispersion curve

Three values of γ were chosen as examples for machine computations of the dispersion curves. In order to extrapolate to other values of γ , consider first Eq. (11). This is a family of straight lines with slopes γ and common point (1, 1) in the η_1, η_T plane. One of these lines, labeled (A), corresponding to the value $\gamma = 4/3$, is shown in Fig. II - 8. Each point on the line corresponds to some unique frequency, with infinite frequency at (1, 1), and progressively lower frequencies along the line as it is traversed in the direction $\eta_1 \rightarrow -\infty$. Clearly, there is a linear relationship between distance along line (A) from point (1, 1) and the abscissa of the dispersion curve in Fig. II - 10. Thus the numbered zones traversed by line (A) correspond to distinct segments of the $1 - \eta_1$ axis.

The families of dispersion curves for all γ have in common the property that

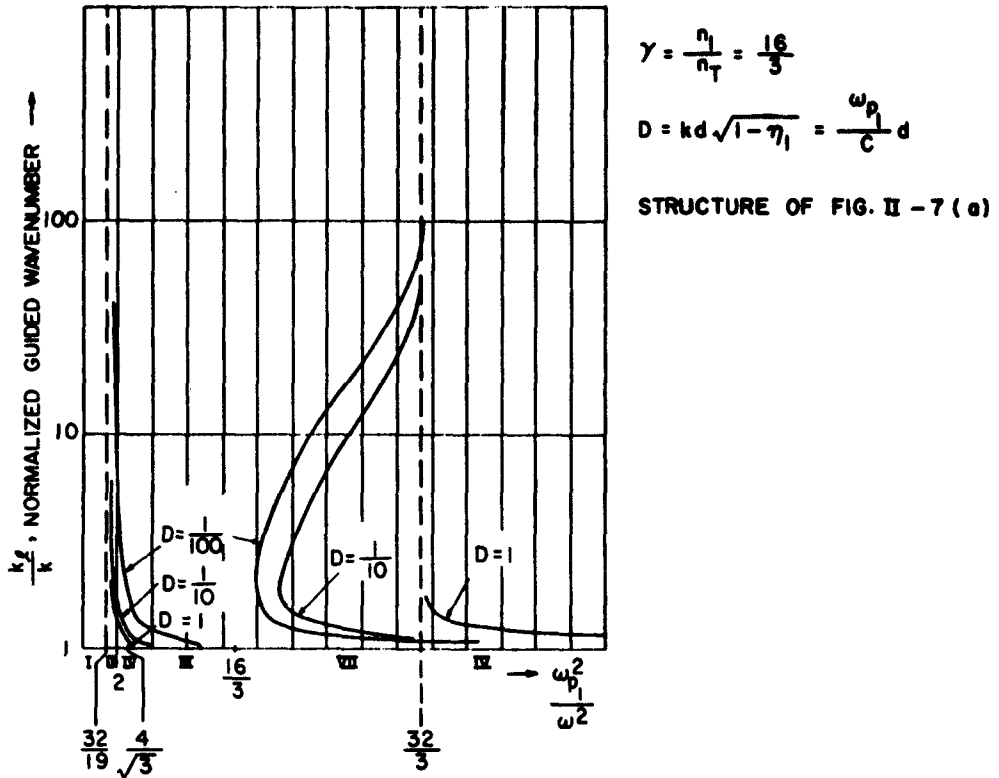


Fig. II-12 Dispersion curve

the frequency point must start in zone I, then progress to zone II, and finally traverse zone VII before ending in IV. (See Figs. II - 10, II - 12). Three different sequences of zones are possible:

- 1) I, II, V, I, VII, IV for $1 < \gamma < 2$
- 2) I, II, V, III, VII, IV for $2 < \gamma < 4$
- 3) I, II, IV, III, VII, IV for $4 < \gamma < \infty$

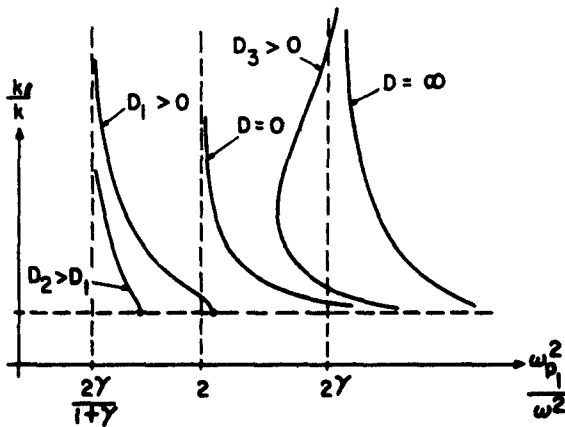


Fig. II-13 Generalized dispersion curve

The values of γ for which dispersion curves were computed were chosen so that one lies in each of these ranges. The only differences are in the traversals of zones III, IV and V when $\eta_T > 0$. On this basis a generalized dispersion curve family can be drawn as in Fig. II-13, which is representative of the curves for all γ such that $1 < \gamma < \infty$. The curves will differ

PLASMA ELECTROPHYSICS AND ELECTRONICS

in their essentials only in that the low frequency cutoff of the higher mode may or may not occur before the lower mode starts to propagate.

Air Force Cambridge Research Laboratory
Office of Aerospace Research
AF-19(604)-4143, AF-19(628)-2357

P. Hirsch, J. Shmoys

Rome Air Development Center, Air Force Systems Command
AF-30(602)-2045

Reference

1. P.S. Epstein, Proc. Nat. Acad. Sci., Vol. 40, p. 1158 (1957).

D. A STUDY OF THE CATHODE FALL REGION IN A PULSED GLOW DISCHARGE

M. Nahemow, N. Wainfan

1. Introduction

The field and space charge configurations in a stable glow discharge have been studied by many investigators.¹ The propagation velocity and dynamics of the initial breakdown wave of a starting discharge have also been the subject of considerable study.² In an effort to trace the progress of a glow discharge from the time the initial breakdown wave starts to the time when the stable glow configuration is reached, a series of time-resolved spectroscopic studies of the cathode fall region of a wall-bound, pulsed discharge in hydrogen was undertaken.³ By examining the Stark splitting of the spectral lines of the hydrogen spectrum, the electric field was mapped in space and time within the cathode fall region of the discharge.

The purpose of this paper is to present the results of the field configuration measurements and to comment briefly on some of the possible processes by which the stable cathode fall region is established.

2. Experimental Arrangements

A block diagram of the experimental arrangement is presented in Fig. II - 14.

The discharge tube is a standard section of two-inch pyrex pipe. Cathodes of titanium and aluminum were used. The anode was made of titanium. The various cathodes were fitted into the pyrex tube with an annular gap of 1 mm to prevent the discharge from propagating back into the annular gap between the cathode and the wall of the discharge tube. The axial gap between the electrodes was 3.6 cm.

Vacuums of the order of 10^{-6} torr were obtained before filling the discharge tube. Hydrogen was introduced, by diffusion, through the walls of an electrically heated thin-walled nickel tube.

PLASMA ELECTROPHYSICS AND ELECTRONICS

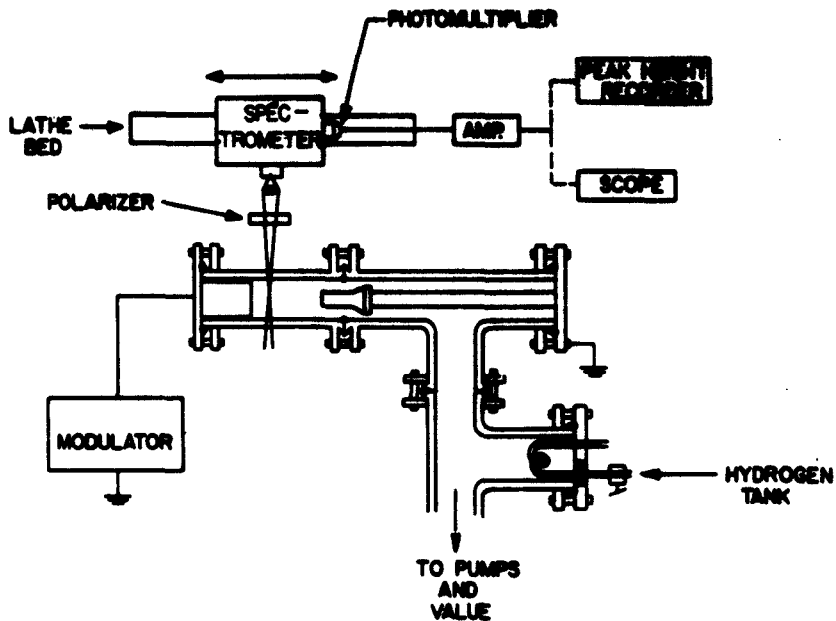


Fig. 11-14 Optical plasma probing system

A one microsecond negative pulse was provided by the modulator which could support a current rise of 5000 amperes per microsecond. Except as otherwise noted the pulse repetition rate employed for the data reported here was 100 per second. It may be noted that no variations in the results were observed as the pulse repetition was varied from 1 to 1000 per second.

The optical radiation from the discharge was observed with a 0.5 meter grating spectrometer. The spectrometer, provided with an optical collimator and polarizer, was mounted on a lathe bed, and thus could be moved, along the axis of this discharge tube. This arrangement provided a spatial resolution of 0.2 mm along the axis of the discharge tube and a spatial precision of 0.05 mm. The amplified output pulse of the spectrometer's photo-multiplier could be viewed directly on a dual beam oscilloscope and could be compared with the simultaneously presented discharge tube current and voltage pulses. In addition, the spectrometer output pulse could be directed to a peak height detector whose output was recorded.

Using this latter arrangement and the motor driven wavelength drive on the spectrometer, a recorded plot of peak light intensity vs. wavelength could be obtained for a given position along the axis of the discharge tube. The rise time of the oscilloscope and the associated electronics was 14 nanoseconds for the current and voltage

signals. The rise time of the total photo-multiplier circuit was 18 nanoseconds with an inherent circuit delay of 112 nanoseconds.

3. Results

The Stark split components of the hydrogen spectrum are linearly polarized when viewed at right angles to the electric field. The components of a Stark split spectral line, polarized parallel to the electric field, are labeled π , and those polarized perpendicular to the field are labeled σ . Since the separation of the π components for the H_{β} line is twice that of the σ components for a given electric field, the π components were used to investigate the electric field. (See reference 4.) Fig. II - 15

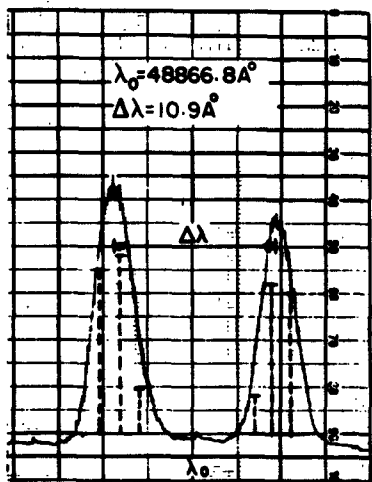


Fig. II-15 Typical π components of the H_{β} line of hydrogen

is a typical recorded trace of the peak light intensity plotted as a function of wavelength for the π components of the H_{β} line of the hydrogen spectrum within the cathode fall region of the discharge. The positions of the unresolved components of the split line are shown by the dotted lines in Fig. II - 15. The low minimum between the peaks in Fig. II - 15 indicates that the high electric field was formed early in the pulse and that the field is nearly constant over the duration of the pulse.

Figure II - 16 presents photographs of the oscilloscope traces of light intensity, voltage, and current signals as a function of time. In Fig. II - 16(b) the light intensity signal was obtained by setting the spectrometer to the wavelength of one of the Stark split peaks seen in Fig. II - 15.

The light intensity is seen to rise early in the pulse and remain constant for the duration of the pulse. This would indicate that the electric field within the cathode fall region reached its stable configuration within the first 100 nanoseconds of the initiation of the discharge pulse. In Fig. II - 16(a) the light signal was obtained by setting the spectrometer to the wavelength corresponding to the unsplit, zero field, position of the H_{β} line. No peak in the light intensity was observed early in the pulse. This supports the notion that by the time the current has begun its rapid rise, the high field region has formed. Otherwise, the initial current rise could be expected to be accompanied

PLASMA ELECTROPHYSICS AND ELECTRONICS

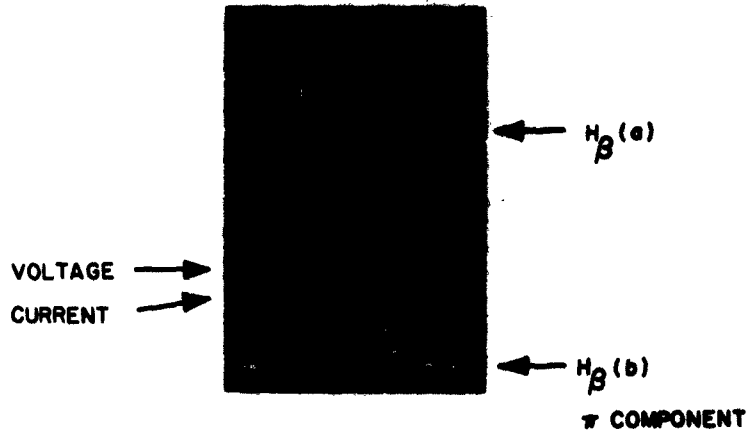


Fig. II-16 Light intensity vs. time; time scale: $.2\mu$ sec/cm.

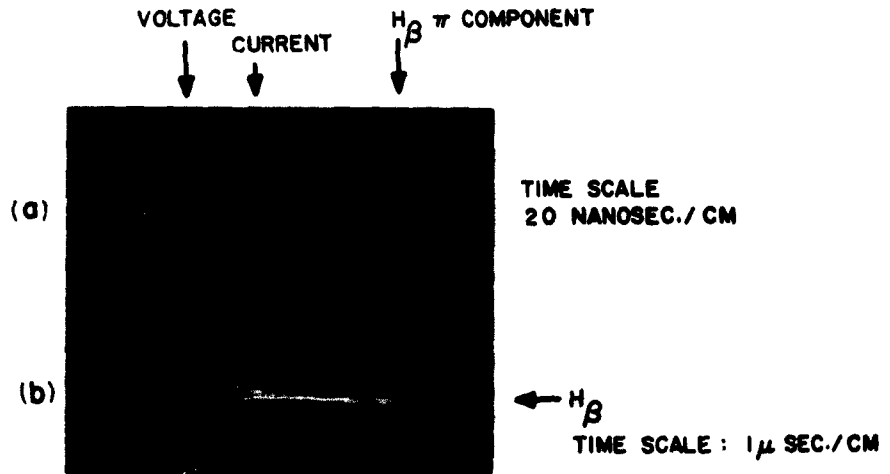


Fig. II-17 Detail of the start and collapse of a pulsed discharge in hydrogen

by a peak in the light intensity at the unsplit wavelength.

Figure II - 17 presents the leading and trailing edges of traces such as seen in Fig. II - 16, with the sweep rate multiplied by a factor of 10 and 2, respectively.

In Fig. II - 17(a) the leading edge of Fig. II - 16(b) is examined. Measuring

PLASMA ELECTROPHYSICS AND ELECTRONICS

time from the start of the voltage pulse it was found that the voltage reached its maximum value in 80 nanoseconds. For the particular potential and pressure employed, the current started 10 nanoseconds later and by 70 nanoseconds had reached 0.8 amperes. At 70 nanoseconds the current started a rapid rise and reached 53 amperes (150 nanoseconds after the start of the voltage pulse.) The light pulse from the Stark split peak, when corrected for the 112 nanosecond circuit delay, begins its rapid rise in coincidence with the current jump at 70 nanoseconds.

It would appear, therefore, that after the initial breakdown process, occupying an interval of about 70 nanoseconds, the electric field configuration reached its steady value within the following 20 nanoseconds. This is of the order of 50 nanoseconds before the current reaches its maximum value.

Figure II - 17(b) presents the trailing edge of a trace such as is presented in Fig. II - 16(a). In this case the light signal is representative of the unsplit wavelength at the center of Fig. II - 15. Here, in the light signal, a peak may be seen corresponding to an inverted peak in the current which occurred after the collapse of the applied voltage pulse. This inverted current peak is a result of the redistribution of the space charge in the cathode fall region after the applied potential goes to zero. The light peak excited by the reverse current pulse shows no Stark splitting.

The magnitude of the electric field within the cathode fall region is calculated as follows. The incompletely resolved Stark split H_{β} line, as illustrated in Fig. II - 16, is corrected for the geometrical "window" of the spectrometer. Using the measured separation of the split components and the published data³ on the Stark effect, the field is calculated. Results obtained by measurements on the π components of the H_{β} line were verified by measurements on the σ components of the H_{β} line and by the consideration of other lines in the Balmer series. The error in the electric field thus obtained is ± 1000 v/cm.

Figure II - 18 presents a set of electric field profiles within the cathode fall region of the discharge. The set of curves presented was obtained using an aluminum cathode, for which the cathode-anode gap was 36.1 mm. Results presented in Figs. II - 16 and II - 17 show that these curves are representative of the relatively stationary electric field distribution which one obtains within 90 nanoseconds of the start of the voltage pulse and which is therefore representative of 90 percent of total pulse time interval. Since almost the entire potential drop appears across the cathode fall region,^{4, 5} it is convenient to normalize the electric field profiles by plotting E/V vs. axial distance from the face of the cathode. The areas under the curves will thus all be unity. The extrapolated intercept of these curves agrees well with the location of the edge of the

PLASMA ELECTROPHYSICS AND ELECTRONICS

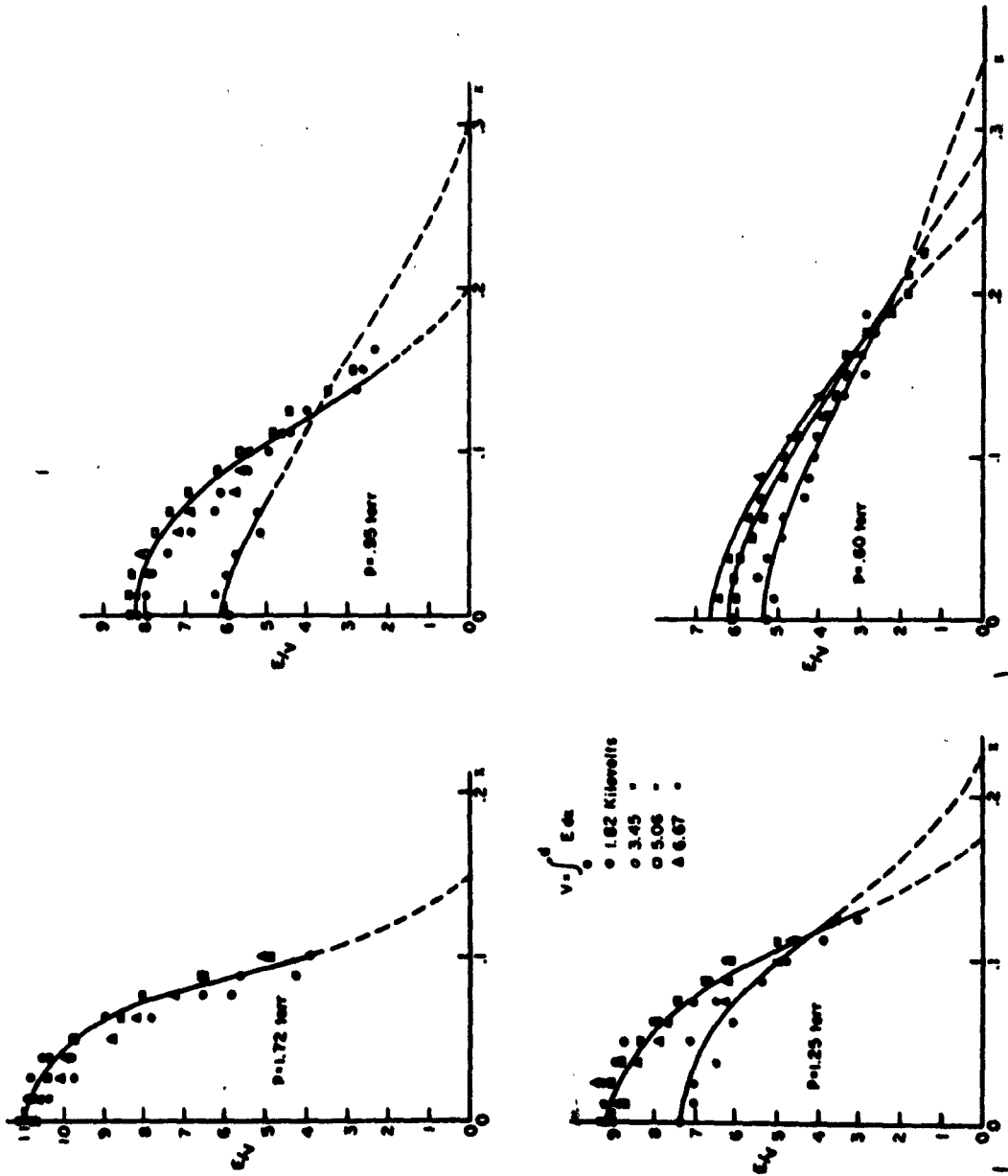


Fig. II-18 Normalized electric field (cm^{-1}) $E/\int_0^d E dx$ vs. $x(\text{cm})$; aluminum cathode in hydrogen: 3.61 cm gap.

cathode fall region as determined by light intensity measurements.

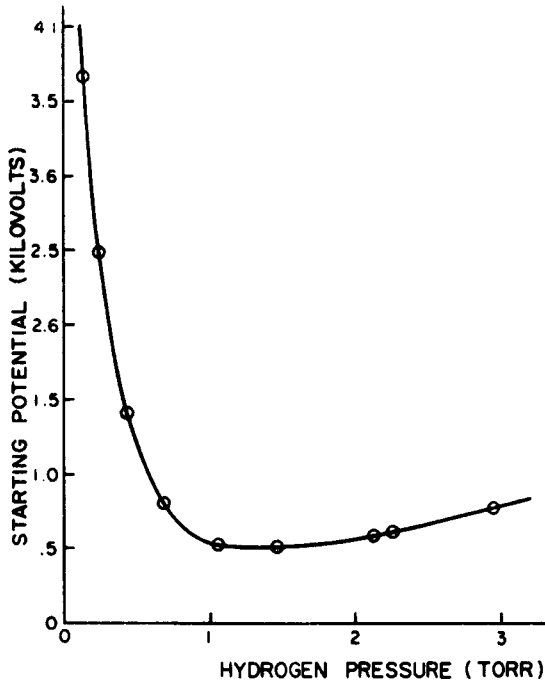


Fig. II-19 Paschen curve for pulsed discharge in hydrogen; aluminum cathode: 36.1 mm gap.

4. Discussion

Conventionally, glow discharges are classified as either normal or abnormal glows. In a normal glow there is available to the discharge more cathode surface than is needed to carry the total current. The abnormal glow begins when the current is increased beyond the value at which all the available cathode surface is participating in the discharge. By this criterion the discharges described in this paper are abnormal glows.

A striking feature of the observations reported here is the rapid formation of the cathode fall region of the discharge. The high electric fields have substantially reached their equilibrium configuration within 100 nanoseconds of the application of the voltage pulse. The rapidity of the formation of this cathode fall indicates that the

Figure II - 19 presents the starting potential as a function of pressure for one microsecond applied voltage pulses. Since the starting delay is observed to be dependent on the applied voltage near the minimum starting potential, the curve obtained, although resembling a classical Paschen curve, does not follow the pd similarity rule. It has been shown⁵ that even for a dc glow in hydrogen the similarity relations do not hold for the left-hand branch of this curve.

Figure II - 20, which presents d , the length of the cathode fall region, as a function of the pressure p , summarizes the information in Fig. II - 18 in a form that can be conveniently compared to the Paschen curve of Fig. II - 19.

In Fig. II - 21 the current density, j , is presented as a function of p , and the applied potential, V ; $j^{2/3}/p$ is plotted against V . It can be seen that in this form all the data presented here falls approximately on the same line except near the starting potential.

PLASMA ELECTROPHYSICS AND ELECTRONICS

space charge cloud associated with the cathode fall region must be formed locally within a few millimeters of the cathode face. The low mobility and short free paths of the positive ions would require times of the order of microseconds if the cathode fall space charge were gathered from the general volume of the discharge.

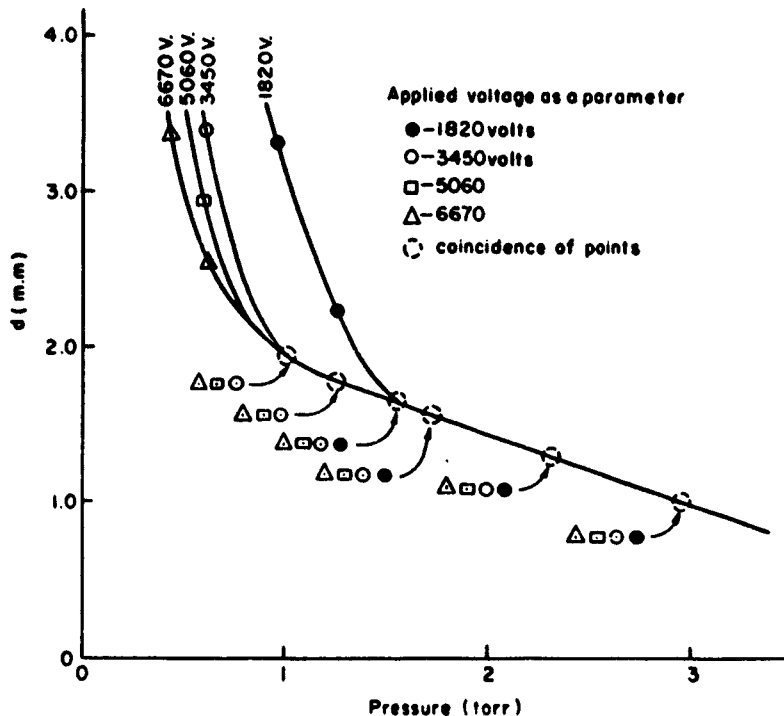


Fig. II-20 Length, d , of the cathode fall region vs. hydrogen pressure

One establishes that the space charge has dispersed in the time between discharge pulses by making the period between pulses long compared with the space charge relaxation time. The results presented in Fig. II - 17(b) demonstrate this. Here the inverse current pulse caused by the redistribution of the space charge may be seen. If the inverse current pulse is integrated to get the total charge represented by the inverse pulse, and if this result is compared with the total space charge obtained by consideration of the electric field profile, it is found that the inverse current peak has accounted for the cathode fall space charge.

Although the rapid local formation of the cathode fall space charge cloud is experimentally demonstrated here, the mechanism of its rapid formation is not

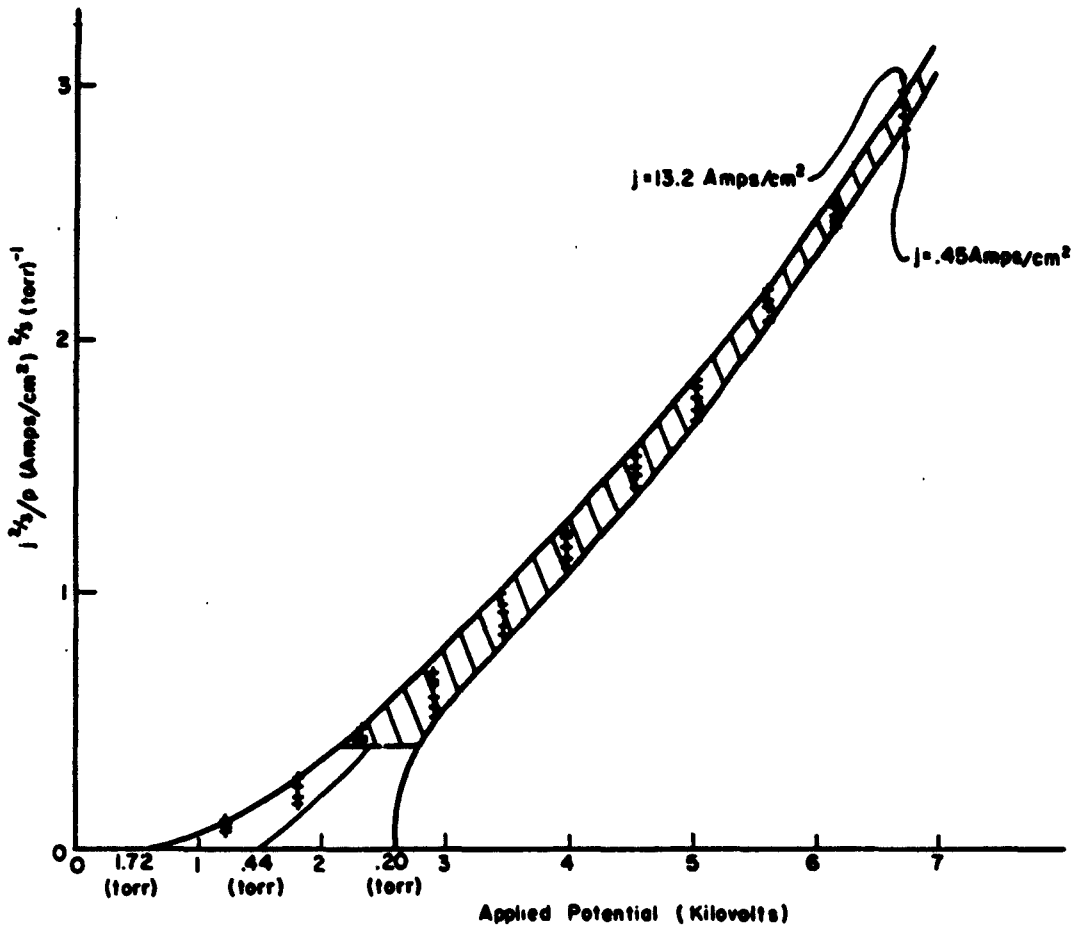


Fig. II-21 Reduced current $j^{2/3}/\rho$ vs. applied potential: .20 to 1.8 torr.

entirely clear.

The characteristics of the pulsed abnormal glow in hydrogen reported here can be compared with previous results. In Figs. II - 19 and II - 20 are compared, one sees that for conditions existing to the left of the minimum of the Paschen curve, the length of the cathode fall region is a function of the overvoltage, and pd is not a constant for a constant overvoltage, but increases with increasing pressure. To the right of the Paschen curve minimum, the length of the cathode fall is essentially independent of the applied potential. These observations yield values of pd that agree well with previous results over the range of pressures considered.

Previous results have indicated that the reduced current density j/p^2 is in-

PLASMA ELECTROPHYSICS AND ELECTRONICS

dependent of p for dc glows.⁷ This arises because j is calculated to be proportional to the mobility, $K_{(p)}$, times the pressure cubed, and $K_{(p)}$ is found to be proportional to $1/p$. From Fig. II - 21 it can be seen that the reduced current density $j/p^{3/2}$ yields a better summary of the data for the large overvoltage discharges discussed here.

The profiles of the electric field at the cathode are in agreement with theory.^{1, 5} At the lower pressures one would expect a solution such as discussed by Warren¹ to hold. The values of the maximum electric fields and cathode fall length found here agree with values obtained by extrapolating Warren's data.¹ At the higher pressures and for high overvoltages, the data presented here appear to be in agreement with the theory presented by McClure.⁵ Thus, the mechanism for maintaining an equilibrium space charge configuration seems reasonably well established. The question remaining to be answered in detail is how the space charge configuration forms.

Joint Services Technical Advisory Committee
AF-AFOSR-62-295

M. Nahemow, N. Wainfan

Air Force Cambridge Research Laboratory
Office of Aerospace Research
AF-33(657)-10820

References

1. R. Warren, Phys. Rev., Vol. 98, p. 1658 (1955).
2. G.W. Paxton and R.G. Fowler, Phys. Rev., Vol. 128, p. 993 (1962).
3. M. Nahemow, N. Wainfan, H. Veron, "A Study of the Dynamics of Pulsed Discharge in Hydrogen," Progress Report No. 22 to the Joint Services Technical Advisory Committee, R-452-22-62, Microwave Research Institute, P.I.B., pp. 28-36.
4. E.V. Condon and G.H. Shortley, "Theory of Atomic Spectra" (Cambridge Univ. Press, 1951), p. 401.
5. G.W. McClure, Phys. Rev., Vol. 124, p. 969 (1961).
6. A.S. Pokrovskaja and B.N. Kliarfeld, Soviet Phys. JETP, Vol. 5, p. 812 (1957).
7. J.D. Cobine, "Gaseous Conductors" (New York: Dover Publications, 1958), p. 228.

E. HIGH-POWER MICROWAVE PLASMA INTERACTIONS

T. Morrone

The object of our investigation is to determine how high-power microwaves interact with a hydrogen plasma. We wish to know how long the field takes to break down the gas, as well as what is the resulting plasma density as a function of space and time, before and after breakdown.

To find the answers we must solve the Boltzmann equation:

$$df/dt + \underline{v} \cdot \nabla f + \underline{F}/m \cdot \nabla_v f = (\delta ef/\delta t) \text{ collisions.}$$

Knowing f , we can determine the ionization collision frequency and study the density build-up process.

For meaningful results we must consider all the collision processes which are important in weakly to moderately ionized molecular hydrogen. They are:

- 1) Electron - neutral elastic collisions;
- 2) Electron - neutral inelastic collisions (vibrational, rotational, ionizing, and excitational);
- 3) Electron - electron collisions.

Small energy loss collisions may be accounted for by expanding the collision integral in powers of $\delta(v)$, the average fraction of energy lost per collision. Large energy loss collisions can only be accounted for by introducing a source and a sink term at each energy " μ ." The source term explains the gain of electrons at " μ ," resulting from higher energy particles losing energy on collision. The sink term results from colliding particles at " μ ," falling to lower energy states.

The effect of electron-electron collisions may be calculated by expanding the collision integral in powers of the average fraction of momentum exchanged per collision. This quantity is small.

The Boltzmann equation is solved by expanding f in a Fourier series in time, and in Legendre polynomials in velocity space. For moderately high field strengths,

$$f = f_0^0 + f_1^1 \cos \theta \cos \omega t + g_1^1 \cos \theta \sin \omega t.$$

PLASMA ELECTROPHYSICS AND ELECTRONICS

Solutions have been obtained thus far in the low density case, where electron-electron collisions are unimportant.

Rome Air Development Center
Air Force Systems Command
AF-30(602)-2045

T. Morrone

F. ONE-DIMENSIONAL ISOTHERMAL FLOW IN AN INFINITELY CONDUCTING FLUID

M. Sandler

The steady-state solutions to the following set of equations were previously considered¹ and a range of existence was established:

$$(\partial B / \partial t) + (\partial B v / \partial x) = \frac{1}{\sigma \mu} (\partial^2 B / \partial x^2) \quad (1)$$

$$(\partial \rho / \partial t) + (\partial \rho v / \partial x) = 0 \quad (2)$$

$$\rho (\partial v / \partial t) + \rho v (\partial v / \partial x) + (\partial p / \partial x) + (B / \mu) (\partial B / \partial x) = 0 \quad (3)$$

$$p = (KT/m) \rho \quad (4)$$

This set of equations is immediately recognized as the one-dimensional form of:

1) Maxwell's equations;

2) the equation of continuity;

3) the equation of momentum;

4) the equation of state for a conducting fluid with crossed electric, magnetic and velocity fields.

This paper is concerned with the solution of the Cauchy problem for this set of equations. To facilitate a solution we consider the case of an infinitely conducting fluid. For this condition, Eqs. (1) and (2) have the same form:

$$(\partial \rho / \partial t) + (\partial \rho v / \partial x) = 0 \quad (2)$$

$$(\partial B / \partial t) + (\partial B v / \partial x) = 0 \quad (1')$$

If we look only for solutions of the form $B = ap$ and initially comply with this condition, the problem is reduced to the solution of the following two equations:

PLASMA ELECTROPHYSICS AND ELECTRONICS

$$(\partial\rho/\partial t) + \rho (\partial v/\partial x) + v (\partial\rho/\partial x) = 0 \quad (2)$$

$$\rho (\partial v/\partial t) + \rho v (\partial v/\partial x) + [(KT/m) + (a^2/\mu) \rho] (\partial\rho/\partial x) = 0 \quad (3')$$

These may be transformed into a linear problem using the hodograph transformation.² The variables may be grouped into $x - vt$ and ρt . The new form of the equations is as follows:

$$\left[\partial(x-vt)/\partial v \right] + (\partial\rho t/\partial\rho) = 0 \quad (5)$$

$$\left[(KT/m\rho) + (a^2/\mu) \right] (\partial\rho t/\partial v) + (\partial/\partial\rho) (x-vt) = 0 \quad (6)$$

To satisfy the initial conditions in the above equations, the technique of separation of variables may be used to advantage. This method is currently being investigated, and will be reported at a later date.

A simpler case may be solved in closed form. A steady state solution is

$$\rho = \rho_0, \quad B = a\rho_0, \quad v = 0.$$

If $\rho(x, 0) = \rho_0 + \rho_1(x)$ where $|\rho_1(x)| \ll \rho_0$, an approximation in the hodograph plane yields:

$$\left[\partial(x-vt)/\partial v \right] + (\partial\rho t/\partial\rho) = 0 \quad (5)$$

$$\left[\frac{c^2 + ((a^2/\mu) \rho_0)}{\rho_0^2} \right] (\partial\rho t/\partial v) + (\partial/\partial\rho) (x-vt) = 0 \quad (6')$$

Reversing the hodograph transformation, we find that Eq. (2) is unchanged. Equation (3') should be approximated as indicated below, to produce Eq. (6') in the hodograph plane:

$$\rho_0 (\partial v/\partial t) + \rho_0 v (\partial v/\partial x) + [(KT/m) + (a^2\rho_0/\mu)] (\partial\rho/\partial x) = 0 \quad (3'')$$

Therefore, if we define $\gamma^2 = [(c^2/\rho_0^2) + (a^2/\mu\rho_0)]$,

$$\rho t = f_- (\rho - \gamma v) + f_+ (\rho + \gamma v) \quad (7)$$

$$\gamma (x-vt) = f_- (\rho - \gamma v) - f_+ (\rho + \gamma v) \quad (8)$$

Consequently,

PLASMA ELECTROPHYSICS AND ELECTRONICS

$$f_{\pm} [(\rho_0 + \rho_1(x))] = \pm (\gamma x/2) \quad (9)$$

If f_{\pm} cannot be found, one would suspect the presence of shock waves. For the simple case of $\rho_1(x) = [\rho_1/(1+x^2)]$ which is well behaved and meets the specified conditions:

$$f_{\pm} = \pm (\gamma/2) \left[([]' - \rho_0)^{-1} \rho_1 - 1 \right]^{1/2}. \quad (10)$$

Therefore, after some manipulation,

$$\pm (\gamma v \pm \rho) = \rho_0 + \frac{\rho_1}{1 + [x - (t/\gamma) (\gamma v \mp \rho)]^2}$$

If we let $A_{\pm} = \gamma v \pm \rho$, we must solve the cubic

$$(A_{\pm} \mp \rho_0) \left[1 + x^2 - (2xt/\gamma) A_{\pm} + (t^2/\gamma^2) A_{\pm}^2 \right] \mp \rho_1 = 0 \quad (11)$$

and

$$\rho = 1/2 (A_{+} - A_{-}) \quad (12)$$

$$v = 1/2 \gamma (A_{+} + A_{-}) \quad (13)$$

It may be shown that for $t = 0$, the initial conditions check. For $|x| = \infty$, or for steady state, $v = 0$ and $\rho = \rho_0$. Furthermore, it may be shown that only one real solution exists for certain values of x and t . This agrees with the uniqueness proof given in reference 3 for this type of problem.

The closed form solution of the truncated problem considered here exhibits the effects of certain nonlinear terms. It should be noted that the usual "complete" linearization of this problem yields the familiar result:

$$\rho_1 = \rho_{1-} (x-vt) + \rho_{1+} (x+vt) \quad (14)$$

$$\rho_0 v_1/\gamma = \rho_{1-} (x-vt) - \rho_{1+} (x+vt) \quad (15)$$

where

$$\rho = \rho_0 + \rho_1; v = v_1; v^2 = c^2 + (a^2 \rho_0 / \mu).$$

PLASMA ELECTROPHYSICS AND ELECTRONICS

In this case this would yield the following solution, which is given here for purposes of comparison:

$$\rho = \rho_0 + 1/2 \left[\frac{1}{1 + (x - vt)^2} + \frac{1}{1 + (x + vt)^2} \right]$$

$$v = 1/2 \left[\frac{1}{1 + (x - vt)^2} - \frac{1}{1 + (x + vt)^2} \right]$$

Rome Air Development Center
Air Force Systems Command
AF-30(602)-2149

M. Sandler

References

1. E. Levi and M. Sandler, "On Hydromagnetic Flow," Symposium on Magneto-hydrodynamic Electrical Power Generation, King's College, University of Durham, Newcastle-upon-Tyne, England, September 1962.
2. R. Courant and K.O. Friedrichs, "Supersonic Flow and Shock Waves" (New York: Interscience, 1948).
3. K.O. Friedrichs, "General Theory of High Speed Aerodynamics (Princeton: Princeton University Press, 1954).

III - SOLID STATE AND MATERIALS RESEARCH

Altschuler, H. M.	Griemsmann, J. W. E.	Marom, E.	Silber, L. M.
Banks, E.	Juretschke, H. J.	Menes, M.	Sobel, A.
Bergstein, L.	Kahn, W. K.	Nahemow, M.	Stark, H. M.
Carlin, H. J.	Kiszenick, W.	Riley, R.	Stevens, M. T.
Eschwei, Mary A.	Levey, L.	Rudner, Beulah	Sucher, M.
Farber, H.	Lohr, R. F.	Schleuning, H. W.	Yang, W.
Freedman, S. J.	Marcuvitz, N.	Shulman, C.	

A. ACOUSTIC EXCITATION OF MAGNETOELASTIC WAVES IN FERRITES

S. J. Freedman

Kittel¹ has shown that the normal modes in an elastic, ferromagnetic solid consist of strongly coupled magnetoelastic waves in the region where the uncoupled elastic and spin wave modes have nearly the same frequency and wavenumber. It can be shown that the difference in group velocity of these waves is a measure of the exchange constant, while observation of the pulse attenuation will yield direct information about relaxation processes. An experiment is currently in progress to investigate these effects in ferrites.

This paper will consider the problem of the acoustic excitation of these modes at the plane interface, $z = 0$, between an elastically isotropic, nonmagnetic solid and an elastically isotropic, cubically magnetoelastic ferrimagnet. The spectrum for z -directed waves in the ferrimagnet is shown schematically in Fig. III - 1. It can

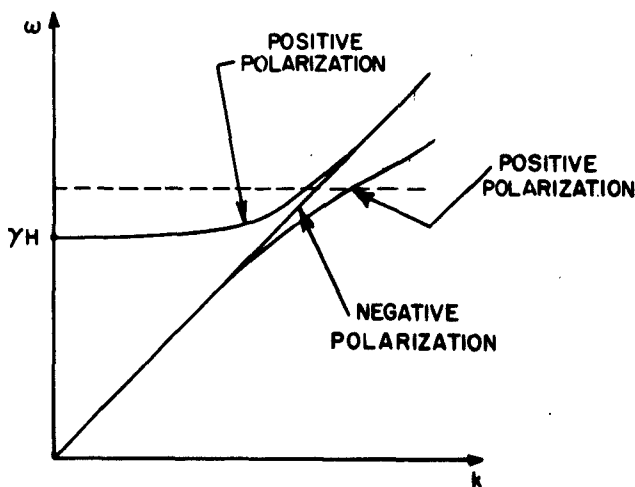


Fig. III-1 Schematic spectrum for coupled magnetoelastic waves in ferrimagnets

be seen from this figure that an acoustic wave may, in general, excite three modes of differing wavenumber: two most conveniently considered to be circularly polarized in a sense which produces ferrimagnetic resonance (positive polarization) and one of opposite circular polarization (negative polarization).

If the static magnetic field H , sufficient technically to saturate the ferrimagnet, is directed along z , and \underline{m} and \underline{R} are the transverse magnetization and elastic displacement respectively, the boundary conditions at the interface may be formulated as follows:

- 1) \underline{R} continuous across boundary;
- 2) Total stress continuous across boundary;
- 3) \underline{m} specified at the interface.

It is important to note that the spin wavelengths involved are much smaller than those characterizing electromagnetic propagation. Hence the latter effects may be neglected.

In order to apply the second boundary condition, one must obtain the stress tensor in a medium exhibiting magnetoelastic coupling. This follows in a straightforward manner from the expression* for the total energy density, ψ (see reference 2):

$$\begin{aligned} \psi = & \alpha \left\{ s_{xx}^2 + s_{yy}^2 + s_{zz}^2 + 2s_{yz}^2 + 2s_{xz}^2 + 2s_{xy}^2 \right\} \\ & + \beta \left\{ s_{xx}^2 + s_{yy}^2 + s_{zz}^2 + 2s_{xx}s_{yy} + 2s_{xx}s_{zz} + 2s_{yy}s_{zz} \right\} \\ & + 2b \left\{ a_y s_{yz} + a_x s_{zx} \right\} \end{aligned} \quad (1)$$

where the s_{ij} are the pure elastic strains; α and β are the elastic constants; b is the magnetoelastic coupling constant; and \underline{a} is a unit vector in the direction of magnetization. The components of the stress tensor, S_{ij} , follow from:

$$S_{ij} = - (\partial \psi / \partial s_{ij}) \quad (2)$$

We obtain for the pertinent components:

$$S_{yz} = 2\alpha (\partial R_y / \partial z) + (2b/M_s) m_x, \quad S_{zx} = 2\alpha (\partial R_x / \partial z) + (2b/M_s) m_y \quad (3)$$

*Expression follows upon assumption $|\underline{m}| \ll M_s$.

SOLID STATE AND MATERIALS RESEARCH

where M_s is the saturation magnetization.

The appropriate conditions on \underline{m} at the surface have not yet been decided experimentally. For the purpose of this calculation, we will use the general isotropic condition:

$$\underline{m} + \lambda (\partial \underline{m} / \partial z) \quad (4)$$

where λ is an adjustable parameter.

At fixed, real, exciting frequency ω , the wavenumbers k_1 and k_2 for the two positive modes are obtained from the dispersion relation:³

$$k^4 \left\{ \frac{a}{\rho} (\gamma D) \right\} - k^2 \left\{ \frac{a}{\rho} (\omega - \gamma H) + \gamma D \omega^2 + (\gamma b^2 / \rho M_s) \right\} + \omega^2 (\omega - \gamma H) = 0 \quad (5)$$

where γ is the gyromagnetic ratio, D is the exchange constant, ρ is the density, and H is the internal (demagnetized) magnetic field.

The wavenumber k_3 for the negative mode is obtained from:

$$k^4 \left\{ \frac{a}{\rho} (\gamma D) \right\} + k^2 \left\{ \frac{a}{\rho} (\omega + \gamma H) - \gamma D \omega^2 + (\gamma b^2 / \rho M_s) \right\} - \omega^2 (\omega + \gamma H) = 0 \quad (6)$$

For a transverse elastic wave of amplitude I , polarized in the $x - z$ plane, incident normally on the interface, application of the boundary conditions leads to the following expressions for the relative amplitudes of the reflected (plane polarized) modes, ρ_x and ρ_y , and also of the transmitted (circularly polarized) modes, R_1 , R_2 , R_3 :

$$\rho_y = \frac{i}{2A^+} \left\{ \frac{[-A^+ + M(C-D)] [A_1 E^- C - A_2 F^- D] + [A^- - M(C-D)] [A_1 E^+ C - A_2 F^+ D]}{[A_1 E^+ C - A_2 F^+ D]} \right\} I$$

$$\rho_x = \frac{1}{2A^+} \left\{ \frac{[A^+ + M(C-D)] [A_1 E^- C - A_2 F^- D] + [A^- - M(C-D)] [A_1 E^+ C - A_2 F^+ D]}{[A_1 E^+ C - A_2 F^+ D]} \right\} I$$

$$R_3 = \frac{1}{2} \{ I + \rho_x - i \rho_y \} \quad (7)$$

$$R_2 = \frac{k_A^a A_1}{2a_B} \frac{\{ I - \rho_x - i \rho_y \}}{A_1 k_2 C - A_2 k_1 D}$$

$$R_1 = -\frac{A_2 D}{A_1 C} R_{2x}$$

where:

$$A^{\pm} = a_A k_A \pm a_B k_3 ;$$

$$E^{\pm} = a_A k_A \pm a_B k_2 ;$$

$$F^{\pm} = a_A k_A \pm a_B k_1 ;$$

$$C = i + \lambda k_1 ;$$

$$D = i + \lambda k_2 ;$$

$$A_1 = -\gamma b k_1 \left(\omega - \gamma H - H_{ex} a^2 k_1^2 \right)^{-1} ;$$

$$A_2 = -\gamma b k_2 \left(\omega - \gamma H - H_{ex} a^2 k_2^2 \right)^{-1} ;$$

$$M = i b a_A A_1 A_2 k_A (k_2 A_1 C - k_1 A_2 D)^{-1} ;$$

and the subscripts A and B refer respectively to the nonmagnetic solid and ferrimagnet.

In continuing research, these calculations will be extended to include attenuation, and machine computations will be started.

Joint Services Technical Advisory Committee
AF-AFOSR-62-295

S. J. Freedman

References

1. C. Kittel, "Interaction of Spin Waves and Ultrasonic Waves in Ferromagnetic Crystals," *Phys. Rev.*, Vol. 110, p. 836 (1958).
2. R. Becker and W. Döring, "Ferromagnetismus" (Berlin: J. Springer, 1939), Chap. 11, p. 136.
3. E. Schlömann, "Generation of Phonons in High Power Ferromagnetic Resonance Experiments," Technical Memorandum T-217, Raytheon Co. (March 16, 1960).

B. HARMONIC GENERATION IN MAGNETIC MATERIALS THROUGH GALVANO-MAGNETIC INTERACTIONS

L. M. Silber, H. Stark

We are undertaking an investigation of the harmonic fields generated by galvanomagnetic interactions in thin films of ferromagnetic metals and ferrites. This is an extension of previous work on galvanomagnetic interactions in thin ferrite films,¹ and nickel films.^{2, 3}

SOLID STATE AND MATERIALS RESEARCH

In an isotropic ferromagnetic material the magnetization \underline{M} interacts with the current density, such that the total current density \underline{J} is given by:

$$\underline{J} = \sigma \left[\underline{E} - (\Delta\rho/M^2)(\underline{J} \cdot \underline{M}) \underline{M} + R(\underline{J} \times \underline{M}) \right] \quad (1)$$

where $\Delta\rho$ is the magnetoresistance anisotropy, and R is the extraordinary Hall coefficient. The interaction of a ferromagnetic material with electromagnetic radiation may then be formally described by Maxwell's equations, the appropriate equation of motion for \underline{M} , and Eq. (1) above. However, the nonlinear terms introduced by (1) are quite small, so that it is appropriate to solve the linear problem, and to include the nonlinear effects as a first-order correction.

Denoting the small oscillating component of \underline{M} by \underline{m} , so that $\underline{M} = \underline{M}_0 + \underline{m}$, the correction terms due to (1) become

$$\underline{j} = -(\Delta\rho/\rho M_0^2)(\underline{J} \cdot \underline{M}_0)\underline{M}_0 + R\sigma \underline{J} \times \underline{M}_0 \\ + \sigma \underline{e} - (\Delta\rho/\rho M_0^2) \{ (\underline{J} \cdot \underline{M}_0)\underline{m} + (\underline{J} \cdot \underline{m})\underline{M}_0 \} + R\sigma (\underline{J} \times \underline{m}).$$

The second line, which can be rewritten

$$\underline{J} = \sigma \left[\underline{e} - (\Delta\rho/M^2) \{ (\underline{J} \cdot \underline{m}) \underline{M}_0 + (\underline{J} \times \underline{m}) \times \underline{M}_0 \} + R(\underline{J} \times \underline{m}) \right] \quad (2)$$

contains terms of zero frequency and second harmonic. This can be seen as follows.

Each of the terms of \underline{J} and \underline{m} is of the form $\text{Re } f(\underline{r}) e^{i\omega t}$ and $\text{Re } g(\underline{r}) e^{i\omega t}$, respectively. Neglecting the vector character, the product is of the form

$$1/2 [f'g' + f''g'' + \text{Re } fg e^{i2\omega t}] ,$$

where the first two terms give the dc fields; the third term, in the usual notation $fg e^{i2\omega t}$ is the second harmonic.

Prof. Juretschke² has suggested that this accounts for observed dc fields. He has computed results for these components for the case of a thin film backed by a short in a waveguide, and has also solved the one-dimensional problem for arbitrary orientation of the dc magnetic field in the plane of the film. Egan and Juretschke subsequently measured the dc field in nickel, confirming the predictions of the theory.³ Both theory and measurements were extended to ferrites, and the dc effect was observed in films of magnetite.⁴

In order to obtain quantitative information from a measurement of the second harmonic fields, it is necessary to know the incident radiation field patterns within

SOLID STATE AND MATERIALS RESEARCH

the magnetic material. Under the assumption that the H_{10} mode in the empty waveguide couples entirely into an H_{10} type mode in the magnetic film, these patterns are obtained quite simply. For a conducting magnetic material the above assumption is reasonable. From the field patterns obtained and the correction term (see Eq. (2)), the second harmonic fields generated in the various modes are obtained.

The results indicate that the second harmonic power in the H_{01} should be of the order of 10^{-16} P incident (both powers in watts) for nickel at 9 kmc. For powers that are easily obtainable (within the magnetron range), 1 kw, for example, the resultant harmonic power is 10^{-10} watts.

In order to detect this, a spectrum analyzer was modified so that the minimum detectable signal is 10^{-12} watts. As a power source, we intend to use a radar beacon whose maximum output is about 15 kw.

The second harmonic power in the source was investigated. We found that with an appropriate low-pass filter it could be reduced to 20 db below the second harmonic power generated in the film.

A measurement of the second harmonic fields would provide a valuable check on the existing theory. In addition, since we can measure both the magnitude and phase of the fields generated, it might prove possible to obtain the material constants in a more direct manner.

National Science Foundation
GP-753

L. M. Silber, H. Stark

References

1. W. Heinz and L. Silber, "DC Effects in Ferromagnetic Resonance in Thin Ferrite Films," J. Appl. Phys. Suppl., Vol. 33, p. 1306 (March 1962).
2. H. J. Juretschke, J. Appl. Phys., Vol. 31, p. 1401 (1960).
3. W. G. Egan and H. J. Juretschke, to be published in J. Appl. Phys., May 1963.
4. Progress Report No. 21 to the Joint Services Technical Advisory Committee, R-452.21-62, Microwave Research Institute, P. I. B., pp. 54-58.

C. ACTIVE STRUCTURES RESEARCH

H. M. Altschuler, R. F. Lohr, Jr.

As discussed in a previous report,¹ difficulty was encountered in measuring active two-ports at the very low power levels required to avoid ruby saturation. Of the various approaches considered for circumventing these difficulties, the increase

SOLID STATE AND MATERIALS RESEARCH

of sensitivity of the detection equipment by noise reduction was initially deemed to be most promising. Systematic steps were taken in this direction as outlined below.

Leakage paths of signal frequency power from the generator and the bridge to the mixer were reduced systematically in number as well as in their transmission efficiencies. This was accomplished by three distinct means:

- 1) additional shielding of equipment, especially of flexible waveguides;
- 2) substantial reduction of the number of waveguide joints potentially involved in leakage paths;
- 3) lapping of all remaining waveguide flanges for maximum flatness, and silver painting the mated flanges.

Leakage at the i-f frequency was also reduced by additional shielding.

Various methods of reducing receiver bandwidth were explored. The following two methods were judged to have promise: the use of a passive 30 mc crystal band-pass filter and the use of filters at a second, lower, i-f frequency. The second method was tentatively tried and found to be successful in principle. In practice, however, higher quality equipment than is available would have to be used in making such a modification. There is little doubt that a high quality state-of-the-art 30 mc crystal filter would also be successful in this instance.

An alternative means of increasing bridge sensitivity has also been found to be effective, and is now in use. If deemed necessary, reduction of receiver bandwidth by filtering can in addition be employed in order to attain still higher sensitivity. The method involves the interchange of the X-band source and the detection system in the bridge setup employed up to this time.²

A detailed analysis has shown that a bridge, such as that employed in this work for measuring arbitrary (potentially nonreciprocal) linear two-ports, can be subjected to source detector interchange provided that any isolators employed within the bridge itself are reversed appropriately as the interchange is made. Fig. III - 2 shows the two situations in bare outline; the normal bridge has been called a "forward" bridge and the bridge after the interchange a "reversed" bridge.

The results of the analysis can be summarized as follows. If, by a given procedure with the forward bridge the scattering matrix S of the unknown two-port is determined, then the identical procedure with the reversed bridge results in the transposed result, i. e., in \tilde{S} . In other words, the steps which lead to S_{12} in one case lead to S_{21} in the other, and vice versa; the same steps are used to obtain S_{11} and S_{22} in both cases. It follows as a corollary that these bridges would yield transposed

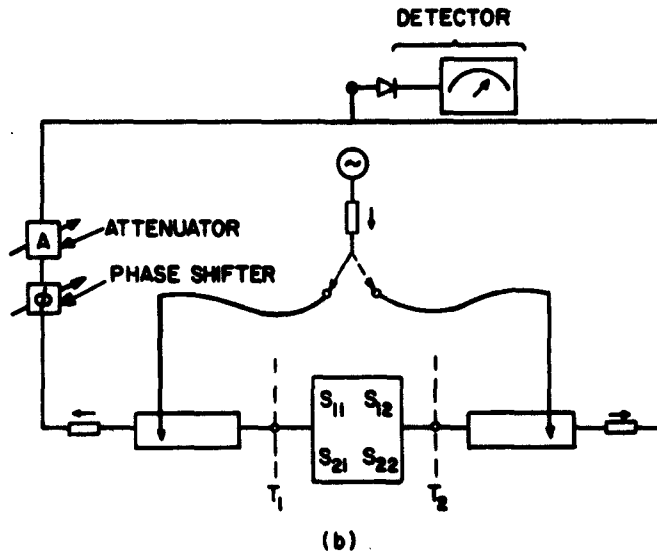
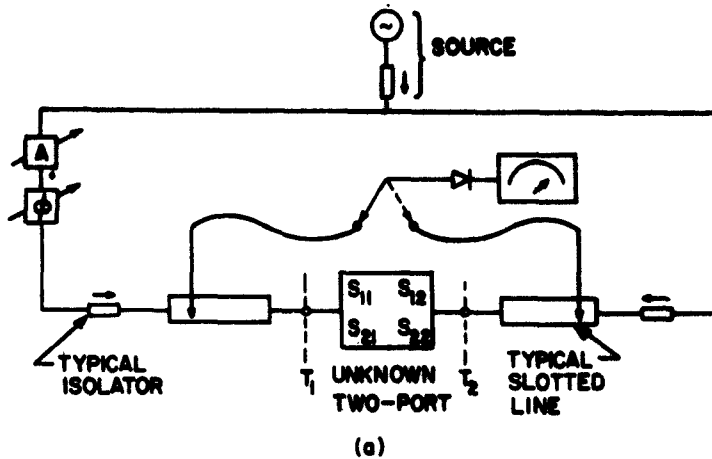


Fig. III-2 (a) Forward bridge: (b) Reversed bridge .

results in impedance and admittance matrix measurements also.

In connection with detector source interchange in bridges, similar interchanges were also considered in the simpler cases of impedance measurements of one-ports (loads), where this technique has long been employed,³ and in the measurement of two-ports by any impedance methods whatsoever. In all these cases the same results are obtained by "forward" and "reversed" measurements.

Known, sufficient conditions³ for the validity of source detector interchange in

SOLID STATE AND MATERIALS RESEARCH

one-port measurements are the following. Both generator and detector must be matched, or in typical slotted line measurements, the probe must be well matched and well decoupled. It has now been found that as long as no approximations whatsoever are made, the necessary and sufficient conditions are as follows. Generator impedance must equal detector impedance. Also, all nonreciprocal two-ports involved in the measurements (other than those "part of" the generator or the detector; see Fig. III - 2) must have constant parameters throughout the measurement. All these conditions were seen to pertain equally well in two-port impedance measurements and in bridge measurements.

Source and detector are interchanged in one-port measurements to provide more signal at the detector when the power level at the unknown structure must be held below a fixed minimum. When sufficient power is available, a reversed measurement may also permit greater withdrawal of the probe in a slotted line as compared with that in a forward measurement. The same ends are served by reversal in two-port impedance and bridge measurements.

While variable phase shifters may have small variable dissipation associated with them, they can give rise to much more serious variations in reflective attenuation when they separate two fixed lossless discontinuities. Such effects have been noted in the bridge used for measuring active structures and a suitable calibration and correction procedure has been devised. It applies specifically to errors arising from this source in the bridge measurement of two-ports by means of circular loci.

Joint Services Technical Advisory Committee
AF-AFOSR-62-295

H. M. Altschuler

References

1. Progress Report No. 22 to the Joint Services Technical Advisory Committee, R-452.22-62, Microwave Research Institute, P.I.B., pp. 68-74.
2. Progress Report No. 14 to the Joint Services Technical Advisory Committee, R-452.14-59, Microwave Research Institute, P.I.B., pp. 12-14.
3. E. L. Ginzton, "Microwave Measurements" (New York: McGraw-Hill, 1957), Sect. 5.13.

D. LOW TEMPERATURE STUDIES

H. Farber

The temperature coefficient of resistance of several cermet resistors has been measured. Problems resulting from radio interference as well as erratic low

frequency ground currents limited the accuracy and reproducibility to $\pm .02^\circ$ K upon cycling to room temperature.

Within these limits, and within the range of 1.7 to 4.2° K the resistors follow a similar law to the carbon resistor, namely $[\log R/T]^{1/2} = A + B \log R$ (see Fig. III - 3). These measurements were made with less than 10^{-8} watts dissipated in

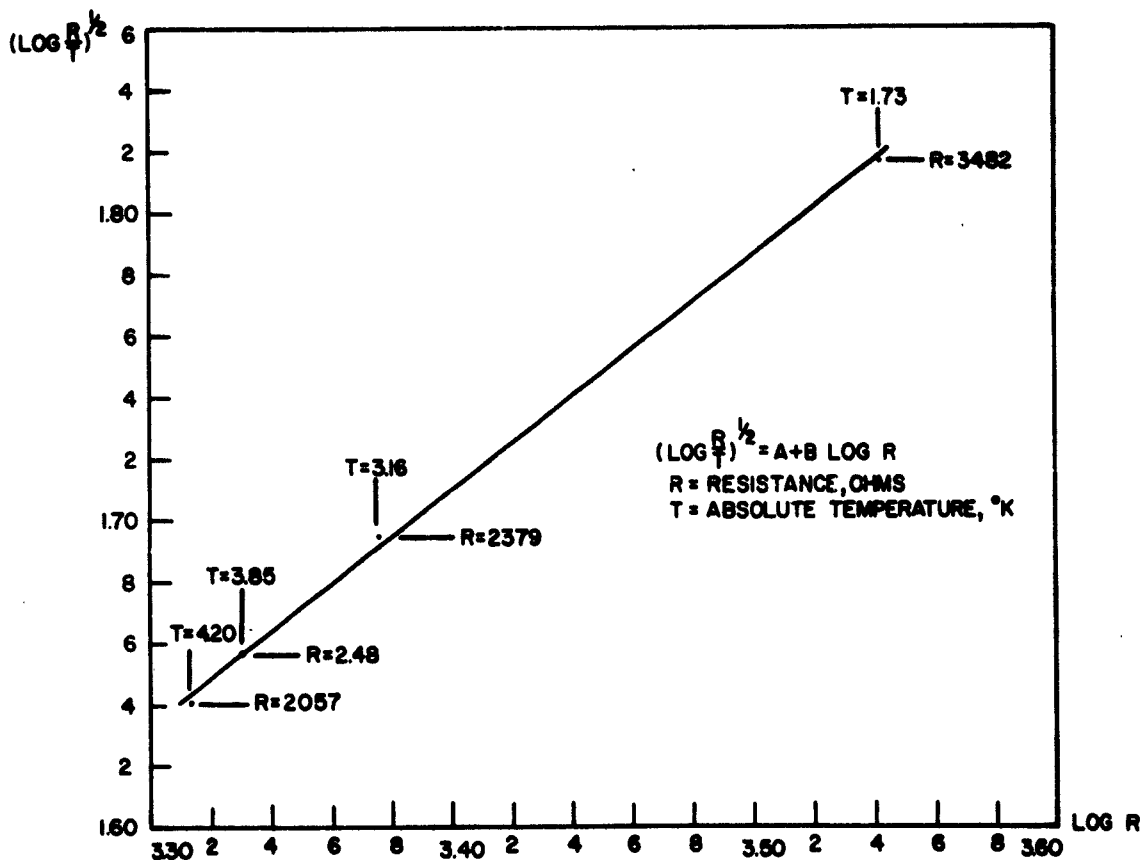


Fig. III-3 Variation of resistance of a cermet resistor with temperature

the sensing resistor. The sensitivity of these resistors $[(1/R) (dR/dT)]$ is 0.3 at 4.2° K.

In forthcoming research attempts will be made to improve the shielding, thus increasing the accuracy and reproducibility of the measuring system prior to starting the study on thin films.

Joint Services Technical Advisory Committee
AF-AFOSR-62-295

H. Farber

SOLID STATE AND MATERIALS RESEARCH

E. BIOMEDICAL ENGINEERING RESEARCH

W. B. Blesser

Medical engineering research at the Polytechnic may be divided roughly into two general, though not mutually exclusive areas (1) analytic studies, and (2) instrumentation. Analytic studies include analysis of physiological responses to applied signals and analog simulation of physiological systems. Instrumentation includes development and design of equipment for medical applications.

This paper presents a brief description of the various projects now in progress. Although the project investigators are in most instances M. A. and Ph. D. students, some project teams include or consist entirely of undergraduate students.

1. Analytic Studies

(a) **E.E.G. Analysis:** Because of the noisy nature of the human electroencephalograph (E.E.G.) it is not possible to perceive signal information directly in the E.E.G. traces. With the use of averaging techniques, however, E.E.G.'s can be processed to yield signal information in response to periodically applied stimuli. Thus, when periodic visual stimuli are applied to a human, a response can be detected in the E.E.G. when average processing techniques are employed.

To date, most of the E.E.G. average response studies have utilized a single known periodic stimulus. We are presently engaged in a project to determine whether the superposition of two periodic signals will yield an E.E.G. response which is the superposition of the two separate responses. The procedure to be followed will be first to determine the E.E.G. response to separately applied visual and auditory stimuli. Then these two periodic signals will be applied simultaneously, and again the E.E.G. average response will be obtained. The three average responses can then be compared to determine whether linear superposition is valid. Two Electrical Engineering M. A. students are the principal investigators for this project.

Most E.E.G. average response investigations deal with the response to externally applied stimuli. Little work, if any, has been done with human E.E.G. responses to self-generated output signals. Two M. A. students are now engaged in an investigation of a subject who delivers a periodic output (e.g., tongue clicks or finger movement). In this case, the periodicity of the signal cannot be accurately controlled so that a special average response program must be developed.

(b) **Dye Dilution Studies:** Dye dilution techniques have long been used by medical researchers to study blood flow in the cardiovascular system. The method is based upon the principle that a fluid volume can be measured if a dye is introduced into the

fluid and the color density of the fluid is compared with some reference density. As applied to cardiovascular studies, the procedure is to introduce a known bolus of dye into the blood stream. Samples of blood are then periodically withdrawn from various body sites (e.g., from the heart). When these samples are analysed, color density vs. time curves can then be drawn. From such curves, information can be obtained about blood flow through the various body organs.

At the present time, interpretation of the dye dilution curves depends primarily on experience gained from repeated tests. The information derived is largely based upon empirical studies. Some work has been done to give a theoretical explanation to the dye curves obtained from specific body organs (the heart and lungs, for example). Relatively little work, however, has been done to explain the curves when the entire cardiovascular system is considered.

One way in which it may be possible to obtain a better quantitative understanding of the dye dilution curves would be to construct a model of the system. The closed loop aspects of the cardiovascular system suggest that one appropriate model might be an analogous electrical feedback model. To construct such a model, the transfer function of the various organs must be at least approximately derived. Preliminary work in this direction has already been initiated. When the various blocks in the system have been described, the entire system will be programmed on a computer. Should the computer results compare favorably with the results of actual dye dilution tests, the computer model could then serve as a useful tool to study blood flow and pathology in the circulatory system.

As an alternate model representation of the circulatory system, we are simultaneously constructing a mechanical model of the heart and other important organs of the system. With such a model it may be possible to simulate the distribution of dye when it is injected into the human blood stream. From actual measurements on the model we can then study the dye dilution as the dye courses through the circulatory system.

(c) Adaption during Tracking: The transfer characteristics of a human engaged in an eye-hand operation has been the subject of much experimental investigation. In most investigations, the overall "average" transfer function has been obtained by averaging the responses of a large number of sample runs. This technique does not permit an examination of the adaptation mechanism of the operator which in a man-machine system is probably as significant as, if not more significant than, the overall transfer function. Instead of average processing a number of overall responses, we are presently attempting to examine each tracking response in an attempt to discern when and how the human operator changes his mode of behavior.

SOLID STATE AND MATERIALS RESEARCH

2. Instrumentation

(a) **Average Response Computer:** While it is true that average response computers are available commercially, most of these are prohibitively expensive for most institutions. We are presently trying to construct a cheaper average response computer which utilizes analog rather than digital signals. This method employs a simple operational amplifier as an averaging device and a tape transport as a delay line. The periodic signal is recorded on the tape sequentially and the amplifier adds each periodic signal to each successive periodic signal. The overall sum is continuously recorded on a different channel of the tape.

(b) **Body Plethysmograph:** The body plethysmograph is generally used to measure body dimensional changes during respiration. The unit is an airtight chamber with controllable breathing vents. When a patient is enclosed, the chest movements cause pressure changes in the chamber and these can be recorded and calibrated to give body volume changes. By special experimental techniques this same unit can be used to record the blood flow through the pulmonary system.

Many of the body plethysmograph units in use today use pressure measurements to indicate volume changes because direct volume measurements cannot be made rapidly or accurately. Such a procedure gives rise to sealing problems, since any small leakage would invalidate the result. The sealing problem, which appears to be a relatively simple engineering problem, has been assigned to two undergraduate Mechanical Engineering students. The students are attempting to design a unit with minimum leakage and maximum practical structural rigidity. Upon completion of the unit, an attempt will be made to incorporate a pressure servo unit into the system. The servo system will act to maintain the plethysmograph internal pressure at some predetermined level by mechanically providing the proper volume changes. By such a procedure, the required volume changes could be directly recorded and the plethysmograph pressure could be maintained at a value close to ambient pressure so as to minimize the effects of leakage.

(c) **Bone Conduction:** When a broken bone is in a cast it is not possible to use X-ray techniques to determine the extent of bone healing. In order to get some measure of the healing of the bone, it has been suggested that one can utilize the sound transmission characteristics of the bone. An Electrical Engineering student is now working on a project to discern how well a bone transmits sound as well as what happens to the wave shape of sound when the bone is broken and progressively heals.

Joint Services Technical Advisory Committee
AF-AFOSR-62-295

W. B. Blesser

IV - MICROWAVE CIRCUITS

Altschuler, H.M.	Hessel, A.	Morrone, T.	Ruddy, J.M.
Birenbaum, L.	Jacenko, D.	Nussbaum, M.L.	Shenkel, H.
Carlin, H.J.	Kahn, W.K.	Oliner, A.A.	Shmoye, J.
Farber, H.	Klinger, M.	Pepper, R.	Stadmire, H.
Goldie, H.	Kohavi, Z.	Reynolds, A.L.	Sucher, M.
Griemsmann, J.W.E.	Levey, L.	Rosenbaum, S.	Weis, A.
Grimza, E.	Malloy, G.	Rosenthal, S.W.	

A. HIGH-POWER FACILITY

E. Grimza, S.W. Rosenthal, M. Sucher

The high-power C-band microwave system is being used at present for a number of experiments. The system is particularly adaptable for this wide variety of experiments because of its inherent flexibility; in effect, it is a high-power microwave signal generator. As indicated in earlier reports, the system is variable in pulse width to 10 μ sec. It has a repetition rate consistent with a duty cycle of .001, power up to 10 megawatts peak, 10 kilowatts average, and it can be swept with respect to frequency.

The experiments presently associated with the system are as follows:

1. Plasma Diagnostics

A hydrogen plasma is being generated by the high-power microwave pulse. Associated with this is a microwave interferometer, operating at 36.5 kmc cw, which will measure the average electron density of this transient hydrogen plasma. This is accomplished by the simultaneous measurement of the signal transmitted through the plasma and the magic tee difference-arm signal, which yields the desired phase shift and hence electron density information.

2. Fast High-Power Microwave Switching

Two high-power microwave, nanosecond switches are being experimented with, using the high-power signal generator. These switches, a thyatron-type switch and a dc triggered high-pressure discharge switch, make use of the variable parameters of the high-power system. The switch experiments, described in Section IV - C of this Progress Report, are leading to the development of a dischargeable C-band traveling-wave resonator.

3. Hypersonic Shock Wave Interaction

The high-power microwave system has been used as a source for experiments involving the interaction of high microwave power and a hypersonic shock wave.

4. Metal Failure

Experiments concerned with the study of the failure characteristics of metals

MICROWAVE CIRCUITS

subjected to high microwave power are in progress. These experiments make use of both the high peak as well as the high average powers available. The flexibility of the system contributes to the wide range of experimental possibilities. These experiments are discussed in detail in Section IV - B of this Progress Report.

Rome Air Development Center
Air Force Systems Command
AF-30(602)-2135

S. W. Rosenthal

B. INTERACTION OF HIGH MICROWAVE FIELDS WITH METALS

H. Farber, G. Malloy, H. Shenkel

The study of the interaction of high microwave fields with metals (aluminum, stainless steel and copper) has been continued. In a previous report¹ it was noted that a coaxial cavity resonant in the TE_{011} mode was being used. The test sample was the inner, hollow conductor (2 - 1/2" x 1/3" diameter x 1/8 - 1/16" wall). In order to differentiate between field effects and heating effects a comparative series of tests was conducted using pulsed power with a duty cycle of 10^{-3} and cw power.*

A summary of the results of these tests is given below:

a) For stainless steel, as little as 50 watts average power into the cavity** heated the sample so that it glowed a dull red, and 400 watts average input power produced an optical temperature of 2000°F within several seconds. The cavity was in an evacuated condition during these tests.

The above tests were carried out using cw and pulsed power and no measurable difference was observed.

b) At power levels of 600-650 watts cw stainless steel samples were melted within 3-30 seconds. The melted regions ranged from 1/16" to 1/4" along the axial dimension.

c) At 450 watts input, a copper center conductor was heated to a dull red heat in one minute.

*These tests were performed at the Sperry Electron Tube division in Gainesville, Florida. Their cooperation is gratefully acknowledged.

**When the center conductor is at the same temperature as the outer walls, 20-60 percent of the input power is absorbed by the center conductor depending on its relative surface resistance to the wall surface resistance, which was that of copper at the start of each test (see paragraph (e) above).

MICROWAVE CIRCUITS

d) For aluminum center conductors, 400 watts average (using pulsed power) were required to melt the sample.

e) In the above tests with stainless steel center conductors, the walls became coated with a nickel-iron mixture. An aluminum coating was obtained when the center conductor was made of aluminum.

f) In one experiment at atmospheric pressure, with a stainless steel center conductor, 450 watts cw were required to raise its temperature to 2000°F instead of the 400 watts reported in paragraph (a).

Breakdown problems in the cavity or the feed waveguide prevented using higher powers. In the case of pulsed power, the high microwave fields in the evacuated (10^{-5} mm Hg) cavity caused multipactor breakdown. In the case of cw power, rf heating probably caused thermal emission which then caused breakdown in the cavity. The cavity could probably be redesigned to decrease these problems so that it would be possible to use higher powers.

The cavity may be considered to be an impedance matching device for coupling the microwave energy into the metallic surface. To compare this with a uniformly illuminated surface in free space, 450 watts coupled into the cavity would result in the same power absorption in a one sq. cm central region of the sample as that produced by an illumination of 450 kw/cm² in free space on an equal (unit) area of the metal.

Rome Air Development Center
Air Force Systems Command
AF-30(602)-2135

H. Farber

Reference

1. Progress Report No. 22 to the Joint Services Technical Advisory Committee, R-452.22-62, Microwave Research Institute, P. I. B., pp. 93-98.

C. DC TRIGGERED MICROWAVE SPARK GAP SWITCH

H. Farber, M. Klinger, M. Sucher

As part of the development of a dischargeable C-band traveling wave resonator, work on two types of fast, high-power, low-loss, microwave switching devices has been in progress. One of these is essentially a microwave hydrogen thyratron having an rf power holdoff capability of more than one megawatt (at one microsecond pulse width) and a switching time of less than 30 nanoseconds. This device was described in detail in a previous report.¹ The present device may be described as a dc triggered

MICROWAVE CIRCUITS

microwave spark gap.

In the present form of the switch, the spark occurs in air at normal atmospheric pressure. It is initiated by a narrow 15 kv dc voltage pulse of half sinusoid shape applied between a central electrode, entering the waveguide through one of the side walls, and two opposing hemispheres on the broad walls which constitute the spark gap. The basic form of the switch is shown in Fig. IV - 1.

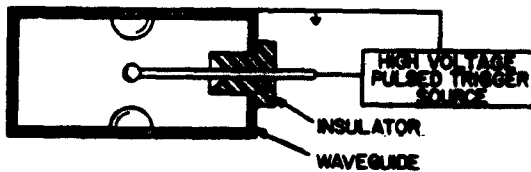


Fig. IV-1 Schematic of dc triggered microwave spark gap.

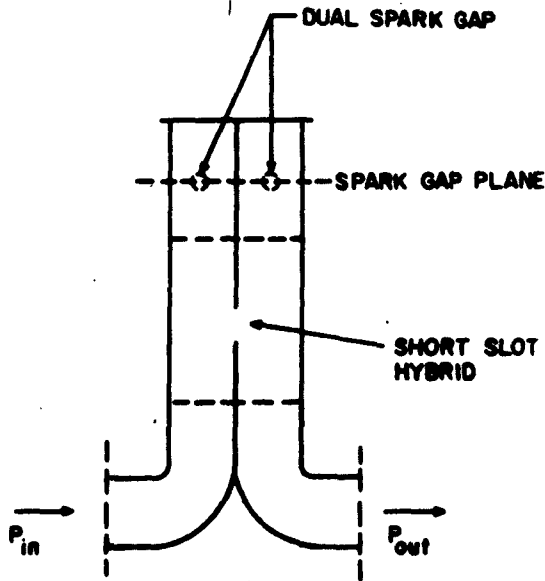


Figure IV-2

is triggered, the stored energy of the resonator is applied to a load or antenna as before, and the pulse duration is the time taken by a wave to travel from one end of the cavity to the opposite end and back.

By properly positioning a short circuit behind the spark gap, a standing wave minimum may be shifted by a quarter guide wavelength upon triggering a discharge. Therefore, by using two similar spark gaps symmetrically arranged in conjunction with a short-slot hybrid, as shown in Fig. IV - 2, one may achieve a 180 degree phase shifter through the switching action of the spark gaps. This device can in turn be used in association with two other hybrids to close the loop of a traveling-wave resonator.

When the switch is in the unfired condition, a traveling wave will circulate in the ring. When the switch is fired, the stored energy of the resonator can be discharged into an external load or fed into an antenna in the form of an enhanced rectangular pulse whose duration equals the time taken for the wave to traverse the length of the ring.

If desired, one may use a long line cavity resonator instead of a ring resonator. In this case, only a single spark gap and hybrid (as shown in Fig. IV - 3) are required. In the unfired state the combination simply acts as a short circuit terminating one end of the cavity. When the discharge

MICROWAVE CIRCUITS

The present switch characteristics (see Fig. IV - 4) are as follows:

Peak rf holdoff power:	About one megawatt (independent of pulse width)
rf switching time:	< 10 nanoseconds
"Cold" insertion loss (unfired condition):	0.1 to 0.2 db
Isolation (fired condition):	17 db (may be appreciably better in dual spark gap arrangement)
Arc loss (fired condition):	0.2-0.3 db (at rf levels above 30 percent of holdoff power)
Jitter:	None could be observed on a Tektronix 545 scope operated at a horizontal sweep of 20 nanoseconds/cm.

The characteristics of the dc trigger are as follows:

Pulse amplitude:	10-15 kv
Pulse shape:	Half sinusoid of 10-15 nanoseconds duration
Pulse rise time:	~ 5 nanoseconds

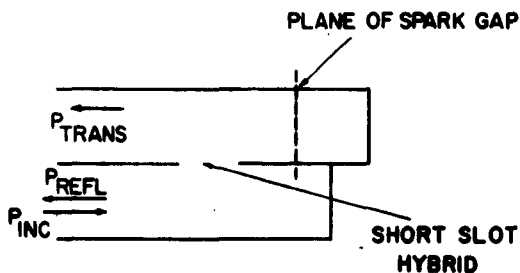


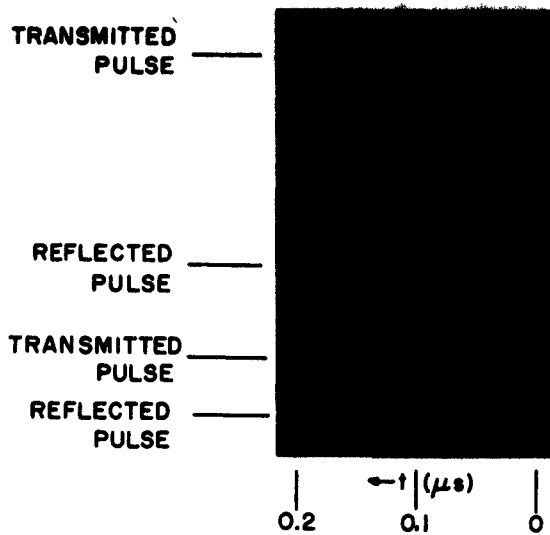
Fig. IV-3 Test arrangement for dc triggered microwave spark. (Terminating shorts are arranged so that P_{trans} is maximum in absence of spark. When spark is triggered, P_{trans} drops and P_{refl} rises. Isolation is defined as $10 \log (P_{inc}/P_{trans})$ and arc loss as $10 \log (P_{inc}/P_{refl})$ for switch in triggered state.)

Switching action during an rf pulse of 2 microseconds duration is illustrated in Fig. IV - 4 for an rf power level of 600 kw. (Because of the expanded time scale, the beginning and end of the rf pulse cannot be seen.)

The pulse generator is capable of supplying a 35 kv video pulse, but 15 kv suffices to break down the gap at atmospheric pressure. With moderate pressurization of the switch it should be possible to utilize the full 35 kv output of the video pulse source and greatly enhance the rf holdoff capability. The switch construction is now being modified so that it can be pressurized.

The switch has also been used to

MICROWAVE CIRCUITS



RF POWER: 600 kw

DC TRIGGER: 15 kv

SCOPE: TEKTRONIX 545 A

SWEEP TIME: 20 NANOSECONDS/cm

Fig. IV-4 Oscillograms of switching by dc triggered microwave spark

discharge the stored energy in a moderately long, copper-walled waveguide cavity resonator (overall length including switch and auxiliary components is about 15 feet). A 10 db directional coupler whose main arm was terminated in a movable short and whose auxiliary arm was part of the cavity resonator was used as the input coupling device. The arrangement is shown in Fig. IV - 5. Oscillograms of the envelope of the rf output pulse are shown in Fig. IV-6.

The peak value of 0.5 Mw attained in the output pulse represented a gain of from 8-10 db above the input, which was in the form of a 4 microsecond rf pulse. The pulse rise time is seen to be about 10 nanoseconds, which is also the response time of the oscilloscope.

There are several modes of operation of this switch depending on the level of microwave power. At relatively low rf levels the discharge is maintained solely by the dc trigger source. At higher microwave power levels the discharge can be maintained jointly by the dc source and microwave fields, while at sufficiently high microwave power the latter alone suffices to maintain the discharge. In this case only a dc voltage pulse of short duration is required (merely to trigger the discharge), and the external dc source power requirements are relatively low.

The rise time for the build-up of a discharge across the gap is a function of the overvoltage ratio, i. e., the ratio of applied electric field to threshold electric field. The threshold electric field is defined as the field which, if maintained indefinitely, will produce breakdown; it is, therefore, the minimum field at which breakdown can occur. When dc and rf fields are superposed, an effective breakdown field can be defined which is a function of both types of field. Breakdown can then be discussed in terms of the effective field.

At low microwave powers the effective breakdown field is essentially the dc

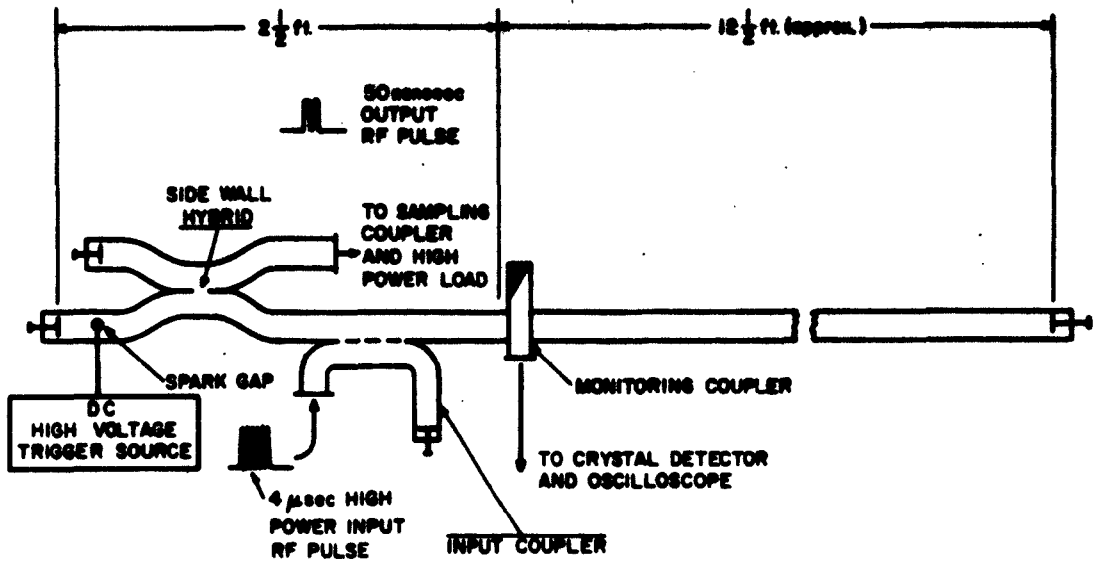
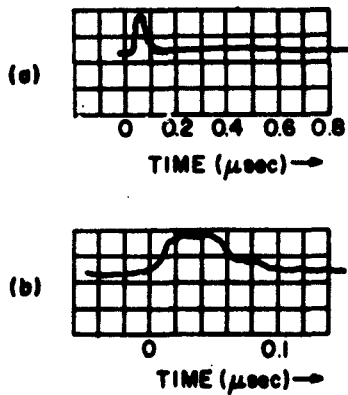


Figure IV-5



RF POWER: 500 kw
 DC TRIGGER: 15 kv
 SCOPE: TEKTRONIX 545A

Fig. IV-6 Oscillograms of the envelope of rf output pulse. (a) $0.1 \mu \text{ sec/cm}$ sweep; (b) 20 nanosec/cm sweep.

MICROWAVE CIRCUITS

field. However, when the microwave power exceeds 70 percent of the self-breakdown power, the effective field becomes strongly dependent on the microwave power level. The rise time for the discharge rapidly decreases as the overvoltage ratio rises above unity and, for a ratio of two, becomes a few nanoseconds for reasonable gap lengths. This is the basis for the rapid switching realizable by means of this device.

An analysis has been made of the relation between breakdown time (based on a streamer-photoionization mechanism) and the overvoltage ratio, taking into account the superposition of the two types of field. This study will be described in a forthcoming memorandum.

Rome Air Development Center
Air Force Systems Command
AF-30(602)-2135

M. Sucher

Reference

1. Progress Report No. 22 to the Joint Services Technical Advisory Committee, R-452.22-62, Microwave Research Institute, P.I.B., pp. 83-93.

D. ELECTRICAL BREAKDOWN AT MICROWAVE FREQUENCIES OF GASES AT RELATIVELY HIGH PRESSURES

H. Farber

Experimental measurements on the static breakdown of gases at very high pressures show that Paschen's Law is not obeyed in this region. At the higher pressures the breakdown potential is less than it would have been if Paschen's Law were obeyed.

The Fowlen-Nordheim theory for emission from a cold cathode surface would require fields of 10^7 - 10^9 v/cm for appreciable electron current to lower the static breakdown potential. On the other hand, the secondary Townsend coefficient should be lowered by the increasing pressure and the result should be an increase in breakdown potential. The lowering of the breakdown potential, relative to the prediction of Paschen's curve occurs at approximately 10^5 v/cm.

At microwave fields one can conveniently generate fields in excess of 10^5 v/cm without using electrode surfaces, e.g., the TE_{01} mode in cylindrical waveguide.

An experimental study of the breakdown of gases in the relevant pressure ranges is being made to determine the influence of field-emitted electrons on the measured values of the breakdown strength. A cylindrical cavity resonant in the TE_{011} mode has been designed and is being constructed (see Fig. IV - 7). Another cavity resonant

MICROWAVE CIRCUITS

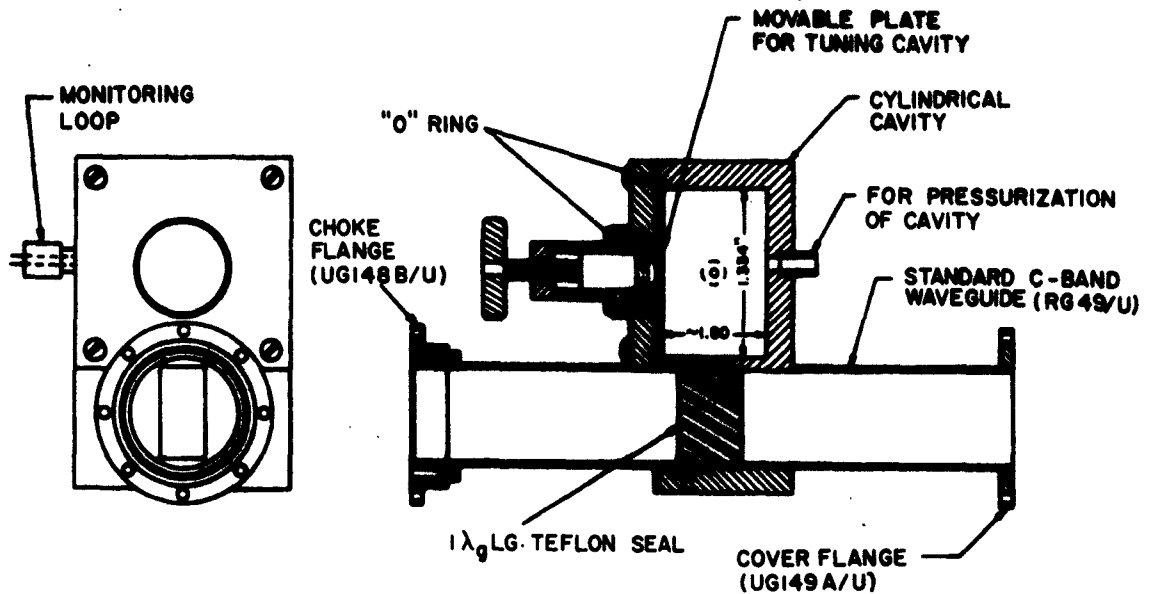


Fig. IV-7 Tunable high pressure cylindrical cavity TE_{011} mode; $f_0 = 5.5$ Gc.

in the TM_{010} mode is currently being designed so that a comparison between electrode and electrodeless breakdown can be made.

Office of Naval Research
Nonr-839(35)

H. Farber

E. ABSORBING MATERIAL USING PARALLEL RESISTIVE SHEETS

J. W. E. Griemsmann, K. Suetake

One class of absorbers utilizes parallel resistive sheets in various forms, such as honeycomb or egg-box construction, as shown in Fig. IV - 8. Resistive sheets are arranged to lie in at least two directions so as to provide for absorption of any polarization. Such grid structures are inherently difficult to analyze and are usually realized through experimentation with various parameters including resistance values and spacing. The analysis presented here can be used to obtain the design data for these parameters.

The configuration to be studied is shown in Fig. IV - 9(a). An absorber is set up with many parallel, infinitely thin resistive sheets which have the surface resistance R_s (ohm per square) and are separated from one another by a lossless, low dielectric

MICROWAVE CIRCUITS

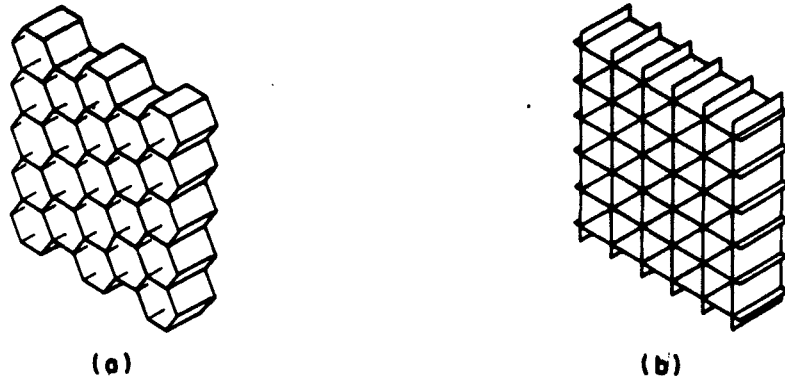


Fig. IV-8 Absorbers utilizing parallel resistive sheets. (a) Honeycomb construction; (b) Egg-box construction.

constant material of thickness p . Only the electromagnetic field associated with the TE mode propagating in the z -direction need be considered since this provides the basic means of absorption.

When both horizontal and vertical resistive sheets are used, the incoming radiation can always be decomposed in such a manner that vertically and horizontally polarized TE_{10} modes are excited. The analysis thus has more general usage than the case analyzed.

For the purposes of analysis, all the resistive sheets are considered to be split into two halves, each having a surface resistance $2R_s$ (ohms). Further, by virtue of symmetry of the configuration, fictitious sheets which have infinite resistance can be considered to be inserted between the split resistive sheets and also to be the center planes between the resistive sheets,

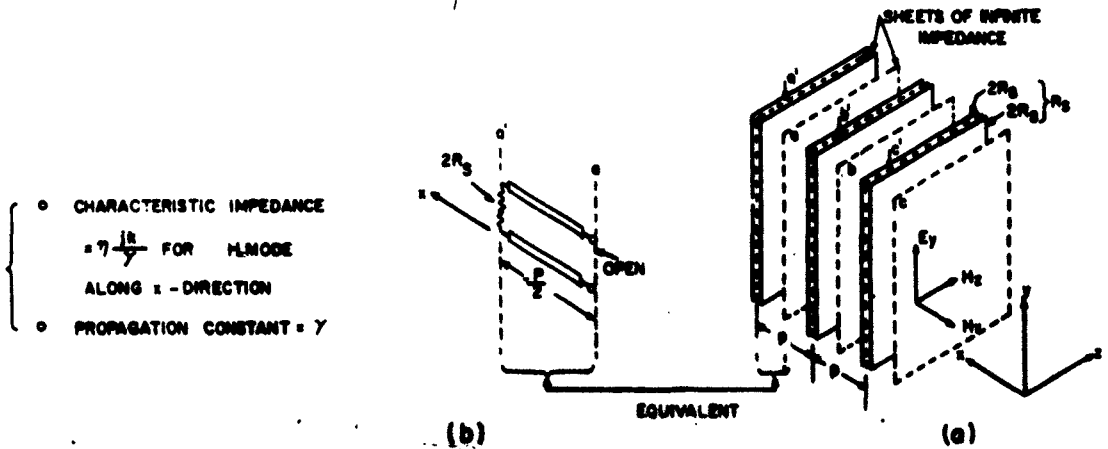


Fig. IV-9 (a) Configuration; (b) Equivalent circuit.

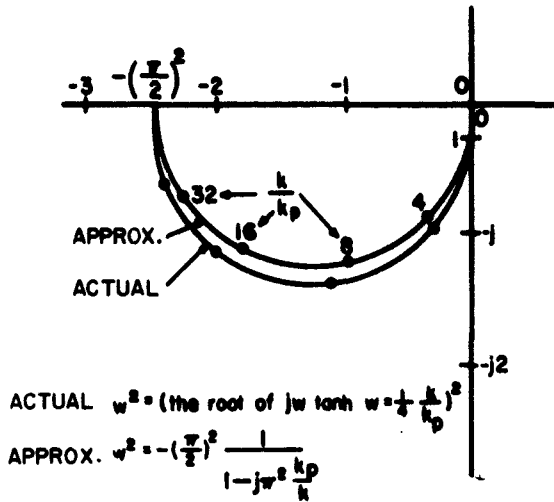


Fig. IV-10 Locus of w^2 vs. k/k_p

This situation will lead to the transverse resonance condition (see Fig. IV-9(b)):

$$2 R_g = -\eta (j k / \gamma) \coth \gamma (p / 2)$$

or (1)

$$z(w) = jw \tanh w = (kp/4) (\eta/R_g)$$

where $w = \gamma (p/2)$, γ is the propagation constant in the transverse x -direction, and $\eta = 120 \pi \sqrt{\mu} \epsilon$ and $k = (2\pi/\lambda) \sqrt{\mu} \epsilon$ are respectively the intrinsic impedance and phase constant of the medium of separation.

If the values of R_g and p are given and w is determined as a root of Eq. (1), then the propagation constant in the z -direction,

Γ , and the characteristic impedance Z_z will be obtained from the relations,

$$\Gamma = j\sqrt{k^2 + \gamma^2} \quad \text{or} \quad \Gamma(p/2) = j\sqrt{[k(p/2)]^2 + w^2} \quad (2)$$

and

$$Z_z = \eta (jk / \Gamma) = \eta \frac{k(p/2)}{\sqrt{[k(p/2)]^2 + w^2}} \quad (3)$$

The complex root, $w = \mu + jv$, however, is not readily obtained, because Eq. (1) is transcendental. This paper presents an approximate simple formula in terms of w^2 (see Fig. IV - 10):

$$w^2 = -(\pi/2)^2 \frac{1}{1 - j\pi^2 (k_p/k)} \quad (4)$$

where

$$k_p = (1/p) (R_g/\eta) .$$

Using this formula, the propagation characteristics of the absorbing material as a function of frequency are obtained, with the help of the conformal mapping technique. The result is shown in Fig. IV - 11.

The maximum attenuation constant, α_{max} , for the electromagnetic waves propa-

MICROWAVE CIRCUITS

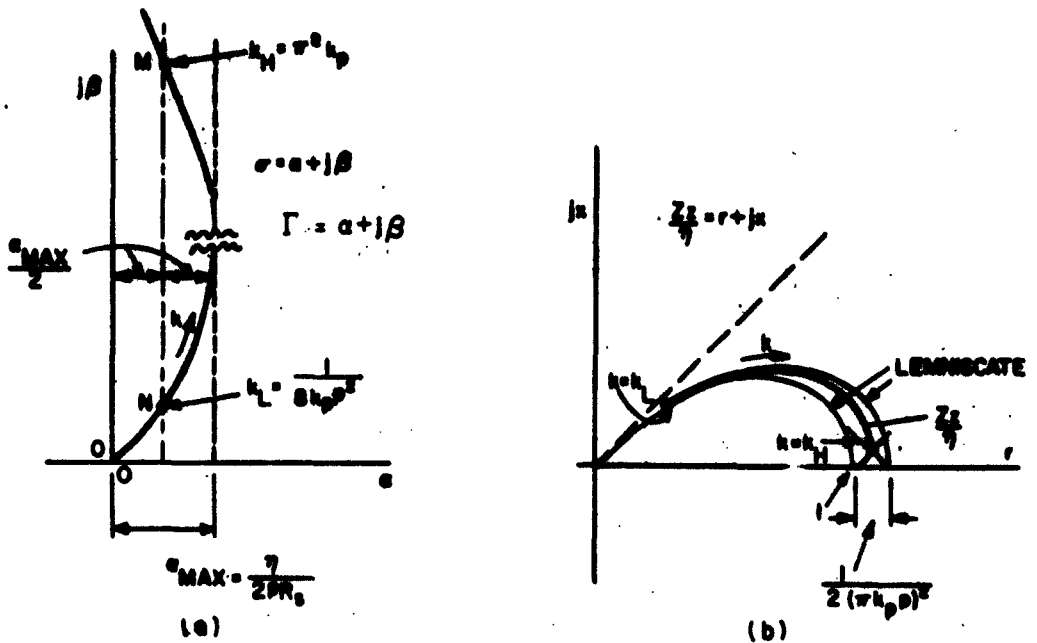


Figure IV-11

TABLE I				
	Formula	Case 1	Case 2	Unit
R_s		377 ($= \eta$)	754 ($= 2 \eta$)	Ω
p		1	0.5	cm
a_M	$(1/2p) (\eta/R_s)$	0.5 4.35	0.5 4.35	Nep/cm db/cm
f_H	$v(\pi/2p) (R_s/\eta)$	50	50	kmc
f_L	$v(1/16 \pi p) (\eta/R_s)$	1.2	1.2	kmc
f_H/f_L	$8\pi^2 (R_s/\eta)^2$	40	160	
$(Z_s/\eta)_{f_H}$	$1 + j(1/2\pi^2) (\eta/R_s)^2$	1 + j 0.05	1 + j 0.01	
$(Z_s/\eta)_{f_L}$	$\approx \frac{1}{\sqrt{1-j8}} =$	0.264 + j0.233		

$\eta = 120 \pi = 377 \Omega$

$v = \text{light velocity cm/sec}$

gating through the absorber is $\eta/(2R_s p)$. A working range of frequency is that in which the attenuation lies between its maximum value and its half values. This range is given by

$$(f_H/f_L) = 8 \pi^2 (R_s/\eta)^2,$$

where f_L is the lowest and f_H is the highest frequency in the working range. The performance data for the typical set of parameters is shown in Table I.

The frequency characteristics are considered to be so wide as a result of the construction of this absorber, which does not contain any periodic structure in the direction of wave propagation z . These results will be useful for construction of some absorbing walls which should have broadband frequency characteristics. The usual absorber design would require that auxiliary matching means be used. However, such considerations are well known and are considered to be beyond the scope of this paper. A detailed study has been presented in a previous report.¹

Air Force Cambridge Research Laboratory
Office of Aerospace Research
AF-19(604)-7499

J. W. E. Griemsmann, K. Suetake

Reference

1. K. Suetake and J. W. E. Griemsmann, "Absorbing Material Using Parallel Resistance Sheets," Report PIBMRI-1060-62, Microwave Research Institute, P. I. B. (August 1962).

F. C-BAND FERRITE SWITCH

L. M. Silber, A. Weis

Some time ago a switching circulator using ferrite rectangular toroids was developed at X-band.^{1, 2} This circulator operated over a 10 percent bandwidth, and could be switched in 10 nanoseconds. It was felt that a similar device operating in the C-band frequency range would be of value for use with the high-power C-band facility. Although it was not then anticipated that a device could be made to handle the full 10 megawatts available, such a device might be useful in switching the power from a traveling wave resonator, or in other experimental arrangements.

The ferrite material developed for the X-band circulator is not suitable for use at C-band because the high magnetization leads to appreciable microwave losses at the lower frequency. It was found that reduction of the magnetization by substitution of aluminum for some of the iron gave a material with reasonably square hysteresis loop and good microwave properties. The final composition adopted was

MICROWAVE CIRCUITS

$Mg_{0.925} Mn_{0.575} Fe_{1.4} Al_{0.6} O_{4.5}$. The saturation magnetization of this material is 1200 gauss, and the Curie temperature 150°C.

A preliminary version of the circulator was built by scaling dimensions of the X-band model. Dielectric cores were not used. It was found that the ferrite sections could be matched to standard waveguide by using quarter wavelength sections of polystyrene. Ferrite sections approximately 4 inches long were needed to obtain the necessary differential phase shift of 90°. A circulator was assembled using two jayrators a reciprocal phase shifter, a magic tee, and a short slot hybrid coupler. The reciprocal phase shifter was required because the two jayrators were assembled from different materials, and had slightly different characteristics.

The assembled circulator was tested at low power levels over a frequency range of 4.8 to 5.8 kmc/sec. With proper adjustment of the reciprocal phase shifter, the loss between coupled ports is 0.9 db, and between uncoupled ports 30 db.

Measurements at high power indicate that the losses do not change appreciably up to power levels of 100 kw peak. At higher powers heating deteriorates the performance and the device becomes reciprocal. Breakdown occurred at peak powers of 300 kw.

The circulator was switched by discharging a length of cable through the wire linking the ferrite tubes. The switching time depends on the peak current, and consequently on the potential to which the cable is charged. Switching times as short as 20 nanoseconds could be obtained. At higher charging voltages sparking occurred where the wire passed through the wall of the waveguide.

An improved version of the circulator is now being developed. Dielectric cores will be used in the ferrite sections to reduce the length of ferrite required. This should reduce the insertion loss, and reduce frequency sensitivity. Air spaces between ferrite and waveguide will be filled with dielectric to help avoid microwave breakdown, and a larger hole will be provided for feeding the wire through the waveguide wall. It should be possible to obtain switching times of the order of ten nanoseconds by these techniques.

Joint Services Technical Advisory Committee, AF-AFOSR-62-295
Rome Air Development Center, Air Force Systems Command
AF-30(602)-2135

L. M. Silber

References

1. Progress Report No. 16 to the Joint Services Technical Advisory Committee, R-452.16-59, Microwave Research Institute, P.I.B., pp. 83-87.
2. L. Levey and L. M. Silber, "A Fast-Switching X-Band Circulator Utilizing Ferrite Toroids," WESCON Convention Record (August 1960).

G. SYMMETRIES OF UNIFORM WAVEGUIDE CONTAINING ANISOTROPIC MATERIALS

W.K. Kahn, Y. Konishi, L.M. Silber

Waveguides, which have symmetry, have simpler electrical characteristics and equivalent circuits than general waveguides. The problem of symmetrical waveguide junctions has been studied by Dicke;¹ their scattering equivalent circuits were treated by Kahn.² The conception of symmetries was utilized to analyze directional coupler and bridge circuits as special cases by several authors.^{3, 4}

These symmetrical characteristics can be kept under some conditions even when the structure contains anisotropic materials. Furthermore, such waveguides may present several interesting characteristics useful in practical applications. From this standpoint, this paper discusses the particular anisotropic conditions under which waveguides can retain symmetries. It considers a uniform waveguide, that is, a waveguide which has a sectional boundary condition independent of distance along the guide, and includes anisotropic materials. Only those symmetries which are concerned with the plane transverse to the propagating direction of the waveguide are examined in detail.

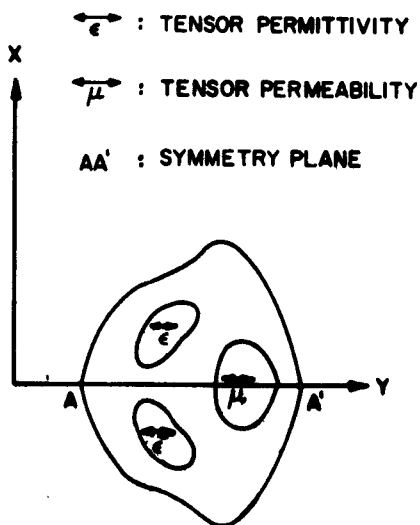


Fig. IV-12 Sectional diagram of waveguide possessing one symmetry plane

First, the distributions and electrical constants of tensor materials which can satisfy the conditions imposed by symmetry about the plane AA', as shown in Fig. IV-12, are described. Secondly, these results are extended to a waveguide which has two orthogonal symmetry planes, and lastly to a waveguide which has a symmetry axis. As a practical consideration this paper discusses what kind of dc magnetic field may be applied to ferrite materials so that electrical symmetry of the waveguide is preserved.

A waveguide is called symmetric about a symmetry plane when it satisfies the following conditions. Given the solution of the field equations for the waveguide shown in Eq. (1):

MICROWAVE CIRCUITS

$$\left. \begin{aligned} \underline{\mathcal{F}}(x, y, z) = \underline{E}_t(x, y, z), \underline{E}_x(x, y, z); \underline{H}_t(x, y, z), \\ \underline{H}_x(x, y, z); \underline{J}_t(x, y, z), \underline{J}_x(x, y, z), \\ \rho(x, y, z), \end{aligned} \right\} \quad (1)$$

where \underline{E} , \underline{H} , \underline{J} , ρ are respectively the electric field, magnetic field, electric current density and electric charge density inside the waveguide. Suffix t indicates the component parallel to the yz plane in Fig. IV - 12.

If the expression shown in Eq. (2) is also a solution of the field equations inside the waveguide, the waveguide has symmetry about yz plane.

$$\left. \begin{aligned} \underline{\mathcal{L}}(x, y, z) = \underline{E}_t(-x, y, z), -\underline{E}_x(-x, y, z); -\underline{H}_t(-x, y, z), \\ \underline{H}_x(-x, y, z); \underline{J}_t(-x, y, z), -\underline{J}_x(-x, y, z); \rho(-x, y, z) \end{aligned} \right\} \quad (2)$$

The solution $\underline{\mathcal{L}}(x, y, z)$ is called the reflected solution corresponding to the solution $\underline{\mathcal{F}}(x, y, z)$.

The linear combinations of $\underline{\mathcal{L}}(x, y, z)$ and $\underline{\mathcal{F}}(x, y, z)$

$$\begin{aligned} \underline{\psi}_e &= \underline{\mathcal{F}} + \underline{\mathcal{L}} \\ \underline{\psi}_o &= \underline{\mathcal{F}} - \underline{\mathcal{L}} \end{aligned} \quad (3)$$

make two field $\underline{\psi}_e$ and $\underline{\psi}_o$; $\underline{\psi}_e$ and $\underline{\psi}_o$ are called even and odd solutions in \underline{E}_t , respectively.

The Waveguide Possessing One Symmetry Plane

As mentioned above, we have to show what conditions the anisotropy must satisfy in order that the reflected expression $\underline{\mathcal{L}}(x, y, z)$ corresponding to the solution $\underline{\mathcal{F}}(x, y, z)$ may also be a solution.

The existence of the reflected solution is established in the following two steps:

1) The reflected expression $\underline{\mathcal{L}}(x, y, z)$ must be shown to satisfy Maxwell's field equation.

2) This expression must also satisfy the boundary condition inside the waveguide shown in Fig. IV - 12.

Conditions on the Proper Tensor Distribution of Anisotropic Materials

If the two fields $\underline{J}(x, y, z)$ and $\underline{L}(x, y, z)$ are substituted in the Maxwell Equations, we can get required conditions on the tensor distribution of material by the relation between \underline{J} and \underline{L} required to render both expressions solutions.

Let us express the magnetization $\underline{M}(x, y, z)$ and the electrical polarization $\underline{P}(x, y, z)$, respectively, through a tensor magnetic susceptibility $\underline{X}(x, y, z)$ and a tensor electric susceptibility $\underline{X}^e(x, y, z)$ as shown in Eqs. (4) and (5).

$$\underline{M}(x, y, z) = \begin{bmatrix} X_{xx}(x, y, z) & X_{xy}(x, y, z) & X_{xz}(x, y, z) \\ X_{yx}(x, y, z) & X_{yy}(x, y, z) & X_{yz}(x, y, z) \\ X_{zx}(x, y, z) & X_{zy}(x, y, z) & X_{zz}(x, y, z) \end{bmatrix} \underline{H}(x, y, z) \quad (4)$$

$$\underline{P}(x, y, z) = \begin{bmatrix} X_{xx}^e(x, y, z) & X_{xy}^e(x, y, z) & X_{xz}^e(x, y, z) \\ X_{yx}^e(x, y, z) & X_{yy}^e(x, y, z) & X_{yz}^e(x, y, z) \\ X_{zx}^e(x, y, z) & X_{zy}^e(x, y, z) & X_{zz}^e(x, y, z) \end{bmatrix} \underline{E}(x, y, z) \quad (5)$$

Substituting Eq. (1) in Maxwell's equation, we can get Eqs. (6) - (9), where the subscripts t and x denote, respectively, components parallel to the symmetry plane and components normal to the symmetry plane.

$$\begin{aligned} \nabla_t \times \underline{E}_x(x, y, z) + \underline{I}_x \times \frac{\partial}{\partial x} \underline{E}_t(x, y, z) + j\omega \mu_0 \underline{H}_t(x, y, z) &= -j\omega \underline{M}_t(x, y, z) \\ &= -j\omega \left\{ \underline{I}_z X_{yx}(x, y, z) - \underline{I}_y X_{zx}(x, y, z) \right\} \times \underline{H}_x(x, y, z) - j\omega \underline{X}_d^e(x, y, z) \underline{H}_t(x, y, z) \end{aligned} \quad (6)$$

$$\begin{aligned} \nabla_t \times \underline{H}_x(x, y, z) + \underline{I}_x \times \frac{\partial}{\partial x} \underline{H}_t(x, y, z) - j\omega \epsilon_0 \underline{E}_t(x, y, z) &= j\omega \underline{P}_t(x, y, z) \\ &= j\omega \left\{ \underline{I}_x X_{yx}^e(x, y, z) - \underline{I}_y X_{zx}^e(x, y, z) \right\} \times \underline{E}_x(x, y, z) + j\omega \underline{X}_d^e(x, y, z) \underline{E}_t(x, y, z) \end{aligned} \quad (7)$$

$$\begin{aligned} \nabla_t \times \underline{E}_t(x, y, z) + j\omega \mu_0 \underline{H}_x(x, y, z) &= -j\omega X_{xx}(x, y, z) \underline{H}_x(x, y, z) \\ &= -j\omega \left\{ -\underline{I}_z X_{xy}(x, y, z) + \underline{I}_y X_{xz}(x, y, z) \right\} \times \underline{H}_t(x, y, z) \end{aligned} \quad (8)$$

MICROWAVE CIRCUITS

$$\begin{aligned} \nabla_t \times \underline{H}_t(x, y, z) - j\omega \epsilon_0 \underline{E}_x(x, y, z) &= j\omega \underline{P}_x(x, y, z) \\ &= j\omega X_{xx}^e(x, y, z) \underline{E}_x(x, y, z) + j\omega \left\{ -\underline{I}_z X_{xy}^e(x, y, z) + \underline{I}_y X_{xz}^e(x, y, z) \right\} \times \underline{E}_t(x, y, z) \end{aligned} \quad (9)$$

where μ_0 , ϵ_0 are the permeability and permittivity of free space, and \underline{I}_x , \underline{I}_y , \underline{I}_z are unit vectors along the x, y, and z axes, and

$$\underline{\overline{X}}_d = \begin{bmatrix} X_{yy} & X_{yz} \\ X_{zy} & X_{zz} \end{bmatrix} \quad \underline{\overline{X}}_d^e = \begin{bmatrix} X_{yy}^e & X_{yz}^e \\ X_{zy}^e & X_{zz}^e \end{bmatrix}$$

If we assume the reflected solution $\underline{A}(x, y, z)$ satisfies Maxwell's equation, Eq. (2) must satisfy Eqs. (6)-(9).

Putting Eq. (2) into Eq. (6), and substituting x' for $-x$, we can get Eq. (10):

$$\begin{aligned} \nabla_t \times \underline{E}_x(x', y, z) + \underline{I}_x \times \frac{\partial}{\partial x'} \underline{E}_t(x', y, z) + j\omega \mu_0 \underline{H}_t(x', y, z) &= j\omega \underline{M}_t(-x', y, z) \\ &= j\omega \left\{ \underline{I}_z X_{yx}(x, y, z) - \underline{I}_y X_{zz}(x, y, z) \right\} \times \underline{H}_x(x', y, z) - j\omega \underline{\overline{X}}_d(x, y, z) \underline{H}_t(x', y, z) \end{aligned} \quad (10)$$

Similarly, putting Eq. (2) into (7)-(9), we get Eqs. (11)-(13).

$$\begin{aligned} \nabla_t \times \underline{H}_x(x', y, z) + \underline{I}_x \times \frac{\partial}{\partial x'} \underline{H}_t(x', y, z) - j\omega \epsilon_0 \underline{E}_t(x', y, z) \\ &= -j\omega \left\{ \underline{I}_z X_{yx}^e(x, y, z) - \underline{I}_y X_{zx}^e(x, y, z) \right\} \times \underline{E}_x(x', y, z) + j\omega \underline{\overline{X}}_d^e(x, y, z) \underline{E}_t(x', y, z) \end{aligned} \quad (11)$$

$$\begin{aligned} \nabla_t \times \underline{E}_t(x', y, z) + j\omega \mu_0 \underline{H}_x(x', y, z) &= -j\omega X_{xx}(x, y, z) \underline{H}_x(x', y, z) \\ &+ j\omega \left\{ -\underline{I}_z X_{xy}(x, y, z) + \underline{I}_y X_{xz}(x, y, z) \right\} \times \underline{H}_t(x', y, z) \end{aligned} \quad (12)$$

$$\begin{aligned} \nabla_t \times \underline{H}_t(x', y, z) - j\omega \epsilon_0 \underline{E}_x(x', y, z) &= j\omega X_{xx}^e(x, y, z) \underline{E}_x(x', y, z) \\ &- j\omega \left\{ -\underline{I}_z X_{xy}^e(x, y, z) + \underline{I}_y X_{xz}^e(x, y, z) \right\} \times \underline{E}_t(x', y, z) \end{aligned} \quad (13)$$

Comparing Eqs. (10)-(13) at $x' = x$ with Eqs. (6)-(9), we can easily get the results shown in Eqs. (14) and (15).

$$\left. \begin{aligned} X_{ii}(x, y, z) &= X_{ii}(-x, y, z), \quad (i = x, y, z) \\ X_{ij}(x, y, z) &= X_{ij}(-x, y, z), \quad (i, j = y, z, i \neq j) \\ X_{ij}(x, y, z) &= X_{ij}(-x, y, z), \quad \left\{ \begin{aligned} (i, j = x, y, i \neq j) \\ (i, j = x, z, i \neq j) \end{aligned} \right\} \end{aligned} \right\} \quad (14)$$

$$\left. \begin{aligned} X_{ii}^e(x, y, z) &= X_{ii}^e(-x, y, z), \quad (i = x, y, z) \\ X_{ij}^e(x, y, z) &= X_{ij}^e(-x, y, z), \quad (i, j = y, z, i \neq j) \\ X_{ij}^e(x, y, z) &= -X_{ij}^e(-x, y, z), \quad \left\{ \begin{aligned} (i, j = x, y, i \neq j) \\ (i, j = x, z, i \neq j) \end{aligned} \right\} \end{aligned} \right\} \quad (15)$$

These equations show that susceptibility tensor of materials inside of waveguide must have a form satisfying Eqs. (14) and (15). They also show that the geometrical distribution of materials must be kept symmetrical about the symmetry plane.

Putting Eqs. (14) and (15) into Eqs. (4) and (5), we get the following relations:

$$\left. \begin{aligned} \underline{M}_x(x, y, z) &= \underline{M}_x(-x, y, z), \quad \underline{P}_x(x, y, z) = \underline{P}_x(-x, y, z) \\ \underline{M}_t(x, y, z) &= -\underline{M}_t(-x, y, z), \quad \underline{P}_t(x, y, z) = -\underline{P}_t(-x, y, z) \\ \underline{B}_x(x, y, z) &= \underline{B}_x(-x, y, z), \quad \underline{D}_x(x, y, z) = \underline{D}_x(-x, y, z) \\ \underline{B}_t(x, y, z) &= -\underline{B}_t(-x, y, z), \quad \underline{D}_t(x, y, z) = -\underline{D}_t(-x, y, z) \end{aligned} \right\} \quad (16)$$

Equations (14), (15) are the results we have obtained in this section.

Boundary Conditions inside the Waveguide

It is readily shown that, with the stipulations on the tensor materials indicated above, $\mathcal{L}(x, y, z)$ satisfies proper boundary conditions if $\mathcal{F}(x, y, z)$ did so.

Waveguide Containing Ferrite Materials

We now examine the dc magnetic field applied to ferrite in a waveguide in order to determine what restrictions on this field are necessary for waveguide symmetries to be preserved. The considerations are presented in the case of one symmetry plane

MICROWAVE CIRCUITS

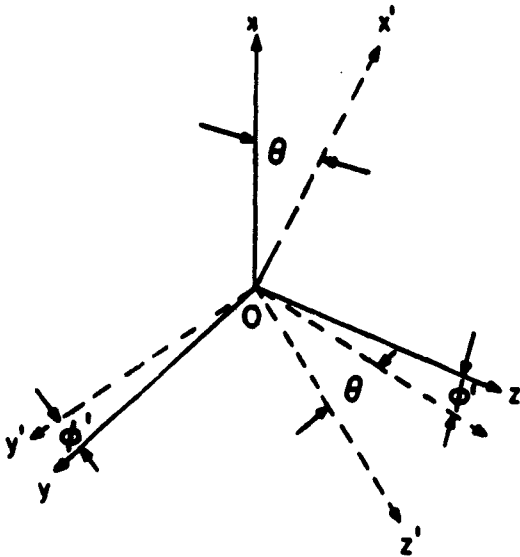


Fig. IV-13 Rotation of coordinate about origin

Two orthogonal planes and complete symmetry axis have been discussed, and are included in a more complete report.⁷

Let us consider the new coordinates $x' y' z'$ of which x' axis coincides with the direction of the dc magnetic field applied to ferrite material at position (x, y, z) in $x y z$ coordinate system.

When the ferrite is saturated by an applied dc magnetic field, the susceptibility tensor \overline{X}' of the ferrite is expressed by Eq. (17) in $x' y' z'$ coordinate system.⁶

$$\overline{X}' = \begin{bmatrix} 0 & 0 & 0 \\ 0 & X & -jK \\ 0 & jK & X \end{bmatrix} \quad (17)$$

However, we can arbitrarily choose y', z' axis, because the susceptibility tensor is invariant under rotations of arbitrary angles about x' axis. Therefore, we choose y' axis along the intersection of the $y z$ plane and the plane normal to x' axis and passing through the origin, as illustrated in Fig. IV - 13.

Let the angle between y and y' axis be ϕ' ($0 \leq \phi' < 2\pi$), and the angle between x and x' axis be θ' ($0 \leq \theta' \leq \pi$). Then ϕ' is also the angle between the $x x'$ and $x z$ planes.

The following relation exists between $x y z$ and $x' y' z'$ coordinate systems:

$$\begin{bmatrix} x \\ y \\ z \end{bmatrix} = \begin{bmatrix} a_1^1 & a_2^1 & a_3^1 \\ a_1^2 & a_2^2 & a_3^2 \\ a_1^3 & a_2^3 & a_3^3 \end{bmatrix} \begin{bmatrix} x' \\ y' \\ z' \end{bmatrix} = \begin{bmatrix} \cos \theta' & 0 & -\sin \theta' \\ \sin \theta' \sin \phi', \cos \phi', \cos \theta' \sin \phi' \\ \sin \theta' \cos \phi', -\sin \phi', \cos \theta' \cos \phi' \end{bmatrix} \begin{bmatrix} x' \\ y' \\ z' \end{bmatrix} \quad (18)$$

The components X_{ij} of the tensor \overline{X}' expressed in $x y z$ coordinate system can be calculated from the components X'_{ij} of the tensor expressed in $x' y' z'$ coordinate system by the following formula:

$$X_{ij} = \sum_k \sum_l a_k^i a_l^j X'_{kl} \quad (19)$$

Taking into account the orthogonal character of the coordinate transformation and the special form (17), we get Eq. (20):

$$\left. \begin{aligned} X_{ij} &= -a_1^i a_1^j X + j(a_3^i a_2^j - a_2^i a_3^j) K \quad (i \neq j) \\ X_{ii} &= \{1 - (a_1^i)^2\} X \end{aligned} \right\} \quad (20)$$

Substituting Eq. (18) in Eq. (20),

$$\left. \begin{aligned} X_{xx}(x, y, z) &= X \sin^2 \theta', \quad X_{yy}(x, y, z) = X(1 - \sin^2 \theta' \sin^2 \phi') \\ X_{zz}(x, y, z) &= X(1 - \sin^2 \theta' \cos^2 \phi') \\ X_{yz}(x, y, z) &= -X \sin^2 \theta' \sin \phi' \cos \phi' - j K \cos \theta' = X_{zy}^*(x, y, z) \\ X_{xy}(x, y, z) &= -X \sin \theta' \cos \theta' \sin \phi' - j K \sin \theta' \cos \phi' = X_{yx}^*(x, y, z) \\ X_{xz}(x, y, z) &= -X \sin \theta' \cos \theta' \cos \phi' + j K \sin \theta' \sin \phi' = X_{zx}^*(x, y, z) \end{aligned} \right\} \quad (21)$$

where the sign * denotes complex conjugate.

Next we consider the new coordinate $x'' y'' z''$ of which x'' axis coincides with the applied dc magnetic field at point $(-x, y, z)$ in $x y z$ coordinate, where the magnitude of dc field is different from the former but also saturates the ferrite.

When we show the angle between x and x'' axis by θ'' and the angle between $x x''$ plane and $x z$ plane by ϕ'' , we can get the same relation as in Eq. (21) except for the replacement of θ' , ϕ' , K , X and $X_{ij}(x, y, z)$ by θ'' , ϕ'' , K' , X' and $X_{ij}(-x, y, z)$.

However, since there exists the relation $X_{yy} + X_{zz} - X_{xx} = X'_{yy} + X'_{zz} - X'_{xx}$ in Eq. (21), K' and X' must equal K and X according to Eq. (14). Therefore, the magnitude of H_{dc} at symmetry points must be equal.

Also, considering the relation between $X_{ij}(x, y, z)$ and $X(-x, y, z)$ shown in Eq. (14), the following relation must be satisfied:

$$\cos \theta' = \cos \theta'', \quad \sin \phi' = -\sin \phi'', \quad \cos \phi' = -\cos \phi'' .$$

Then we get Eq. (22):

$$\theta' = \theta'', \quad \phi' = \phi'' + \pi . \quad (22)$$

MICROWAVE CIRCUITS

Therefore

$$\underline{I}_x \times (\underline{I}_x + \underline{I}_{x'}) = 0,$$

(23)

where $\underline{I}_x, \underline{I}_{x'}$ are unit vectors along the x, x' axes.

TABLE I		
CLASSIFICATION OF SYMMETRY	DISTRIBUTION OF TENSOR SUSCEPTIBILITY	ARRANGEMENT OF FERRITE AND PATTERN OF DC MAGNETIC FIELD
One-Symmetry Plane	$X_{ii}(xyz) = X_{ii}(-xyz)$ $(i = x, y, z)$ $X_{ij}(xyz) = X_{ij}(-xyz)$ $(ij = x, y)$ $X_{ij}(xyz) = -X_{ij}(-xyz)$ $(ij = x, z)$ <p>Eqs. (14, 15)</p>	
Two-Symmetry Planes	$X_{ii}(xyz) = X_{ii}(x , y , z)$ $(i = x, y, z)$ $X_{ij}(xyz) = -X_{ij}(-x, y, z)$ $= X_{ij}(x, -y, z)$ $(i, j = x, z)$ $X_{ij}(xyz) = X_{ij}(-xyz) = X_{ij}(x-yz)$ $(i, j = y, z)$ $X_{ij}(xyz) = -X_{ij}(-xyz)$ $= -X_{ij}(x, -y, z)$ $(i, j = x, y)$	
Symmetry Axis	$\underline{\underline{X}} = \begin{bmatrix} X_{\xi\xi}(r), & 0 & , & 0 \\ 0 & , & X_{\eta\eta}(r), & X_{\eta\xi}(r), \\ 0 & , & X_{\xi\eta}(r), & X_{\xi\xi}(r), \end{bmatrix}$ <p>Same tensor on the circle whose center is the z axis.</p>	

MICROWAVE CIRCUITS

Conversely, we can easily verify that the susceptibility tensor at points (x, y, z) and $(-x, y, z)$ satisfies the relation of Eq. (14) when the resultant vectors of dc magnetic field at (x, y, z) and $(-x, y, z)$ have no components along the y, z axes. Thus, the condition, Eq. (34), is necessary and sufficient.

The applied dc magnetic field satisfying Eq. (18) generally has the field pattern illustrated at the top of Table I.

As a special case, the dc magnetic field applied parallel to x axis can keep symmetry of waveguide which includes symmetrically arranged ferrite pieces.

The condition on waveguide containing anisotropic materials to keep its symmetries has been clarified. The important results carried out in this paper are tabulated in Table I.

Joint Services Technical Advisory Committee
AF-AFOSR-62-295

Y. Konishi

References

1. Montgomery, Dicke and Purcell, "Principles of Microwave Circuits" (New York: McGraw-Hill, 1948), pp. 401-478.
2. W.K. Kahn, "Scattering Equivalent Circuits for Common Symmetrical Junctions," IRE Trans. on Circuit Theory, Vol. CT-3, pp. 121-127 (June 1956).
3. J. Reed and G.J. Wheeler, "A Method of Analysis of Symmetrical Four-Port Networks," IRE Trans. on Microwave Theory and Techniques, Vol. MTT-4, p.246 (October 1956).
4. E.M.T. Jones and J.T. Bolljahn, "Coupled Transmission Line Directional Couplers," IRE Trans. on Microwave Theory and Techniques, Vol. MTT-4, pp. 75-81 (April 1956).
5. Montgomery, Dicke and Purcell, "Principle of Microwave Circuits" (New York: McGraw-Hill, 1948), p. 412.
6. R. Sohos, "Theory and Application of Ferrites," Prentice-Hall Electrical Engineering Series, p. 64.
7. Y. Konishi, "Symmetries of Uniform Waveguide Containing Anisotropic Materials," Report PIBMRI-1052-62 (August 1962).

V - NETWORK THEORY

Altschuler, H.M.
Ansell, H.G.
Bellmer, W.
Boesch, F.T.
Carlin, H.J.

Deutsch, S.
Felsen, L.B.
Hou, H.S.
Kahn, W.K.
Kohler, W.

Laemmel, A.E.
Nanda, V.
Papoulis, A.
Reynolds, A.L.
Smilen, L.I.

Smith, E.J.
Wohlers, M.
Youla, D.C.
Zysman, G.

A. THE THEORY OF ACTIVE MODE GENERATION USING TUNNEL DIODES

L.I. Smilen

A tunnel diode is capable of generating active or oscillatory modes when placed across a passive immittance. The circuit in which a lossless, linearized tunnel diode is terminated by a passive one-port is shown in Fig. V - 1.

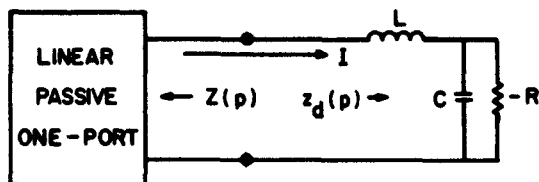


Figure V-1

The active modes, in the complex p -plane, are determined from the solutions to the equation

$$\left[Z(p) + z_d(p) \right] I = 0, \quad (1a)$$

of the form $I = I_0 e^{pt}$ where $\text{Re } p \geq 0$. These, in turn, are governed by the solutions to the equation

$$Z(p) + z_d(p) = 0 \quad (1b)$$

in $\text{Re } p \geq 0$.

Due to the parasitic reactive elements associated with the equivalent circuit of the tunnel diode, certain restrictions exist which limit the locations of these modes in the right half p -plane. These limitations are contained in the following theorem.

Theorem: The modes p_i ($i = 1, 2, \dots, n$) with $\text{Re } p_i > 0$, generated by a lossless tunnel diode, must satisfy the following inequalities:

$$\frac{1}{RC} - \sum_{i=1}^n p_i \geq 0 \quad (2a)$$

and

$$\frac{(3R^2 C - L)}{LR^3 C^3} + \sum_{i=1}^n p_i^3 \geq 0 \quad (2b)$$

The inclusion of modes on the real frequency axis requires that the inequality signs in (2a) and (2b) be deleted. It has been proven that it is always possible to find a passive impedance, $Z(p)$, in which to terminate the diode, such that any set

NETWORK THEORY

of active modes which satisfies the theorem is individually generated.

A lossless impedance is capable of generating modes solely in $\text{Re } p > 0$. In this case the equality sign in (2a) must be used. A synthesis utilizing lossy impedance is always possible, provided equality is not achieved in (2a) and (2b).

The proof of the theorem and the synthesis procedures are contained in

reference 1. The following two illustrations are taken from that reference.

(a) Using a diode for which

$$\begin{aligned} -R &= -50 \Omega, \\ C &= 20 \text{ pf}, \\ L &= 10 \text{ nh}, \end{aligned}$$

design a lossless impedance to generate a set of modes at $p_{1,2} = 3 \times 10^8 \pm j 4 \times 10^8$ rad/sec and $p_3 = 4 \times 10^8$ rad/sec. The circuit is shown in Fig. V - 2.

(b) Using a diode for which

$$\begin{aligned} -R &= -50 \Omega, \\ C &= 10 \text{ pf}, \\ L &= 10 \text{ nh}, \end{aligned}$$

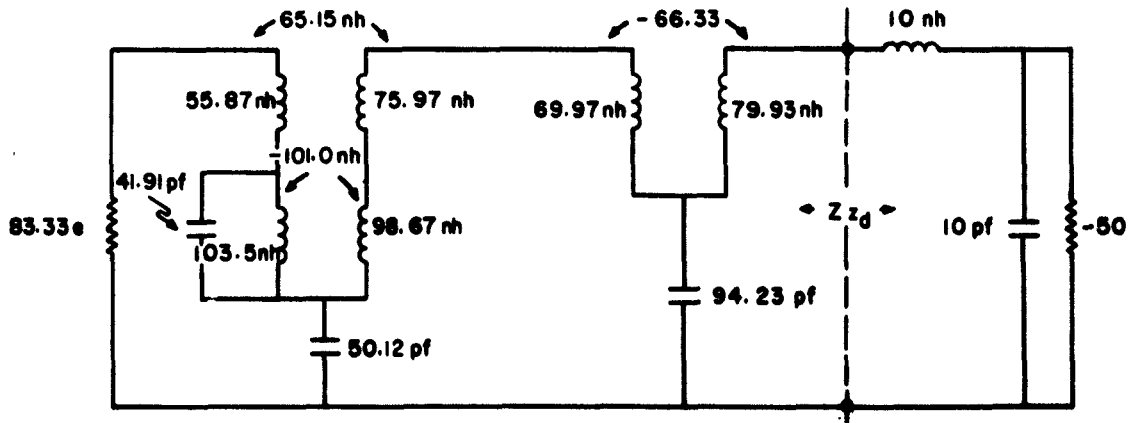


Figure V-3

NETWORK THEORY

design a lossy impedance to generate the same set of modes used in part (a). The circuit is shown in Fig. V - 3.

Rome Air Development Center
Air Force Systems Command
AF-30(602)-2868

L. I. Smilen

Reference

1. L. I. Smilen, "The Theory of Active Mode Generation Using Tunnel Diodes," Report PIBMRI-1134-63, Microwave Research Institute, P. I. B.

B. TOPOLOGY AND RESISTOR NETWORKS

F. T. Boesch

Many of the algebraic properties of resistor networks are intimately connected with the topology of the network. Indeed, most of the algebraic properties of the network may be derived in a relatively simple fashion by an appropriate topological argument.

Specific results which require a rather tedious algebraic derivation are the following: the rank of the incidence matrix; the significance of linearly independent columns of the incidence matrix; the Kron transformation; the inverse of a tree incidence matrix; the algebraic connection between a fundamental cut-set matrix and the associated tree incidence matrix; and the Cederbaum algorithm for the determination of the fundamental cut-set matrix from the node-pair admittance matrix. These results are derived by utilizing the topological properties of the network.

The rank of the incidence matrix of a connected graph is obtained immediately by introducing the concept of a tree, and demonstrating that any connected network contains a tree. The properties of a tree incidence matrix are obtained immediately by simple topological arguments. The properties of the linearly independent columns of the incidence matrix are derived by relating them to a tree. These results are then used to yield a simple derivation of the Kron transformation. The inverse of a tree incidence matrix is studied topologically and used to prove that a fundamental cut-set matrix is the product of the graph's incidence matrix by the inverse of a tree incidence matrix of the graph.

The Cederbaum algorithm is then derived by utilizing the previous concepts. (The Cederbaum algorithm is a procedure for determining the fundamental cut-set matrix of a node-pair admittance matrix formulation from a given node-pair admittance matrix.)

The advantage of the topological derivation is quite dramatic in this case since

the original algebraic proof is rather complicated. The algorithm is then used to demonstrate that the problem of realizing a fundamental cut-set matrix, i.e., finding a graph which has a fundamental cut-set matrix which is equal to the given matrix, is equivalent to the network problem of synthesis of a n-port short-circuit admittance matrix as a transformerless resistor network on n + 1 nodes.

These topics will be discussed in detail in a forthcoming report.

Joint Services Technical Advisory Committee
AF-AFOSR-62-295

F. T. Boesch

C. CANONICAL FORM OF TWO TANDEM-CONNECTED FOUR-PORTS

W.K. Kahn, A.L. Reynolds

As was shown by Kahn and Kyhl,¹ a four-port is either degenerate or the interconnection of two three-ports. It may also be represented as an ideal directional coupler together with certain lossless reciprocal two-ports connected at the outputs

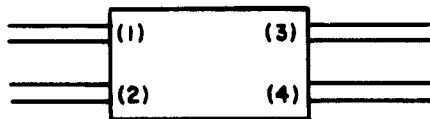


Fig. V-4 Schematic of a four-port

of this directional coupler. Such a representation is here called the canonical form of a given four-port. The question which has been examined is the relation of the directional coupler core of the resultant four-port of two tandem-connected four-ports with the cores of each of the two component four-ports.

The scattering matrix of the directional coupler core of a four-port such as indicated in Fig. V-4 has one of three simple forms:

$$S_1 = \begin{bmatrix} 0 & 0 & a & j\beta \\ 0 & 0 & j\beta & a \\ a & j\beta & 0 & 0 \\ j\beta & a & 0 & 0 \end{bmatrix}, \quad S_2 = \begin{bmatrix} 0 & a & 0 & j\beta \\ a & 0 & j\beta & 0 \\ 0 & j\beta & 0 & a \\ j\beta & 0 & a & 0 \end{bmatrix}, \quad S_3 = \begin{bmatrix} 0 & j\beta & a & 0 \\ j\beta & 0 & 0 & a \\ a & 0 & 0 & j\beta \\ 0 & a & j\beta & 0 \end{bmatrix}$$

On interconnection of two four-ports, as indicated in Fig. V - 5, it is found that the resultant four-port has cores 1, 2 or 3 in accordance with the scheme of Table I. Several subsidiary results of interest have been obtained.²

NETWORK THEORY

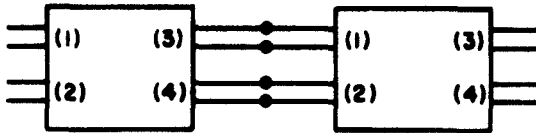


Fig. V-5 Schematic of two four-ports in tandem

TABLE I - RESULTANT CORE TYPES			
Type of core of first four-port \ Type of core of second four-port	①	②	③
①	①②	all	all
②	all	①,③	all
③	all	all	③

Joint Services Technical Advisory Committee
AF-AFOSR-62-295

W.K. Kahn

References

1. W.K. Kahn and R.L. Kyhl, "The Directional Coupler Core of an Arbitrary, Lossless, Reciprocal 4-Port," Proc. IRE, Vol. 49, No. 11 (November 1961).
2. A.L. Reynolds, "Canonical Forms of Two Tandem-Connected Four-Ports," Master's Thesis in Electrophysics, Polytechnic Institute of Brooklyn, June 1963.

VI - SYSTEMS AND CONTROL

Bellmer, W.	Devieux, C.	Kohavi, Z.	Palin, J.	Schwartz, M.
Belove, C.	Dorato, P.	Laemmel, A.E.	Panzer, M.	Shaw, L.
Bergstein, L.	Drenick, R.F.	Lavallee, P.	Papoulis, A.	Shoeman, M.L.
Bially, T.	Haddad, R.	Lynch, W.A.	Rudner, B.	Smith, E.J.
Blessner, W.B.	Hess, D.	Mendel, J.M.	Schachter, H.	Truxal, J.G.
Bongiorno, J.J.	Horing, S.	Mishkin, E.	Schilling, D.L.	Warshauer, J.
Boorstyn, R.R.	Karsky, M.	Mow, W.C.-W.	Schillinger, A.	Wohlers, F.
Deutsch, S.	Kliger, I.	Nelson, E.		

A. STABILITY AND CONVERGENCE PROPERTIES OF LINEAR TIME-VARYING SYSTEMS

J.J. Bongiorno, Jr.

1. Introduction

In a recent report,¹ earlier work on linear time-varying systems^{2, 3} was extended to multi-input multi-output systems. The extension to multi-input multi-output systems is especially significant in that it enables one to investigate readily the stability of parametric devices and satellite attitude control systems. In particular, bounds on the time-varying system parameters which are sufficient for stability can be obtained from real-frequency data. Since only real-frequency data is required, the stability test is easily applied to high-order systems.

2. The Main Theorem

Before stating the main theorem, it is appropriate here to define $\|A\|$, norm of A , where A is a matrix. By definition, the $\|A\|$ is the positive square root of the largest eigenvalue of A^*A , where the $*$ indicates conjugate transpose. When A is a matrix function of a real or complex variable t , $A = A(t)$, then

$$\|A(t)\|_{\max} = \text{l. u. b.}_{t_0 \leq t \leq t_1} \|A(t)\| \quad (1)$$

where $t_0 \leq t \leq t_1$ is the range of definition of $A(t)$.

Theorem: If $K(t)$ is a periodic matrix function of t and $w(t)$ is the impulse response matrix of a linear, lumped, constant-parameter system, and if

$$(a) \quad G(s) = \mathcal{L}\{w(t)\} \text{ analytic for } \text{Re } s > \sigma_c, \sigma_c \leq \mu_c \quad (2)$$

$$(b) \quad \|K(t)\|_{\max} \|G(\mu_c + j\omega)\|_{\max} < 1, \quad (3)$$

SYSTEMS AND CONTROL

then the vector signal \underline{y} in the system shown in Fig. VI - 1 satisfies the integral equation

$$\underline{y} = \underline{y}_0 + \int_0^t w(\tau) K(t - \tau) \underline{y}(t - \tau) d\tau, \quad (4)$$

where \underline{y}_0 represents the open-loop response of $w(t)$ to initial conditions, and is of the form

$$\underline{y} = \sum_{i=1}^n e^{\mu_i t} P(t) \underline{\phi}(t) \quad (5)$$

with

$$\text{Re } \mu_i < \mu_c, \quad i = 1, 2, \dots, n. \quad (6)$$

All elements of the matrix $P(t)$ are polynomials in t and $\underline{\phi}(t)$ is a periodic vector with the same period as $K(t)$. When the above statements hold with $\mu_c = 0$, then the system shown in Fig. VI - 1 with $\underline{z} \cong 0$ is stable in the sense that every \underline{z} with bounded norm yields an output \underline{y} with bounded norm.

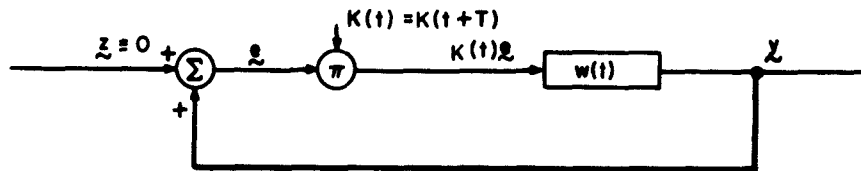


Figure VI-1

The proof of the above theorem is contained in a report⁴ presently in preparation. Only an outline of the proof is given here since it is lengthy. Conditions (a) and (b) of the theorem are sufficient to ensure that all solutions of (4) of the form

$$\underline{y} = e^{\mu t} \underline{\phi}(t), \quad \underline{\phi}(t) = \underline{\phi}(t + \tau)$$

satisfy

$$\text{Re } \mu < \mu_c \quad (8)$$

Since $w(t)$ is the impulse response matrix of a linear, lumped, constant-parameter system, and since $K(t) = K(t + \tau)$, the system shown in Fig. VI - 1 is a Floquet system. That is, all solutions \underline{y} must be of the form (5). The result (6) then immediately follows from (5), (7), and (8). When the theorem holds with $\mu_c = 0$, the undriven system is asymptotically stable. It readily follows that for every input \underline{z} with bounded norm, an output \underline{y} with bounded norm results.

3. Application to Parametric Devices

The generalized parametric device shown in Fig. VI - 2 is now investigated. M is a network of n coupled capacitors with terminal description

$$\dot{\underline{y}} = - (C \underline{y})_t, \quad C(t) = C(t + \tau). \tag{9}$$

The subscript t indicates differentiation with respect to t. The terminal description of the network N is

$$\underline{y}(t) = \underline{y}_0 + \int_0^t H(\tau) \dot{\underline{y}}(t - \tau) d\tau, \tag{10}$$

where H(t) is the n x n impulse response matrix describing N. Clearly,

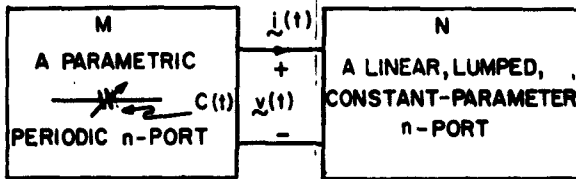
$$z(s) = \int_0^\infty H(t) e^{-st} dt$$

is the impedance matrix of N.

Combining (9) and (10) and integrating by parts yields

$$\underline{y} = \left[\underline{y}_0 + H(t) C(0) \underline{y}(0) \right] - \int_0^t \left[H_t(\tau) + H(\tau) \delta(\tau) \right] C(t - \tau) \underline{y}(t - \tau) d\tau, \tag{11}$$

where $\delta(t)$ is the unit impulse function.



When the identifications

$$\underline{y}_0 = \underline{y}_0 + H(t) C(0) \underline{y}(0), \tag{12}$$

$$w(t) = H_t(t) + H(t) \delta(t), \tag{13}$$

and

$$K(t) = C(t) \tag{14}$$

Figure VI-2

are made, then (11) becomes

$$\underline{y} = \underline{y}_0 - \int_0^t w(\tau) K(t - \tau) \underline{y}(t - \tau) d\tau \tag{15}$$

which, except for the first term in the right side of the equality sign, is identical in form with (4).

SYSTEMS AND CONTROL

In the original proof of the theorem stated in Section 2, the condition (a) on the analyticity of $G(s)$ arose from the two conditions:

$$(a) \lim_{t \rightarrow \infty} \int_0^t e^{-\sigma t} w(t) dt = 0, \quad \sigma \geq \mu_c \quad (16)$$

$$(b) \int_0^{\infty} \| e^{-\sigma t} w(t) \| dt < \infty, \quad \sigma > \mu_c. \quad (17)$$

In order to apply the theorem to the parametric device under consideration here, it is therefore necessary to impose the restriction

$$\lim_{t \rightarrow \infty} [\dot{x}_0 + H(t) C(0) x(t)] e^{-\sigma t} = 0, \quad \sigma \geq \mu_c \quad (18)$$

in addition to (17). Both (17) and (18) can be shown to be satisfied when

$$s Z(s) \text{ analytic for } \operatorname{Re} s > \sigma_c, \quad \sigma_c \leq \mu_c. \quad (19)$$

Also,

$$G(s) = \mathcal{L}\{w(t)\} = \mathcal{L}\{H_t(t) + H(t)\delta(t)\} = s Z(s) - H(0) + H(0) = s Z(s) \quad (20)$$

Thus, when (19) is satisfied for $\mu_c = 0$,

$$\|K(t)\|_{\max} \|G(j\omega)\|_{\max} = \|C(t)\|_{\max} \|\omega Z(j\omega)\|_{\max} < 1 \quad (21)$$

is a sufficient condition for asymptotic stability.

4. Application to Satellite Attitude Control

The linearized equations of motion of an earth satellite in an elliptic orbit can be put in the following form⁵ when the desired satellite attitude is such that one of the body-fixed axes is along the line connecting the satellite and earth centers and either error rate, rate gyro, or gravitational damping is employed:

$$\begin{aligned} & \left[\ddot{\theta}_x + a_1 \dot{\theta}_x + a_2 \theta_x + a_3 \dot{\theta}_z + a_4 \theta_z \right] \\ & + \left[f_1(t) \theta_x + f_2(t) \dot{\theta}_z + f_3(t) \theta_z \right] = L_x \end{aligned} \quad (22)$$

$$\left[\ddot{\theta}_y + b_1 \dot{\theta}_y + b_2 \theta_y \right] + g_1(t) \theta_y = L_y - g_2(t) \quad (23)$$

$$\begin{aligned} & \left[\ddot{\theta}_z + c_1 \dot{\theta}_z + c_2 \theta_z + c_3 \dot{\theta}_x + c_4 \theta_x \right] \\ & + \left[h_1(t) \theta_z + h_2(t) \dot{\theta}_x + h_3(t) \theta_x \right] = L_z, \end{aligned} \quad (24)$$

where a_i , b_i , and c_i are constants; f_i , h_i , and g_i are periodic functions with orbital period and amplitudes dependent on orbit eccentricity; and the L 's are disturbance torques. The angles θ_x , θ_y , and θ_z are the well-known Euler angles which give the position of the satellite relative to the desired orientation. The desired satellite attitude results when $\theta_x = \theta_y = \theta_z = 0$.

Equation (23) is uncoupled from the remaining two equations of motion and is considered first. It describes the system shown in Fig. VI - 3, which is identical in form with the system shown in Fig. VI - 1. Furthermore, $G(s)$ is a 1×1 matrix and the transform of a lumped system.

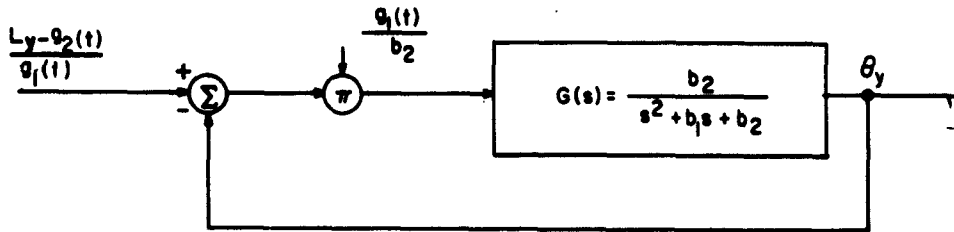


Figure VI-3

When b_1 and b_2 are both positive and the notation $b_1 = 2\zeta_y \omega_y$ and $b_2 = \omega_y^2$ is employed, then $G(s)$ is analytic in $\text{Re } s > -\zeta_y \omega_y$. Since

$$\|G(j\omega)\|_{\max} = |G(j\omega)|_{\max} = \begin{cases} 1, & \zeta_y \geq 1/\sqrt{2} \\ 1/(2\zeta_y \sqrt{1 - \zeta_y^2}), & 0 \leq \zeta_y \leq 1/\sqrt{2} \end{cases} \quad (25)$$

it immediately follows from the theorem stated in Section 2 with $\mu_c = 0$ that

SYSTEMS AND CONTROL

$$\left| \frac{1}{b_2} \right| \left\| g_1(t) \right\|_{\max} = \frac{1}{\omega_y^2} \left| g_1(t) \right|_{\max} < \begin{cases} 1, & \zeta_y \geq 1/\sqrt{2} \\ 2\zeta_y \sqrt{1 - \zeta_y^2}, & \zeta_y \leq 1/\sqrt{2} \end{cases} \quad (26)$$

is a sufficient condition for stable θ_y for all bounded $[L_y - g_2(t)]/g_1(t)$.

The remaining two equations of motion, (22) and (24), can be written as

$$\dot{\underline{\theta}} = A \underline{\theta} + K(t) [\underline{\theta} + \underline{z}], \quad (27)$$

where

$$\underline{\theta} = [\theta_x \quad \dot{\theta}_x \quad \theta_z \quad \dot{\theta}_z]^T \quad (28)$$

(the superscript T indicates transpose),

$$A = \begin{bmatrix} 0 & 1 & 0 & 0 \\ -a_2 & -a_1 & -a_4 & -a_3 \\ 0 & 0 & 0 & 1 \\ -c_4 & -c_3 & -c_2 & -c_1 \end{bmatrix}, \quad (29)$$

$$K(t) = \begin{bmatrix} 0 & 0 & 0 & 0 \\ -f_1 & 0 & -f_3 & -f_4 \\ 0 & 0 & 0 & 0 \\ -h_3 & -h_2 & -h_1 & 0 \end{bmatrix}, \quad (30)$$

and

$$K(t) \underline{z} = [0 \quad L_x \quad 0 \quad L_y]^T. \quad (31)$$

The differential equation (27) describes the system shown in Fig. VI - 4, which is again identical in form with the system shown in Fig. VI - 1. Provided that $G(s)$ is analytic in $\text{Re } s > 0$, it follows that a sufficient condition for stable θ_x and θ_z is

$$\|K(t)\|_{\max} \|G(j\omega)\|_{\max} < 1, \quad (32)$$

where $G(s)$ is the inverse of the matrix $sI - A$.

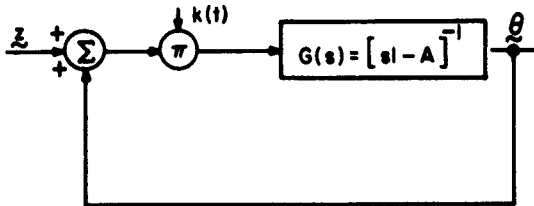


Figure VI-4

5. Conclusion

Although only stability was investigated in the examples presented, it is possible to obtain decaying exponential bounds on the signals in the undriven systems. Clearly, when σ_i in the theorem presented is negative, a $\sigma_c < \mu_c < 0$ can be chosen. It would then follow from (5) and (6) that

$$\|y\| \leq C e^{\mu_c t}, \quad \mu_c < 0 \quad (33)$$

provided that (3) is satisfied.

Finally it is evident that the computation of $\|A(x)\|_{\max}$ when $A(x)$ is $n \times n$ with $n > 2$ is tedious. However, considerable simplification, at the expense of a less precise result, can be made. It is not difficult to show that when A is an $n \times n$ matrix function of x ,

$$\|A(x)\|_{\max} \leq \sqrt{n} |a_{rk}(x)|_{\max} \quad (34)$$

where the a_{rk} are the elements of A and the maximum is taken over all x and all $r, k = 1, 2, \dots, n$.

Office of Scientific Research
 AFOSR-62-280
 Joint Services Technical Advisory Committee
 AF-AFOSR-62-295

J. J. Bongiorno, Jr.

References

1. D. C. Youla, "Some Results in the Theory of Active Networks," Report PIBMRI-1063-62, Microwave Research Institute, P. I. B. (August 1962).
2. J. J. Bongiorno, Jr., "An Extension of the Nyquist-Barkhausen Stability Criterion to Linear, Lumped-Parameter Systems with Time-Varying Elements," Proceedings of the Joint Automatic Control Conference, New York University, June 1962 (to be published in the IRE Trans. on Automatic Control, April 1963).
3. J. J. Bongiorno, Jr., "Convergence Properties of a Model-Reference Adaptive Control System from a Simple Stability Criterion," Proceedings of the National Electronics Conference, Vol. 18, pp. 250-259 (October 1962).

SYSTEMS AND CONTROL

4. J.J. Bongiorno, Jr., "Real-Frequency Stability Criteria for Linear Time-Varying Systems," in preparation.
5. R. Schindwolf, "Geocentric Attitude Control of an Earth Satellite," Ph.D. Dissertation in Electrical Engineering, Polytechnic Institute of Brooklyn, June 1962.

B. STUDIES IN OPTIMAL CONTROL THEORY

P. Dorato

Two investigations in optimal control theory are currently in progress. One is in the field of optimal distributed systems. The object of this study is to develop an optimal control theory for systems with more than one independent variable.

In particular, two independent-variable systems are under investigation: a time variable t and a space variable x . The output variable $Q(x, t)$ is assumed to be related to the input variable $u(x, t)$ by an integral equation of the form:

$$Q(x, t) = \int_0^x \int_0^t K(x, t; \xi, \tau) u(\xi, \tau) d\xi d\tau \quad (1)$$

with a performance criterion

$$P = \int_0^{x_1} \int_0^{t_1} M(Q, u(x, t); x, t) dx dt \quad (2)$$

The object is to determine $u(x, t)$ which minimizes (or maximizes) P . This study is based on the work of Butkovskii¹ and is being carried out by C. Hsieh (Junior Research Fellow).

In the other area of study, which is in the field of optimal parameter-adjustment, the problem is to determine $\underline{u} = \phi(\underline{x})$ which minimizes a performance criterion

$$S = \int_t^T F(\underline{x}) dt, \quad (3)$$

given a system:

$$\dot{\underline{x}} = \underline{A}(\underline{u}) \underline{x} \quad (4)$$

Some second-order examples are currently under investigation by A. Bhojwani (Junior Research Fellow).

Joint Services Technical Advisory Committee
AF-AFOSR-62-295

P. Dorato

Reference

1. A.G. Butkovskii, "The Maximum Principle for Optimum Systems with Distributed Parameters," Automation and Remote Control, Vol. 22, No. 10 (March 1962).

C. THE RESPONSE OF AN AUTOMATIC PHASE CONTROL SYSTEM TO FM SIGNALS AND NOISE

D.L. Schilling

Introduction

An Automatic Phase Control (APC) System was analyzed to determine its response to frequency modulated signals and narrow-band Gaussian noise. Emphasis was placed on the system's response to signals having "ramp" type fm.

The response of the APC system to an fm signal is obtained using a perturbation and a piecewise linear technique. The complete response to an fm signal and noise is then discussed using an iteration technique, and extending the results previously obtained. The techniques utilized in obtaining the system's response yield results which are far more accurate than the results obtained previously using a linearized version of the system.

1. Results

The APC system analyzed in this paper is shown in Fig. VI - 5.

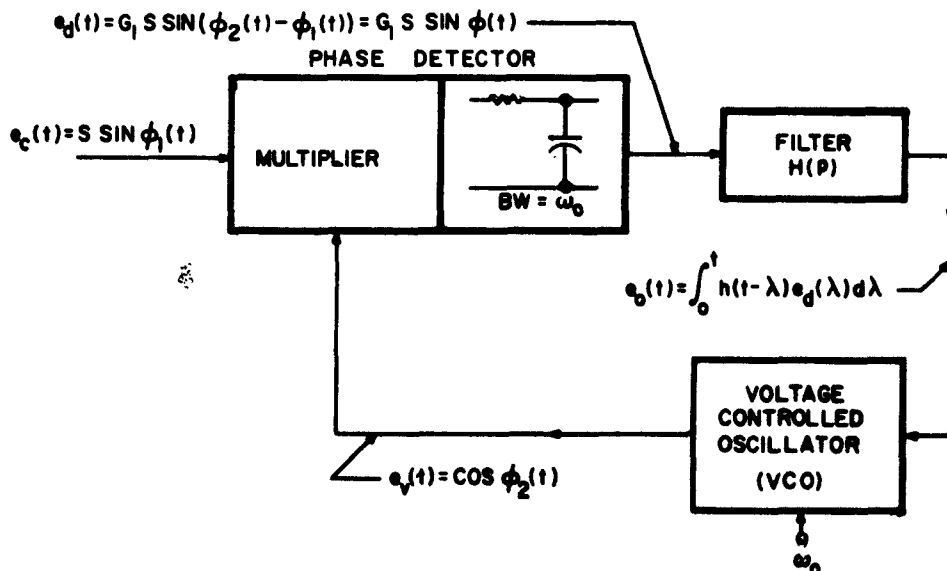


Fig. VI-5 An automatic phase control system

SYSTEMS AND CONTROL

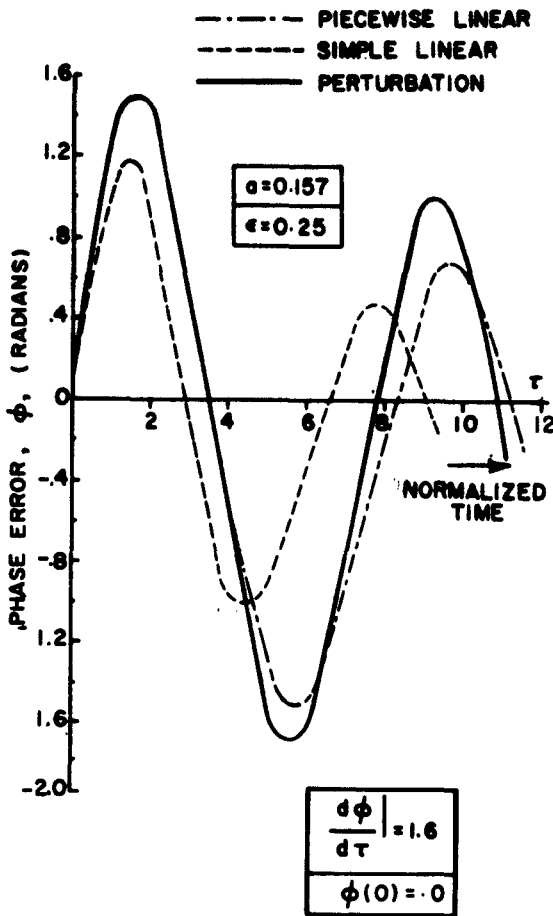


Fig. VI-6 A comparison of the approximate solutions used to obtain the response of the APC system to a frequency ramp modulated signal

linear technique and the simple linear technique used by other authors is shown in Fig. VI - 6.

When no signal is present, the input voltage consists solely of noise. The system responds as though it were an open circuit. Thus,

$$e_c(t) = N(t) \tag{6a}$$

and

$$e_v(t) = \cos(\omega_o t + \phi_n(t)) \tag{6b}$$

If the input signal, $e_c(t)$, is

$$e_c(t) = S \sin \phi_1(t) \tag{1}$$

and the output voltage of the voltage controlled oscillator (vco), $e_v(t)$, is

$$e_v(t) = \cos \phi_2(t) , \tag{2}$$

an indication of how closely the voltage, $e_v(t)$, follows the signal voltage, $e_c(t)$, is given by the phase error, ϕ_s , where

$$\phi_s = \phi_2(t) - \phi_1(t) . \tag{3}$$

The phase error can be calculated as a function of time using the equation

$$\ddot{\phi}_s + \epsilon \cos \phi_s \dot{\phi}_s + \sin \phi_s = -\ddot{\phi}_1 . \tag{4}$$

When $|\epsilon| < 1$ and $|\dot{\phi}_1| < 1$, the solution can be obtained using a perturbation technique, and perturbing about the solution to the pendulum problem

$$\ddot{\phi}_s + \sin \phi_s = 0 \tag{5}$$

When $|\epsilon| \geq 1$ a piecewise-linear technique can be used, although the results obtained are not as accurate as those obtained using the perturbation technique. A comparison of the results obtained using the perturbation technique, piecewise-

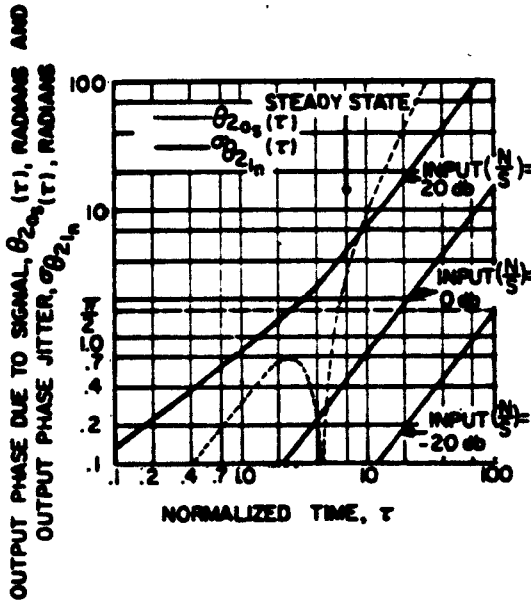


Fig. VI-7 Comparison of output phase $\theta_{2\phi_s}$ with the output phase jitter $\sigma_{\theta_{2\phi_n}}$

and the statistics of the product $[e_c(t)] \times [e_v(t)]$ are the same as $e_c(t)$. Hence the input noise $N(t)$ and the output noise $\phi_n(t)$ are uncorrelated.

When the signal is embedded in noise

$$e_c(t) = S \sin \phi_1(t) + N(t) \quad (7a)$$

and

$$e_v(t) = \cos(\phi_1(t) + \phi_s(t) + \phi_n(t)) \quad (7b)$$

where to a first approximation $\phi_s(t)$ and $\phi_n(t)$ are the phase errors obtained respectively when the signal alone is present, and when the noise alone is present.

Knowing $\phi_s(t)$ and the statistics of $\phi_n(t)$, the problem of whether or not $e_v(t)$ would follow $e_c(t)$, for $0 \leq t \leq T$, was investigated. Since this is a transient problem the phase jitter $\phi_n(t)$, is non-stationary,

and its standard deviation increases with time. An output S/N ratio,

$$(S/N)_{\text{output}} = \frac{\phi_1 + \phi_s}{\sigma_{\phi_n}} \quad (8)$$

was defined as in Eq. (8). Experimentally it was shown that at "steady state," the system will "lock" to the incoming signal if the output S/N ratio is greater than or equal to unity. Thus, for the particular example considered in Fig. VI-7 (ramp type fm), synchronization occurs when the input N/S ratio is less than 12 db.

In order to obtain locking, even when the input N/S ratio is very high, the APC system must be properly adjusted. When the noise is large, one tries to reduce the system bandwidth and hence reduce the noise. However, when the signal is frequency ramp modulated, the bandwidth is proportional to the rate of change of frequency. Thus we must decide on some optimum "bandwidth" to reduce the noise, but follow the modulation.

In addition, the probability of lock depends on whether the system is underdamped, critically damped or overdamped. It can be shown that a critically damped ($\zeta = 2$) system operates in an optimal manner, and that the bandwidth should be between

SYSTEMS AND CONTROL

four to nine times the rate of change of frequency.

2. Conclusions

The results obtained describe the operation of an APC system to an input signal in noise. It is shown that when ramp modulation is applied, the system operates best when it is critically damped with a bandwidth of four to nine times the rate of change of the fm. The maximum N/S ratio possible can also be obtained. It was shown to be 12 db for the critically damped system.

Joint Services Technical Advisory Committee
AF-AFOSR-62-295

D. L. Schilling

References

1. D. L. Schilling, "The Response of an Automatic Phase Control System to FM Signals and Noise," Report PIBMRI-1040-62, Microwave Research Institute, P.I.B. (June 1962).
2. D. L. Schilling and M. Schwartz, "The Response of an APC System to FM Signals and to Noise," 1962 IRE Convention Record, Vol. 10, Part 8.
3. D. L. Schilling, "The Response of an APC System to FM Signals and Noise," (to be published in 1963 IRE Convention Record).

D. SYNTHESIS OF OPTIMAL CONTROL SYSTEMS WITH CONTROL INPUT CONSTRAINTS

P. Dorato, I. Kliger

The following problem is currently under investigation by I. Kliger (Senior Research Fellow) under the supervision of Prof. P. Dorato.

Given a plant with dynamics

$$\dot{\underline{x}} = \underline{A} \underline{x} + \underline{B} \underline{u} \quad (1)$$

and a performance criterion

$$S = \int_0^T \underline{x}^T \underline{C} \underline{x} dt \quad (2)$$

determine a closed-loop control law $\underline{u}(t) = \underline{\phi}(\underline{x}, t)$, which minimizes S with control input constraints of the following types:

(a) Energy Constraints

$$\int_0^T \underline{u}^T \underline{Q} \underline{u} dt \leq L$$

(b) Amplitude Constraints

$$-a_i \leq u_i \leq a_i$$

The special object of this study is to obtain computational algorithms for the optimal closed-loop control law $\underline{\phi}(\underline{x}, t)$.

The optimal control law for both constraints (a) and (b) is shown to be nonlinear. The control law is obtained by iterated approximations. In particular, when the control law involves a switching surface (constraint (b)) it is shown that the first approximation yields a linear switching surface.*

The iterations start with the uncontrolled system $\underline{u} = \underline{0}$; hence a stable plant is assumed. Two iteration schemes are employed. One is essentially an approximation in "policy space" approach; the other is an approximation in "control amplitude" approach. In the latter method, solutions are obtained for increasingly larger values of a_i , from $a_i = 0$ to its full given value. A final report should be completed by June 1963.

Army Research Office (Durham)
DA-ARO(D)-31-124-G144

P. Dorato, I. Kliger

E. SMALL SAMPLE SEQUENTIAL DETECTION

R. R. Boorstyn

The problem discussed here is the application of sequential testing of statistical hypotheses to binary feedback communication systems with short transmission times, or, what is the statistical equivalent, low average sample sizes. This yields excellent results in systems where transmission time is at a premium, and where added complexity in the receiver (and to a lesser degree in the transmitter) and an essentially error-free feedback channel from receiver to transmitter are either available or practicable. Error-free feedback is already available in such systems as radar and satellite communications.

Statistical hypothesis testing with a fixed sample size has been applied by many to problems in binary communications. The optimum test is found by using the probability ratio of a sequence of random variables. A fixed number of signal repetitions (or samples) are determined to achieve a specified probability of error and signal-to-

*This result has been incorrectly interpreted as yielding the complete optimal control law. See C. Jen-Wei, "Synthesis of Relay Systems from the Minimum Integral Quadratic Derivation," *Automation and Remote Control*, Vol. 22, No. 12 (1961).

SYSTEMS AND CONTROL

noise ratio, and the signal is repeatedly transmitted. After the complete reception of all these samples, the receiver decides which of two possible signals has been sent. On a particular trial it often occurs that the same decision could have been reached if the test had been terminated before all the required number of samples were drawn: the probability that the remaining samples will change this decision is very small. Indeed, using the sequential test the average sample size can be reduced by half for a broad class of problems.

The sequential test, developed by Wald, and again utilizing the probability ratio for optimality, requires that the receiver consider all past samples in deciding not only which signal is present but also if another sample is required to make a more accurate decision. The transmitter is then so advised by means of the feedback channel and the process is continued until termination, when a decision is finally made.

A disadvantage is that the sample size is now a random variable. Although on the average it is smaller than that required by any other test, it may be extremely large for a particular trial. The test could then be prematurely terminated or truncated after a fixed number of samples have been drawn. Also, error in the feedback channel may cause instability or at least will deteriorate performance.

For large average sample sizes, Wald has developed excellent and simple approximations for the design and analysis of such tests. However, these do not hold for very small sample sizes. The work reported here contains (a) methods for the solution of such problems, (b) examples of communications interest -- the normal and Rayleigh distributions, (c) comments on truncation and optimality, and (d) a comparison with fixed sample size tests and sequential tests without memory (null-zone detection).

It has been determined that a considerable improvement over fixed sample size tests is obtained with average sample sizes as low as 1 to 1.2. For example, with the normal distribution an average sample size of 1.01 (that is, a second sample is required only once every 100 trials; the test can even be truncated at two without any adverse effects); probability of error of 10^{-8} ; and signal-to-noise ratio (ratio of distance between means to standard deviation) of 8, it has been found that a fixed sample size test of length 2 must be used to obtain comparable results. Thus a saving of 50 percent in length is obtained. Equivalently, a reduction in signal-to-noise ratio of 3 db is found over a fixed sample size test of length 1. It is interesting that for $P_e = .01$, $S/N = 1$, the average sample size is 9 (using Wald's large sample results) whereas the fixed size test requires a length of 22 (a 41 percent saving). All this work has been calculated assuming equal a priori probabilities.

SYSTEMS AND CONTROL

The course of some of the future work envisioned now is an investigation of (a) error in the feedback channel, (b) effects of truncation, and more ambitiously, (c) non-binary applications, parameter estimation, fading signals or non-stationary sequences of random variables, and dependent sequences of random variables.

A detailed report on the above topics has been published as a technical report, Report PIBMRI-1128-63.

Joint Services Technical Advisory Committee
AF-AFOSR-62-295

R. R. Boorstyn

F. RELIABILITY RESEARCH

C. Belove, M. L. Shooman

Reliability research is progressing in three areas. The first area is the study of combinatorial methods which can be used to express system reliability in terms of sub-system or component reliability. One important and difficult problem being studied is the physical interpretation of conditional failure probabilities. Most present approaches avoid this problem by assuming independent failures, which greatly simplifies the computations.

The second area of interest is a continued study of statistical models which describe component or unit failure rates. Several piecewise linear models and regression models are being evaluated with respect to their computational difficulty and accuracy. Much of the future work will center on the computation of model parameters from life test data. Especially important situations to be studied are those in which units are removed or additional units are added while the test is in progress.

The third area involves the statistical computation of system performance parameters in terms of the constituent component statistics. Some work has been done in this field using a Gaussian model for the component statistics. However, if the relation between the performance parameter and component parameters is more complex than a simple linear combination, the change-of-variables computation required is difficult and may result in an unknown distribution. It appears that in many cases the computations are simpler and the results more meaningful if a rectangular distribution model is used for the parameters.

Work is presently proceeding on the selection of appropriate distribution models to use in this study, and on various methods of approximating the change-of-variables technique. Some of this material is being incorporated in a set of course notes written for a graduate course in reliability analysis (IE 625).

SYSTEMS AND CONTROL

In the work on reliability, some major subdivisions of interest have been formulated. In discussing system reliability, one must deal with discrete (catastrophic) failures and continuous (drift) failures. Prof. Charles Belove is studying the continuous failure problem. As a prelude to a stochastic treatment of part variations and their effect on system reliability, he has studied the variation in pole-zero positions of a system transfer function as the lumped circuit parameters change in a deterministic manner. A probabilistic treatment of the continuous failure problem will be begun at the conclusion of this work.

Initial work on the probabilistic solution to the discrete failure problem has included the formulation of mathematical models to describe the probability of success of a single component. The models are based on the part conditional failure rate $z(t)$ and give the reliability as

$$R(t) = e^{-\int_0^t z(\xi) d\xi}$$

Several piecewise linear and curvilinear models have been fitted to $z(t)$. Statistical point estimates for the model parameters based on experimental failure data have been computed. At present, work is proceeding on the problem of relating these part (unit) reliability models to circuit (system) reliability models. Many of these latter results were included in the graduate course IE 625 during the Fall 1962 semester. It is hoped that thesis work in these areas will be started in the near future.

Joint Services Technical Advisory Committee
AF-AFOSR-62-295

M. L. Shooman

G. THEORY OF SWITCHING CIRCUITS

Z. Kohavi, P. Lavalley, W.C.-W. Mow, E.J. Smith

1. SYNTHESIS BY LINEAR GRAPHS

In the final steps of the synthesis of contact networks by linear graph theory,¹ matrices of integers of the field modulo 2 appear in conjunction with constrained variables. For any practical problem, the number of different matrices generated by these constrained variables may be quite large. To yield the realizability of fundamental circuit matrices, an algorithm characterized by simplicity and generality of solution is desirable.

The procedure rests on the following theorem. Let

$$B_f = \begin{bmatrix} I & B_{f_{12}} \end{bmatrix}$$

where I is the identity matrix.

Theorem:

(1) If $B_{f_{12}}$ constrains a row (w) with non-zero elements in columns i, j, k, \dots , then a necessary condition for the realizability of B_f is that the matrix (K) formed by columns i, j, k, \dots , must be realizable as a linear-tree structure.

(2) Order of the linear trees:² if there exists an arrangement of columns of the matrix (K) defined by row (w), such that no two ones are separated by one or more zeros, then this matrix (K) is always realizable as a fundamental circuit matrix of a graph defined by the edges of the sub-tree considered.

- a) The sub-tree is linear;
- b) The edges are ordered in the same way as the columns of the matrix (k) defined by row (w), after rearrangement.

With this procedure, matrices can be examined quickly for realizability. The procedure also forms an important tool in the examination of matrices with constrained variables (0 or 1).

Methods of synthesis are evolved for specifications of the type

$$\{F_i\}_i$$

that is, the simultaneous synthesis of i functions. As an extension of the tools provided by the realizability criterion and the simultaneous synthesis, one-port, non-bilateral switching functions are considered. While previous work³ was restricted to a linear-tree type configuration, this study extends the tree configuration to any possible type by using only the field of integers, modulo 2 (a non-oriented matrix), and orienting the matrix according to the specifications and constraints on the matrix.

P. Lavallee

References

1. R. Gould, "Application of Graph Theory to the Synthesis of Contact Networks," Ph.D. Dissertation, Harvard University, 1957.
2. R. B. Ash and W. H. Kin, "On the Realizability of a Circuit Matrix," IRE Trans. on Circuit Theory, Vol. CT-6, pp. 219-223 (June 1959).
3. E. J. Smith, C. M. Healy, W. C.-W. Mow, "Synthesis of Two-Terminal, Contact-Diode Networks," Report PIBMRI 1144-63, Microwave Research Institute, P. I. B.

SYSTEMS AND CONTROL

2. SECONDARY STATE ASSIGNMENT IN SEQUENTIAL MACHINES

Research is under way to develop methods which result in an economical state assignment for finite-state sequential machines. The problem of assigning the secondary variables to represent the internal states of the machines is of great importance. A poor assignment may result in a very complicated and expensive machine, while a better assignment may reduce the complexity of the resulting network.

It has been shown^{1, 2} that an assignment with self-dependent subsets generally reduces the complexity of the network. Such assignments can be achieved if the state table, which corresponds to the sequential machine, possesses a partition with the substitution property.

The importance of the partition with substitution property is increased by its being a necessary and sufficient condition for a cascade and parallel decomposition of sequential machines. Since the class of machines which possesses the partition with substitution property is very limited, a method is being developed to find equivalent machines for which there exists a partition with substitution property.

A forthcoming report will show that for every finite-state sequential machine M there exists at least one equivalent finite-state sequential machine $M' \cong M$ which possesses a partition with substitution property. A similar method has been developed for equivalent machines for which there exists a partition pair.

In this study, techniques were developed to find equivalent machines which possess the above-mentioned properties, and to develop the manner of assigning to them the secondary variables in such a way that a decomposition and/or economical network would result. Finally, it is noteworthy to mention that the methods have been developed for completely and incompletely specified sequential machines.

Joint Services Technical Advisory Committee
AF-AFOSR-62-295

Z. Kohavi

References

1. J. Hartmanis, "On the State Assignment Problem for Sequential Machines," Parts I and II, IRE Trans. on Electronic Computers, Vol. EC-10, No. 2 (June 1961); Vol. EC-10, No. 4 (December 1961).
2. Z. Kohavi, "Sequential Switching Circuits," Report PIBMRI-1090-62, Microwave Research Institute, P. I. B. (January 1963).

H. NARROW-BAND TELEVISION SYSTEM

S. Deutsch

The first phase of research on narrow-band television systems has been completed. The 10 kc/sec system employs pseudo-random scan¹ with the following standards:

Frame frequency: 0.375 cps
 Horizontal sweep frequency: 24 cps
 Vertical sweep frequency: 768 cps
 Nominal bandwidth: 9.216 kc/sec
 Coarse scan: 24 rows x 32 columns of dots
 Pseudo-random scan: 8 vertical x 8 horizontal elements
 Nominal resolution: 192 vertical x 256 horizontal elements

The experimental results are as follows. Despite the use of a long-persistence P 26 picture-tube phosphor, the dot structure is excessively annoying. The dot structure vanishes when the cathode-ray tube beam is defocussed, yielding a picture that has, in effect, the following standards:

Frame frequency: 1.5 cps
 Horizontal sweep frequency: 24 cps
 Vertical sweep frequency: 768 cps
 Nominal bandwidth: 9.216 kc/sec
 Coarse scan: 24 rows x 32 columns of dots
 Pseudo-random scan: 4 vertical x 4 horizontal elements
 Nominal resolution: 96 vertical x 128 horizontal elements

Although the latter picture nominally contains only 12,288 elements, the resolution is adequate for many purposes and the entertainment value is good. Steps are under way for the establishment of a short-wave experiment using these standards. At the same time, a thesis student is installing a scan conversion tube and associated circuitry in an attempt to achieve the original nominal resolution of 49,152 elements without excessive dot structure.

Magnetic tape recording of the 10 kc/sec signal is easily accomplished at a tape speed of 15 inches/sec. With better equipment, a speed of 7.5 inches/sec should be sufficient. The tape speed must be constant to a high degree of accuracy to prevent excessive frequency modulation of the synchronizing signals.

The next phase of the project is the construction of a high resolution system with

SYSTEMS AND CONTROL

the following standards:

Frame frequency: 1.25 cps
Horizontal sweep frequency: 40 cps
Vertical sweep frequency: 2560 cps
Nominal bandwidth: 122.88 kc/sec
Coarse scan: 96 rows x 64 columns of dots
Pseudo-random scan: 4 vertical x 8 horizontal elements
Nominal resolution: 384 vertical x 512 horizontal elements

This 122.88 kc/sec signal can be sampled by four groups of pulses which yield four channels, each with a bandwidth of 30.72 kc/sec. The latter can be recorded on 4-track magnetic tape at a speed of 15 inches/sec. Work is being performed on the "electronics" for this recorder.

Although the above system is narrow-band, compensation of the video amplifier is still required for good transient response.² Specifically, a 5-reactance, 3-terminal peaking circuit has been analyzed for flat amplitude, flat-time delay, and critically damped transient responses.³

The system employs a sampling technique to get maximum bandwidth reduction without loss of information. It appears that nearly optimum smoothing is provided by ladder networks whose poles form a semicircular array with equal spacing in the vertical direction.⁴

The derivation of a network function $F(s)$ when its phase function $\theta(\omega)$ is given has also been investigated.⁵

Joint Services Technical Advisory Committee
AF-AFOSR-62-295

S. Deutsch

References

1. S. Deutsch, "Narrow-Band TV Uses Pseudo-Random Scan," *Electronics*, Vol. 35, pp. 49-51 (April 27, 1962).
2. S. Deutsch, "Critically Damped Compensation for Broadband Amplifiers," Report PIBMRI-1051-62, Microwave Research Institute, P.I.B. (July 1962).
3. L. Foley, "A Five-Reactance Three-Terminal Peaking Circuit," Report PIBMRI-1119-63, Microwave Research Institute, P.I.B. (February 1963).
4. R.I. Disman and S. Deutsch, "Filters with Poles Having Equal Vertical Spacing," Report PIBMRI-1077-62, Microwave Research Institute, P.I.B. (September 1962).
5. S. Deutsch, "The Derivation of Network Functions from Phase Functions," Report PIBMRI-1006-62, Microwave Research Institute, P.I.B. (March 1962).

PUBLICATIONS AND REPORTS

MEETING PAPERS

Eighth Annual Conference on Magnetism and Magnetic Materials, Pittsburgh, Pa., September 1962

E. Banks and M. Robbins, "The Effect of Fluoride-Compensated Co^{2+} Substitution on the Anisotropy of $\text{BaFe}_{12}\text{O}_{19}$ "

Symposium on Relay Systems and Finite Automata, Moscow, U. S. S. R., September 24 - October 2, 1962

National Electronics Conference, Chicago, Ill., October 8-10, 1962

J. J. Bongiorno, Jr., "Convergence Properties of a Model Reference Adaptive Control System from a Simple Stability Criterion"

M. Schwartz, "Signal-to-Noise and Threshold Effects in fm"

Fall URSI -IRE Meeting, Ottawa, Canada, October 15-17, 1962

A. A. Oliner, "A Dispersion Curve Approach to the Analysis of Log-Periodic Antennas"

First Congress on the Information System Sciences, Hot Springs, Va., November 1962

R. F. Drenick, "Outline of a Future Systems Theory"

1962 Conference on Magnetism and Magnetic Materials, Pittsburgh, Pa., November 13, 1962

H. J. Juretschke, "DC Detection of Spin Resonance in Thin Metallic Films"

American Physical Society Meeting, New York, January 1963

M. Nahemow and N. Wainfan, "High-Field Effects in a Pulsed Wall-Bound Discharge in Hydrogen"

IEEE Winter General Meeting, New York, January 26-30, 1963

M. Sandler, "On Electromechanical Pulse Generators"

American Educational Research Association, Chicago, Ill., February 1963

R. F. Drenick, "Systems Theory"

IDA Pulse High Power Conference, Washington, D. C., February 4-5, 1963

E. Levi, "Pulse Generators with Solid Conductors"

IEEE Convention, New York, March 1963

M. Ettenberg, "Survey of High Power Microwave Tubes"

Optical Society of America Meeting, Jacksonville, Fla., March 1963

L. Bergstein, "Reflection and Transmission of Bounded Waves by Layered Media"

PUBLICATIONS AND REPORTS

Polytechnic Institute of Brooklyn, Thirteenth Annual Symposium: Optical Masers, New York, April 17, 1963

L. Bergstein and H. Schachter, "Stationary Modes in Optic and Quasioptic Cavities"

SWIRECO Meeting, Dallas, Texas, April 19, 1963

L. Braun, "Basic Concepts of Adaptive Control"

6th Midwest Symposium on Circuit Theory, Madison, Wisconsin, May 6, 1963

F. T. Boesch and D. C. Youla, "On the Synthesis of Resistor N-Ports"

JOURNAL ARTICLES

- E. Banks and M. Robbins, "The Effect of Fluoride-Compensated Co^{2+} Substitution on the Anisotropy of $\text{BaFe}_{12}\text{O}_{19}$ " (to be published in J. Appl. Phys.).
- E. Banks (see Ribnick, Post and Banks).
- L. Bergstein, "Reflection and Transmission of Bounded Waves by Layered Media" (to be published in J. Opt. Soc. Am.).
- H. Bertoni and M. Ettenberg, "Determination of Electron Density Profile" (to be published in J. Appl. Phys.).
- H. Carlin and D. C. Youla, "On the Realizability of the Complex Ideal Transformer" (IRE Trans. on Circuit Theory, Vol. CT-9, No. 4, December 1962).
- W. Egan (see Juretschke and Egan).
- S. Epstein (see Juretschke and Epstein).
- M. Ettenberg (see Bertoni and Ettenberg).
- L. R. Felsen, "Radiation from a Uniaxially Anisotropic Plasma Half Space" (to be published in IRE Trans. on Antennas and Propagation, July 1963).
- L. B. Felsen (see Marcinkowski and Felsen).
- H. J. Juretschke, "DC Detection of Spin Resonance in Thin Metallic Films" (J. Appl. Phys. Suppl., March 1963).
- H. J. Juretschke and W. Egan, "DC Detection of Ferromagnetic Resonance in Thin Nickel Films" (J. Appl. Phys., May 1963).
- H. J. Juretschke and S. Epstein, "Galvanomagnetic Effects and Band Structure of Pure and Tin Doped Single Crystal Antimony" (Phys. Rev., Vol. 129, p. 1148, 1963).
- W. K. Kahn, "Power Transmission through General Uniform Waveguides" (IRE Trans. on Microwave Theory and Techniques, pp. 329-331, September 1962).
- C. J. Marcinkowski and L. B. Felsen, "On the Geometric-Optical Properties of Curved Surfaces with Periodic Impedance Properties" (J. Res. Natl. Bur. Standards, Vol. 66D, No. 6, p. 699, 1962).
- C. J. Marcinkowski and L. B. Felsen, "On the Limitations of Geometrical Optics Solutions for Curved Surfaces with Variable Impedance Properties" (J. Res. Natl. Bur. Standards, Vol. 66D, No. 6, p. 707, 1962).

PUBLICATIONS AND REPORTS

- N. Marcuvitz, "Propagation of Waves in Plasma" (Phys. Today, Vol. 15, No. 12, December 1962, December 1962).
- M. Nahemow and N. Wainfan, "High-Field Effects in a Pulsed Wall-Bound Discharge in Hydrogen" (Bull. Am. Phys. Soc., Series II, Vol. 8, No. 1, p. 58).
- A. A. Oliner (see Tamir and Oliner).
- H. Pande, "Current Source Excitation-Type Electro-Mechanical Pulser" (to be published in Trans. IEEE, Pt. 1, Paper 63-1006).
- G. Persky, "The Sinusoidal Variation of Dissipation along Uniform Waveguides" (IRE Trans. on Microwave Theory and Techniques, Vol. 10, pp. 592-595, November 1962).
- B. Post (see Ribnick, Post and Banks).
- A. Ribnick, B. Post and E. Banks, "Phase Transitions in Sodium Tungsten Bronzes" (to be published in Advances in Chemistry Series).
- D. L. Schilling (see Schwartz and Schilling).
- M. Schwartz and D. L. Schilling, "The Response of an Automatic Phase Control System to FM Signals and Noise" (1962 IRE Convention Record).
- L. Shaw, "Discussion of the Paper 'A General Solution for Linear Sampled Data Control' by Gunckel and Franklin" (to be published in ASME J. Basic Eng., 1963).
- L. Shaw, "Dual Mode Filtering of Polynomial Signals Noise" (IEEE Trans. on Automatic Control, April 1963).
- T. Tamir and A. A. Oliner, "Guided Complex Waves: Part I -- Waves at an Interface" (Proc. IEE [London], Vol. 110, p. 310, February 1963).
- T. Tamir and A. A. Oliner, "Guided Complex Waves: Part II -- Relation to Radiation Patterns" (Proc. IEE [London], Vol. 110, p. 325, February 1963).
- T. Tamir and A. A. Oliner, "The Spectrum of Electromagnetic Waves Guided by a Plasma Layer" (Proc. IEEE, Vol. 51, p. 317, February 1962).
- D. C. Youla (see Carlin and Youla).
- N. Wainfan (see Nahemow and Wainfan).

LETTERS TO THE EDITOR

- J. J. Bongiorno, Jr., "An Extension of the Nyquist-Barkhausen Stability Criterion to Linear, Lumped-Parameter Systems with Time-Varying Elements" (IRE Trans. on Automatic Control, April 1963).
- P. J. Crepeau and T. Keegan, "A Beam-Plasma Surface Wave Interaction" (IRE Trans. on Microwave Theory and Techniques, September 1962).
- S. Deutsch, "Critically Damped Compensation for Broadband Amplifiers" (IEEE Trans. on Circuit Theory, March 1963).
- W. K. Kahn, "A Molecular Beam High Power Meter" (to be published in Proc. IEEE).
- T. Keegan (see Crepeau and Keegan).
- J. M. Mendel, "Experimental Measurements Useful in Determining the Damping Ratio ζ for a Second-Order Response" (IRE Trans. on Automatic Control, January 1963).

PUBLICATIONS AND REPORTS

- A. A. Oliner and I. Palocz, "Cerenkov Radiation and Leaky Waves" (to be published in Proc. IEEE).
- A. A. Oliner (see Tamir and Oliner).
- I. Palocz (see Oliner and Palocz).
- M. Sandler, "Comment on Magnetohydrodynamics and Electrohydrodynamics" (Phys. Fluids, December 1962).
- T. Tamir and A. A. Oliner, "Comments on Surface Waves along Plasma Slabs" (IEEE Trans. on Antennas and Propagation, Vol. AP-11, May 1963).

RECENT BOOKS

- W. R. Bennett (see Schwartz, Bennett and Stein).
- L. Braun, Jr. (see Mishkin and Braun).
- E. Mishkin and L. Braun, Jr., eds., "Adaptive Control Systems" (New York: McGraw-Hill, 1960) (to be translated into Japanese [Tokyo, Japan: Corona Publishing Co., 1963]); (to be translated into Polish, 1964).
- M. Schwartz, W. R. Bennett and S. Stein, "Communication Systems and Techniques" (to be published by McGraw-Hill, 1964).
- S. Stein (see Schwartz, Bennett and Stein).

CONTRIBUTIONS TO RECENT BOOKS

- E. Arbel and L. B. Felsen, "On the Theory of Radiation from Sources in Anisotropic Plasmas-- Parts I and II," in Proc. Symposium on Electromagnetic Theory and Antennas (to be published by Pergamon Press, 1963).
- J. J. Bongiorno, Jr., "Convergence Properties of a Model-Reference Adaptive Control System from a Simple Stability Criterion," in Proc. National Electronics Conference, Vol. 18, pp. 250-259.
- L. Braun, Jr., ed., Electrical Engineering Section, Perry's Chemical Engineers' Handbook, 4th ed. (to be published in September 1963).
- R. F. Drenick, "Outline of a Future Systems Theory," in Fundamentals of Information System Science and Engineering, ed. E. M. Bennett (to be published).
- L. B. Felsen (see Arbel and Felsen).
- C. M. Healy (see Smith, Healy and Mow).
- W. C.-W. Mow (see Smith, Healy and Mow).
- L. Shaw, "Optimum Stochastic Control," in Cybernetics Engineering, ed. J. Peschon (to be published by Ginn and Co., January 1964).
- E. J. Smith, C. M. Healy, and W. C.-W. Mow, "Synthesis of Contact-Diode Networks," in Proc. Symposium on Relay Systems and Finite Automata (to be published).

PUBLICATIONS AND REPORTS

TECHNICAL REPORTS

- 1077 R. I. Disman and S. Deutsch, **Filters with Poles Having Equal Vertical Spacing.**
- 1078 J. Lieutand, **Optimization of Multivariable Sampled-Data Control Systems.**
- 1079 F. Jazede, **A Study of Stabilization of an Earth Satellite.**
- 1080 G. Zysman, **Properties of Cascaded Microwave C-Section and Transmission Line Networks (Networks and Waveguides Group Memo No. 73),**
- 1081 P. Shivdasani, **Sensitivity of Some Low Order Bang-Bang Control Systems,**
- 1082 K. Lian, **An Electrodeless Gaseous Plasma Switch Tube for High Power Pulse Modulators - Part IV (Systems and Control Group Memo No. 51).**
- 1083 L. B. Felsen, **Modal Analysis and Synthesis.**
- 1084 W. C.-W. Mow, **On the Minimal Set of Compatibles for Closure.**
- 1085 J. J. Borgiorno, **Final Report - Computer Controlled and Model-Reference Adaptive Feedback Control Systems,**
- 1086 W. Heinz, **DC Effects under Microwave Excitation of Thin Ferrite Films.**
- 1087 S. Geldston, **Probability Distribution at the Output of a Logarithmic Receiver.**
- 1088 J. G. Truxal, **Active and Time Varying Systems and Linear Networks - Final Report.**
- 1089 H. J. Carlin and W. Kohler, **Equiripple Transmission Line Networks.**
- 1090 Z. Kohavi, **Analysis and Synthesis of Sequential Switching Circuits.**
- 1091 W. Ku, **A Theory for Broadband Varactor Parametric Amplifiers.**
- 1092 A. Reynolds, **Canonical Form of Two Tandem-Connected Four-Ports.**
- 1093 P. Hirsch and J. Shmoys, **Surface Waves on Plasma Slabs (Electrophysics Group Memo No. 85),**
- 1094 D. S. Wilson, **Spectroscopic Measurement of Electron Temperature (Systems and Control Group Memo No. 50).**
- 1095 P. Dorato and J. G. Truxal, **Feedback Design and Optimal Control Theory (Systems and Control Group Memo No. 52).**
- 1099 M. Menes, **Final Report on Magnetic Resonance Research. .**
- 1100 T. Morrone, **Electron Ion Two-Stream Instability.**
- 1101 R. J. Nawrocky, **Sinusoidal Steady-State Analysis of a Limit Cycling Control System Containing an Ideal Contactor.**
- 1102 A. E. Laemmel, **Measurement of Ionospheric Paths as a Time-Varying Network.**
- 1103 A. Kerdock, **Coherent Detection on Pulsed Radars.**
- 1104 L. Mantgiaris, **Dual Mode Control.**
- 1105 D. C. Youla, **On the Stability of Linear Systems (Networks and Waveguides Group Memo No. 72).**
- 1106 L. Braun and P. Dorato, **Final Report - Analysis of Flight Control Data and Information.**

PUBLICATIONS AND REPORTS

- 1107 M. Ettenberg, **Special Scientific Report on Investigations in Gaseous Electronics.**
- 1108 R. F. Drenick, **A Statistical Theory of Feedback Control.**
- 1109 K. T. Lian, **Response of a Plasma Slab to an Electric Field (Systems and Control Group Memo No. 55).**
- 1110 H. Berger, **Non-Reciprocal Directional Couplers and Applications in TWR Circuits.**
- 1111 H. Goldie, **A Fast Broadband High Power Microwave Gas Switch.**
- 1112 L. B. Felsen, **Final Report - Exploratory Research in Electromagnetics Networks and Related Solid State and Plasma Topics.**
- 1113 P. J. Crepeau and P. McIsaac, **Consequences of Symmetry in Periodic Structures.**
- 1114 M. P. Barr, **Bibliography from Report "Modulation at Millimeter Wavelengths" (Networks and Waveguides Group Memo No. 74).**
- 1115 E. Levi, **On Hydromagnetic Flows (Systems and Control Group Memo No. 56).**
- 1116 K. T. Lian, **The Effect of Cumulative Ionization on Breakdown Time (Systems and Control Group Memo No. 57).**
- 1117 R. Wohlers, **On the Normalization of Scattering Matrices to Positive Real Function (Networks and Waveguides Group Memo No. 75).**
- 1118 R. Wohlers, **The Problem of Compatible Impedances.**
- 1119 L. Foley, **A Five Reactance 3-Terminal Peaking Circuit.**
- 1120 A. Papoulis, **Marginal and Joint Normal Densities (Systems and Control Group Memo No. 58).**
- 1121 A. Papoulis, **An Estimate of the Variation of a Band-Limited Process (Systems and Control Group Memo No. 59).**
- 1122 E. S. Cassedy and A. A. Oliner, **Dispersion Relations in Time-Space Periodic Media, Part I - Stable Interactions.**
- 1123 J. W. E. Griemsmann, **The Equivalent Circuit of a Lossless Reciprocal 3-Port Having One Matched Port (Networks and Waveguides Group Memo No. 77).**
- 1124 L. B. Felsen and N. Marcuvitz, **Modal Analysis and Synthesis of Electromagnetic Fields.**
- 1125 S. Freedman, **Analysis of Non-Linear Control Systems with Stochastic Inputs (Systems and Control Group Memo No. 60).**
- 1127 J. Ruddy, **Preliminary Analysis on Low Loss Groove Guide (Networks and Waveguides Group Memo No. 78).**
- 1128 R. Boorstyn, **Small Sample Sequential Detection.**
- 1129 E. Levi, **Electromechanical Pulser.**
- 1130 A. E. Laemmel, **Final Report - Pattern Recognition and Detection by Machine.**
- 1131 J. M. Mendel, **The Identification of Over-Damped Processes in the Time Domain.**
- 1132 J. J. Jonsson, **An Approximate Time-Optimal Bang-Bang Discrete Control System Based on a Fast Future State Model (Systems and Control Group Memo No. 61).**

PUBLICATIONS AND REPORTS

- 1133 E. S. Cassedy, Generalized Time-Space Periodic Modulations in Cyclotron Parametric Amplifiers (Electrophysics Group Memo No. 86).
- 1135 W. Bellmer and B. Rudner, Experiments in Radio Station Recognition.
- 1136 A. Matsumoto and D. C. Youla, Darlington Type-D Sections Made with 2 Hunks of 2-Wire Lines (Networks and Waveguides Group Memo No. 79).
- 1137 H. M. Altschuler, The Matrix Manipulation of Bilinear Transformations.
- 1138 H. Pande, Electromechanical Pulsers.
- 1139 K. T. Lian, Evaluation of an Electrodeless Gaseous Plasma Switch Tube for High Power Pulse Modulations: Part I - Plasma Theory.
- 1140 K. T. Lian, Evaluation of an Electrodeless Gaseous Plasma Switch Tube for High Power Pulse Modulations: Part II - Experimental Investigations of Pulsed High Current Electrodeless Discharges in Hydrogen.
- 1141 K. T. Lian, Evaluation of an Electrodeless Gaseous Plasma Switch Tube for High Power Pulse Modulations: Part III - Modulator Design Theory and Experiment.
- 1142 D. C. Youla, An Introduction to the Analytic Theory of Parametric Networks - Part I (Networks and Waveguides Group Memo No. 80).
- 1143 F. T. Boesch, On the Synthesis of Resistor N-Ports.
- 1144 C. M. Healy, W. C.-W. Mow and E. J. Smith, Synthesis of Two-Terminal Contact-Diode Networks.
- 1145 A. Hessel and J. Shmoys, Conversion of Transverse Electromagnetic Waves into a Longitudinal Wave at a Dielectric Plasma Boundary (Electrophysics Group Memo No. 87).
- 1146 P. Lavallee, Switching Networks by Linear Graph Theory.
- 1147 M. Messinger and H. E. Parker, The Dynamics of Gyroscope Damping for Geocentric Attitude Control.
- 1148 H. M. Altschuler, Long Line Effect in Connection with Cavity Resonances.
- 1149 H. M. Altschuler, The Interchange of Source and Detector in Microwave Measurements.

COLLOQUIA AND SEMINARS

- April 25 **Synthesis of Optimal Control Systems with Amplitude Constraints:
Linear Plant, Quadratic Performance Index**
I. Kliger
- May 2 **Optimal Control of Continuous-Time Stochastic Systems**
Prof. P. Dorato
- May 9 **The Identification of Overdamped Processes in the Time-Domain**
J. Mendel

ELECTROMAGNETICS SEMINARS

- October 23, 1962 **Log-Periodic Antennas and Their Analysis in Terms of Brillouin
Diagrams**
Prof. A. A. Oliner
- October 30 **Dispersion Equations Involving Temperature Effects in Plasmas**
Prof. H. Motz, Oxford University, England
- November 13 **Reflection from an Inhomogeneous Plasma**
P. Hirsch
- November 20 **Landau Damping**
Prof. E. Levi
- December 4 **Landau Damping - Part II**
Prof. E. Levi
- January 31, 1963 **Report on the Millimeter and Submillimeter Conference**
Prof. L. Levey
- January 31 **Scattering by Obstacles in a Gyrotropic Medium**
Dr. S. R. Seshardri, Harvard University
- February 8 **Diffraction of Electromagnetic Waves by Elliptic Cylinders Embed-
ded in a Uniaxial Material**
B. Rulf
- February 15 **Hill's Vortex in Magnetohydrodynamics**
Dr. F. K. Moore, Cornell Aeronautical Laboratory
- March 13 **Molecular Solids**
Prof. H. A. Pohl
- March 15 **Inhomogeneous Materials**
Prof. H. Juretschke
- March 15 **Pulse Diffraction by a Half-Plane**
Dr. M. Papadopoulos, Mathematics Research Center,
University of Wisconsin
- March 20 **Covalent Solids**
Prof. F. Collins
- April 8, 12, 22 **The Calculation of the Effect of Discontinuities in Waveguide**
L. Lewin, Standard Telecommunication Laboratories,
Harlow, Essex, England

COLLOQUIA AND SEMINARS

- April 19 **Microwave Research in the University of Sheffield, England**
 A. L. Cullen, University of Sheffield, Sheffield, England
- April 23 **Some Aspects of Propagation in Inhomogeneous Media**
 Prof. D. S. Jones, University College of North Staffordshire,
 Keele, Staffordshire, England
- April 24 **Smoothing Filters for Sampling Pulses**
 Prof. S. Deutsch
- April 26 **On the Relation between Leaky Waves and Lateral Waves**
 Prof. T. Tamir
- May 1 **Wiener's Mean Squared Prediction Theorem**
 Prof. A. Papoulis
- May 3 **Research at Standard Telecommunication Laboratories**
 L. Lewin, Standard Telecommunication Laboratories,
 Harlow, Essex, England
- May 10 **Microwave Optics and Antennas**
 C. J. Sletten, Air Force Cambridge Research Center
- May 17 **Light Emission from Semiconductors**
 Dr. S. Mayberg, General Telephone and
 Electronics Laboratories

ELECTROPHYSICS SEMINARS

- October 15, 1962 **Electronic Beam Steering for Radar Systems**
 G. Ross, Sperry Gyroscope Company
- October 26 **New Techniques in the Synthesis of Resistor n -Ports Described on**
 $n + 1$ Modes
 F. Boesch
- February 15, 1963 **Radiation from an Electromagnetic Source in a Plasma Half Space**
 S. R. Seshadri, Harvard University
- March 1 **Review of Third International Congress on Quantum Electronics**
 W. K. Kahn
- April 5 **Reflection of Plane Waves from an Inhomogeneous Plasma**
 P. Hirsch
- April 12 **On the Relation between Lateral Waves and Leaky Waves**
 Prof. T. Tamir

COLLOQUIA AND SEMINARS

**ANNOUNCEMENT OF 1963 SUMMER CLINIC ON
MICROWAVE FIELD AND NETWORK TECHNIQUES**

Polytechnic Institute Graduate Center

June 3-7, 1963

The short course on "Microwave Field and Network Techniques" is presented by the Electrophysics Department. The course will emphasize basic physical concepts and mathematical techniques as well as their application to specific current problems.

PROGRAM

MONDAY, JUNE 3

9:00 - 9:15 a. m. H. J. Carlin, Head, Electrophysics Department, Introduction
9:15 - 12:15 p. m. L. B. Felsen, "Quasi-optic Diffraction"
12:15 - 1:30 p. m. LUNCHEON AND INFORMAL DISCUSSION
1:30 - 3:30 p. m. J. Shmoys, "Waves in Compressible Plasmas"

TUESDAY, JUNE 4

9:15 - 10:45 a. m. A. Hessel, "Network Methods in Radiation Problems"
10:45 - 12:15 p. m. T. Tamir, "Waves along Smooth Open Structures"
12:15 - 1:30 p. m. LUNCHEON AND INFORMAL DISCUSSION
1:30 - 4:30 p. m. A. A. Oliner, "Radiating Periodic Structures"

WEDNESDAY, JUNE 5

9:15 - 12:15 p. m. J. W. E. Griemsmann, "Oversized Guides and Multimode Techniques"
12:15 - 1:30 p. m. LUNCHEON AND INFORMAL DISCUSSION
1:30 - 4:30 p. m. INFORMAL TOUR OF LABORATORIES

THURSDAY, JUNE 6

9:15 - 11:15 a. m. W. Kahn, "Waveguide Junctions"
11:15 - 12:15 p. m. H. Altschuler, "Measurement of Active and Non-reciprocal Microwave Structures"
12:15 - 1:30 p. m. LUNCHEON AND INFORMAL DISCUSSION
1:30 - 4:30 p. m. H. J. Carlin, "Network Synthesis with Transmission Line Elements"

FRIDAY, JUNE 7

9:15 - 12:15 p. m. D. Youla, "Analytic Theory of Parametric Networks"

COLLOQUIA AND SEMINARS

ANNOUNCEMENT OF SEMINAR IN SPACE COMMUNICATIONS

Polytechnic Institute Graduate Center

June 17-21, 1963

The seminar in "Space Communications" presented by the Electrical Engineering Department is intended to introduce the practicing engineer to the theoretical and practical problems arising in this new area of communications. Lectures will include topics in classical communication theory as well as engineering aspects of existing systems such as Telstar, Relay, and Ranger.

PROGRAM

MONDAY, JUNE 17

10:00 - 10:15 a. m.

Welcoming Address

10:30 - 12:30 p. m.

SESSION 1

M. Ferguson, "Formulation of the Problems Arising in the Design of Space Communication Systems"

M. Ferguson, "Channel Characterization"

12:45 - 1:45 p. m.

LUNCHEON

2:00 - 5:00 p. m.

SESSION 2

W. Wright, "Propagation, Antennas"

TUESDAY, JUNE 18

9:30 - 12:30 p. m.

SESSION 3 - LOW NOISE RECEIVERS

W. J. Tabor, "Masers"

D. C. Hanson, "Parametric Amplifiers"

A. J. Giger, "Diplexers, Filters, and System Considerations of Low Noise Receivers"

12:45 - 1:45 p. m.

LUNCHEON

2:00 - 5:00 p. m.

SESSION 4

M. Schwartz, "Signals in Noise"

WEDNESDAY, JUNE 19

9:30 - 12:30 p. m.

SESSION 5

D. L. Schilling, "Phase Locked Loops"

12:45 - 1:45 p. m.

LUNCHEON

2:00 - 5:00 p. m.

SESSION 6

S. Stein, "Digital Communications"

6:00 p. m.

BANQUET

COLLOQUIA AND SEMINARS

THURSDAY, JUNE 20

9:30 - 12:30 p. m.

SESSION 7

A. G. Schillinger, "Coding and Decoding"

12:45 - 1:45 p. m.

LUNCHEON

2:00 - 5:00 p. m.

SESSION 8 - SATELLITE COMMUNICATIONS: TELSTAR

E. G. Jaasma, "The Telstar Satellite Communication System"

R. C. Chapman, Jr., "The Andover Satellite Ground Station"

S. B. Bennett, "Parameters of the Telstar System and Results"

FRIDAY, JUNE 21

9:30 - 12:30 p. m.

SESSION 9 - SATELLITE COMMUNICATIONS

J. Kiesling, "Relay"

J. C. Graebner, "Ranger"

12:45 - 1:45 p. m.

LUNCHEON

DISTRIBUTION LIST

Contract No. AF-AFOSR-62-295

Semi-Annual Progress Reports to Joint Services Technical Advisory Committee

<u>To:</u>	<u>No. of Copies</u>	<u>To:</u>	<u>No. of Copies</u>
Commander Air Force Office of Scientific Research ATTN: SRPP Washington 25, D. C.	3	Director, Naval Research Laboratory ATTN: Technical Information Officer Washington 25, D. C.	6
Dr. Arnold Shostak, Code 427 Department of the Navy Office of Naval Research Washington 25, D. C.	5	Director, Army Research Office ATTN: Scientific Information Branch Department of the Army Washington 25, D. C.	1
Dr. Edward M. Reilley Director Institute for Exploratory Research U. S. Army Signal Research and Development Laboratory Fort Monmouth, New Jersey	1	Chief, Physics Branch Division of Research U. S. Atomic Energy Commission Washington 25, D. C.	1
Commander Wright Air Development Center ATTN: WWAD Wright-Patterson Air Force Base Ohio	4	U. S. Atomic Energy Commission Technical Information Extension Post Office Box 62 Oak Ridge, Tennessee	1
Commander Air Force Cambridge Research Labs. ATTN: CRREL L. G. Hanscom Field Bedford, Massachusetts	1	National Bureau of Standards Library Room 203, Northwest Building Washington 25, D. C.	1
Commander Rome Air Development Center ATTN: RCOIL-2 Griffiss Air Force Base Rome, New York	1	Director, National Science Foundation Physics Program Washington 25, D. C.	1
Commander Detachment 1 Hq. A. F. Research Division The Shell Building 47 Rue Cantersteen Brussels, Belgium (Air Mail)	2	Director, Army Research Office, Durham Box CM, Duke Station Durham, North Carolina	1
DDC (Defense Documentation Center) Arlington Hall Station Arlington 12, Virginia	10	Arnold Air Force Station AEDC (AEOIM) ATTN: Technical Library Tullahoma, Tennessee	1
Director of Research and Development Headquarters USAF ATTN: AFRDR Washington 25, D. C.	1	AFFTC (AFOTL) ATTN: Technical Library Edwards Air Force Base California	1
		Air Force Office of Scientific Research ATTN: SRMA Washington 25, D. C.	1
		Commander Air Force Special Weapons Center ATTN: SWOI Kirtland Air Force Base New Mexico	1

DISTRIBUTION LIST

<u>To:</u>	<u>No. of Copies</u>	<u>To:</u>	<u>No. of Copies</u>
Commander Air Force Missile Development Center ATTN: HD0I Holloman Air Force Base, New Mexico	1	Dr. John S. Burgess Scientific Director Rome Air Development Center Griffiss Air Force Base Rome, New York	1
Commander Army Rocket and Guided Missile Agency Redstone Arsenal ATTN: ORDXR-OTL Alabama	1	Technical Director Rome Air Development Center Griffiss Air Force Base Rome, New York	1
Commandant Air Force Institute of Technology (AU) Library MCLI-LIB, Bldg. 125, Area B Wright-Patterson Air Force Base Ohio	1	Air Force Office of Scientific Research ATTN: SRY Washington 25, D. C.	1
Commanding Officer Office of Naval Research Br. Off. Navy No. 100 Fleet Post Office Box 39, New York, N. Y.	1	Mr. M. M. Pavane U. S. Air Force AFSC Scientific and Technical Liaison Office 111 E. 16 St. New York 3, New York	1
Commander Air Force Research Division ATTN: RRRTL Washington 25, D. C.	1	Director Air University Library Maxwell Air Force Base Alabama	1
Chief Bureau of Naval Weapons Main Navy Bldg. 18th and Constitution Ave., N. W. Washington 25, D. C.	3	Commander Patrick Air Force Base Cocoa, Florida	1
Commanding Officer Naval Air Development Center Johnsville, Pennsylvania ATTN: NADC Library	1	Commanding Officer Naval Electronics Laboratory San Diego, California	2
Commanding Officer Naval Air Missile Test Center Pt. Mugu, California	1	Dr. S. Seeley, Head Engineering Division National Science Foundation Washington 25, D. C.	1
Chief of Naval Operations Pentagon OP 34 Washington 25, D. C.	1	Commanding Officer USNUSL New London, Connecticut	2
Scientific and Technical Information Facility ATTN: NASA Representative (S-AK/DL) National Aeronautics and Space Administration P. O. Box 5700 Bethesda, Maryland	6	Commanding Officer NOL White Oak, Maryland	2
		Chief, BuShips, Navy Department Washington, D. C.	3
		Aeronautical Research Laboratories ATTN: Technical Library Building 450 Wright-Patterson Air Force Base Ohio	1

DISTRIBUTION LIST

<u>To:</u>	<u>No. of Copies</u>	<u>To:</u>	<u>No. of Copies</u>
Office of Naval Research Department of the Navy ATTN: Code 420 Washington 25, D. C.	1	Hdqs. Aeronautical Systems Division AF Systems Command ATTN: George R. Branner, ASSRNEA-2 Wright-Patterson AFB, Ohio	1
Director, Department of Commerce Office of Technical Services Washington 25, D. C.	1	Dr. G. D. Goldstein, Code 437 Office of Naval Research Department of the Navy Washington 25, D. C.	1
Commanding General U. S. Army Signal Research and Development Laboratory ATTN: SIGFM/EL-RPO Ft. Monmouth, New Jersey	1	Professor D. O. Pederson, Director Electronics Research Laboratory University of California Berkeley, California	1
Director Advanced Research Projects Agency Pentagon Washington 25, D. C.	1	Professor P. Kusch, Executive Director Columbia Radiation Laboratory Columbia University 538 West 120th Street New York 27, New York	1
Director, National Security Agency Fort George G. Meade, Maryland ATTN: C3/TDL	1	Prof. F. Karl Willenbrock Division of Engrg. and Appl. Physics Price Hall, Harvard University Cambridge 38, Massachusetts	1
Mr. H. E. Cohen, SIGRA/SL-XA Mathematics Division Institute for Exploratory Research U. S. Army Signal Research and Development Lab. Fort Monmouth, New Jersey	1	Dr. William R. Rambo Electronics Laboratory Stanford University Stanford, California	1
Advisory Group on Electron Tubes 8th Floor 346 Broadway New York 13, N. Y.	2	Professor Daniel Alpert, Director Coordinated Science Laboratory University of Illinois Urbana, Illinois	1
Commanding Officer U. S. Army Research Office (Durham) ATTN: CRD-AA-IP, Mr. Ulah Box CM, Duke Station Durham, North Carolina	1	Professor Arthur Von Hippel Laboratory for Insulation Research Massachusetts Institute of Technology Cambridge 39, Massachusetts	1
Diamond Ordnance Fuze Laboratories U. S. Ordnance Corps ATTN: ORDTL-450-638, Mr. Raymond H. Comyn Washington 25, D. C.	1	Prof. E. L. Ginzton Microwave Laboratory W. W. Hansen Lab. of Physics Stanford University Stanford, California	1
U. S. Army Engineer Research and Development Laboratories ATTN: Technical Documents Center Fort Belvoir, Virginia	1	Library School of Engineering Dept. of Electrical Engineering Rensselaer Polytechnic Institute Troy, New York	1
Hdqs. Aeronautical Systems Division ATTN: ASRNET-3 Wright-Patterson AFB, Ohio	1	Syracuse University Research Institute Building B-6, Collendale Campus Syracuse 10, New York	1

DISTRIBUTION LIST

<u>To:</u>	<u>No. of Copies</u>	<u>To:</u>	<u>No. of Copies</u>
Prof. M. Kline, NYU Institute of Mathematical Sciences Washington Square New York, N. Y.	1	Prof. Donald C. Stinson University of Arizona Dept. of Electrical Engr. Tucson 25, Arizona	1
University of Michigan Engineering Research Institute Electron Tube Laboratory ATTN: Dr. J. E. Rowe Ann Arbor, Michigan	1	Prof. Joseph Meixner Technische Hochschule Aachen, Germany	1
W. H. Huggins Prof. of Electrical Engr. The Johns Hopkins University School of Engineering Baltimore 18, Maryland	1	A. D. Moore Associate Professor The University of British Columbia Dept. of Electrical Engineering Vancouver 8, Canada	1
Dr. Seymour Cohn, Manager Aircraft Systems Radiation Lab. Stanford Research Institute Stanford, California	1	Prof. A. L. Cullen University of Sheffield Department of Electrical Engr. Sheffield, England	1
Prof. E. C. Jordan, Chairman Dept. of Electrical Engr. University of Illinois Urbana, Illinois	1	Prof. George Sinclair Dept. of Electrical Engineering University of Toronto Toronto, Ontario Canada	1
Prof. R. E. Beam Dept. of Electrical Engr. Northwestern University Evanston, Illinois	1	Prof. T. Tice Supervisor, Antenna Lab. Ohio State University Columbus, Ohio	1
Prof. R. W. P. King Cruft Laboratory Harvard University Cambridge, Massachusetts	1	Prof. L. J. Chu Dept. of Electrical Engineering Massachusetts Institute of Technology Cambridge, Massachusetts	1
Prof. K. Siegel, Head Radiation Laboratory University of Michigan Ann Arbor, Michigan	1	Prof. G. Held Dept. of Electrical Engineering University of Washington Seattle, Washington	1
Prof. S. Silver University of California Berkeley, California	1	W. F. Hauser Massachusetts Institute of Technology Lincoln Laboratory Lexington 73, Massachusetts	1
Prof. J. B. Wiesner Research Laboratory of Electronics Massachusetts Institute of Technology Cambridge 38, Massachusetts	1	Prof. Rolfe E. Glover University of North Carolina Department of Physics Chapel Hill, North Carolina	1
Technical Reports Collection Gordon McKay Library Oxford Street Cambridge 38, Massachusetts	1	Head Dept. of Electrical Engineering Case Institute of Technology University Circle Cleveland 6, Ohio	1

DISTRIBUTION LIST

<u>To:</u>	<u>No. of Copies</u>	<u>To:</u>	<u>No. of Copies</u>
Dr. Kjell Johnsen Norwegian Inst. of Technology Trondheim, Norway	1	Mr. Charles H. Peyton The University of Arizona College of Engineering Tucson, Arizona	1
Professor John Peatman University of Missouri Dept. of Electrical Engineering Rolla, Missouri	1	Prof. T. Kahan, Institut Henri Poincare, 11 Rue Pierre Curie, Paris, France	1
Prof. John R. Gibson Electrical Engineering Dept. Purdue University Lafayette, Indiana	1	Prof. A. Gozzini, Institute of Physics University of Pisa, Pisa, Italy	1
Electrical Engineering Dept. California Institute of Technology Pasadena, California ATTN: Dr. R. W. Gould	1	Prof. G. Barzilai, Institute of Electronics University of Rome Via Eudossiana 18, Rome, Italy	1
University of Illinois College of Engineering Urbana, Ill. ATTN: Paul D. Coleman	1	Prof. G. Latmiral Istituto Universitario Navale Naples, Italy	1
Instrumentation Engineering Program University of Michigan ATTN: Professor E. G. Gilbert Ann Arbor, Michigan	1	Prof. G. Toraldo di Francia Centre Microonde del C. N. R. Via Panchiaticchi, 56 Firenze, Italy	1
Professor Julius Tow Department of Electrical Engineering Purdue University Lafayette, Indiana	1	Prof. Ching-Chung Li University of Pittsburgh Dept. of E. E. Pittsburgh, Penna.	1
Professor T. J. Higgins Department of Electrical Engineering University of Wisconsin Madison, Wisconsin	1	University of Pittsburgh Department of Electrical Engineering ATTN: Library Pittsburgh, Pennsylvania	1
R. A. Johnson The University of Manitoba Dept. of Electrical Engineering Winnipeg, Canada	1	Electronic Systems Laboratory Department of Electrical Engineering Massachusetts Institute of Technology Cambridge 39, Massachusetts	1
Electronic Systems Laboratory Department of Electrical Engineering Massachusetts Institute of Technology Cambridge 39, Massachusetts	1	Institute of Electronics National Chiao Tung University Hsinchu, Taiwan, China	
Institute for Defense Analyses Communications Research Division von Neumann Hall Princeton, New Jersey	1	Computer and Control Systems Laboratory University of Saskatchewan Saskatoon, Canada	1
Alderman Library University of Virginia Charlottesville, Virginia ATTN: Librarian	1	Research Laboratory of Electronics Chalmers University of Technology Gibraltargatan 5 G Gothenburg, Sweden	1

DISTRIBUTION LIST

<u>To:</u>	<u>No. of Copies</u>	<u>To:</u>	<u>No. of Copies</u>
Stanford Linear Accelerator Center Stanford University Stanford, California ATTN: Library/LA	1	Sylvania Electronic Systems Mountain View Operations P. O. Box 188 Mountain View, California	1
Princeton University The James Forrestal Research Center Library Princeton, New Jersey	1	Raytheon Manufacturing Co. Research Division Waltham 54, Massachusetts ATTN: Librarian, Research Division Library	1
Reference Librarian Northeastern University The Dodge Library Boston 15, Massachusetts	1	Laboratory for Applied Research on Crossed-Field Devices Microwave and Power Tube Division Raytheon Manufacturing Co. Research Division Waltham 54, Massachusetts	1
Mrs. Marian S. Veath Librarian Sylvania Electronic Systems 1100 Wehrle Drive Buffalo 21, New York	1	Mr. K. S. Kelleher, President Aero Geo Astro Corp. 1914 Duke Street Alexandria, Virginia	1
Library Airborne Instruments Laboratory Walt Whitman Road Melville, Long Island, N. Y.	1	G. E. C. Research Laboratories East Lane North Wembley Middlesex, England ATTN: W. E. Willshaw	1
Institute of the Aerospace Sciences ATTN: Librarian 2 East 64th Street New York 21, New York	1	Philips Laboratories Irvington-on-Hudson, New York ATTN: Aaron L. Fessler, Librarian	1
Midwest Research Institute 425 Volker Boulevard Kansas City 10, Missouri ATTN: Librarian	1	Mr. John Dyer, Vice President Airborne Instruments Lab. Division of Cutler Hammer 160 Old Country Road Mineola, New York	1
U. S. Navy, ONR New York Branch Office 207 W. 24 St. New York 11, New York	1	Mr. Robert E. Booth, Head Microwave Tubes and Components Section	1
Sperry Phoenix Company Division of Sperry Rand Corp. Phoenix, Arizona	1	Electronic Defense Lab. P. O. Box 205 Mountain View, California	
IBM Research Center Boardman Road, Bldg. 701 Poughkeepsie, New York ATTN: Dr. G. L. Tucker	1	Sylvania Electric Products, Inc. Special Tube Operations Microwave Components Labs. 500 Evelyn Avenue Mountain View, California	1
Technical Library General Electric Microwave Lab. 601 California Avenue Palo Alto, California	1	Mr. Robert S. Elliott Technical Director Rantec Corporation Calabasas, California	1

DISTRIBUTION LIST

<u>To:</u>	<u>No. of Copies</u>	<u>To:</u>	<u>No. of Copies</u>
Rand Corporation 1700 Main Street Santa Monica, California	1	The Library United Aircraft Corporation 400 Main Street East Hartford 8, Connecticut	1
American Systems Incorporated 3412 Century Boulevard Inglewood, California	1	University College of North Staffordshire Keele, Staffordshire, England ATTN: Prof. D. Jones	1
Chairman Canadian Joint Staff For DRB/DSIS 2450 Massachusetts Ave., N. W. Washington 25, D. C.	1	Documents Library Central Electric Co. Missile and Space Vehicle Dept. Room 3446, 3198 Chestnut St. Philadelphia 4, Pennsylvania	1
ASDD Library IBM, Box 344 Yorktown Heights, New York	1	Massachusetts Inst. of Tech. Dept. of Aeronautics and Astronautics Instrumentation Laboratory Cambridge 39, Mass. ATTN: Library	1
Convair Division of General Dynamics Corp. San Diego Division San Diego 12, California ATTN: K. G. Blair, Chief Librarian M. Z. 6-157	1	Bell Telephone Labs. Whippany Library Technical Reports Center Whippany, New Jersey	1
Bibliothèque du C. N. R. S. Centre de Documentation 15, Quai Anatole France Paris 7, France	1	Westinghouse Electric Corp. Air Arm Division Friendship Int'l Airport Box 746 Baltimore 3, Maryland ATTN: Library	1
Library Melpar, Inc. Applied Science Division 11 Galen Street Watertown 72, Massachusetts	1	M. A. G. Tompson Dept. of Mechanical Engineering University of Adelaide South Australia	1
Ing. Santiago F. Pinasco Ayacucho 63, 1er. piso, Dto. II Buenos Aires, Argentina	1	Ohio Semiconductor 1205 Chesapeake Ave. Columbus 12, Ohio ATTN: Dr. Warren E. Beriman, General Manager	1
Ing. A. Gilardini, Selenia Via Tiburtina Km 12, 400, Rome, Italy	1	Scientific and Technical Information Facility ATTN: NASA Representative (S-AK/DL) P. O. Box 5700 Bethesda, Maryland	1
Prof. F. Carassa Magneti-Marelli Co. Milan, Italy	1		
Dr. L. Robin, Ingenieur en Chef Des Telecommunications Department Recherches Mathematiques, 3 Avenue de la Republique Issy-les-Moulineaux, Seine, France	1		

DISTRIBUTION LIST

<u>To:</u>	<u>No. of Copies</u>	<u>To:</u>	<u>No. of Copies</u>
Dr. R. W. Grow Microwave Devices Laboratory University of Utah Salt Lake City, Utah	1	Sandia Base Albuquerque, New Mexico ATTN: Library, Sandia Labs.	1
NASA Headquarters Office of Applications Code FC 400 Maryland Avenue, S. W. Washington 25, D. C.	1	Advanced Techniques Branch (ASRNEA) Electronics Technology Laboratory Aeronautical Systems Division Wright-Patterson AFB, Ohio	1